Evaluation of the Redostat™ Device for the Study of Ferrous Iron Biological Oxidation Kinetics

By

Thierry Kamunga Kazadi

BSc in Chemical Engineering
(University of Lubumbashi/DRC)

A Thesis Submitted to the

University of Cape Town

in **FULL** fulfillment of the requirements for the degree of

Master of Science in Engineering

Department of Chemical Engineering
University of Cape Town
Rondebosch, 7701
South Africa

February 2007

I know the meaning of plagiarism and declare that all of the work in the document, save for that which is properly acknowledged, is my own.

It is the glory of God to conceal a matter, But the glory of kings is to search out a matter. Pr. 25:2

… seek, and you will find… Mat. 7:7
Says the Lord Almighty

Acknowledgements

It is by your grace **Almighty God** that I have completed this work.

My sincere gratitude to Dr. Jochen Petersen for your invaluable guidance and support for my work.

Thanks to all the Fe & S group: Prof. Sue Harrison, Prof. G. Hansford, Dr. Rob van Hille, Emmanuel Ngoma, Tunde Ojumu, Seun, James, Charlie, Nick, Fran, and my friend Mume Kabwe.

Special thanks to my pastor Tshalo Katshunga, brothers Louis and Michel for your spiritual support.

Thanks to IMIRA International for funding this project.

Dedication

To my lovely wife Solange Kamunga for your ever-present support

To my son David and my sister in law Deborah may this be an example set for you

Abstract

Mining of low grade ores is becoming more and more predominant, since high grade ores are becoming increasingly depleted. Below a certain grade, ores cannot be processed economically by conventional methods, such as smelting, roasting or pressure oxidation since they cannot be economically concentrated due to increased milling requirements for the same metal recovery. Therefore, low cost processing methods such as heap bioleaching are becoming attractive. Heap bioleaching is an established metallurgical route for the recovery of copper from low grade sulphide ores and pretreatment of refractory gold bearing sulphides. However, metal recovery is generally low (80 to 85% copper recovery is achieved in about a year) due to the slow heap bioleaching kinetics. It is believed that more metal values can be recovered in a shorter timeframe, if the kinetics of ferrous iron biological oxidation can be accelerated. This requires careful study of the bio-oxidation kinetics under heap-like conditions.

Two different experimental methods are commonly used for the study of ferrous iron biological oxidation kinetics, namely batch and continuous culture techniques. However, the continuously changing conditions in batch culture and the slowness and bacterial wash out in continuous culture are significant weaknesses for these experimental methods. This work has evaluated the Redostat™ device for faster and controlled ferrous iron biological oxidation kinetics studies. The Redostat™ device offers controlled conditions as in continuous culture but the speed and concentration range of batch culture.

Two series of experiments were carried out in the Redostat™ device, consisting of oxidizing ferrous iron in the presence and absence of *Leptospirillum ferriphilum*. The kinetic data generated with the Redostat™ current was compared with that generated under similar conditions by using two other established experimental methods viz., the batch and off-gas analysis methods.

For the abiotic ferrous iron oxidation, it was found that the kinetic data generated with the Redostat™ current is in good agreement with that generated with the batch method. Activation

energies of 61.32 and 63.61kj.mol^{-1} were calculated in the temperature range of 41.4 to 68°C and pH 1.1. These values are consistent with the activation energy values reported in the literature. A value of 69.74kj.mol^{-1} was calculated by using the off-gas analysis method. This slightly higher value was probably due to the low measurement accuracy of this method for low variations of oxygen concentration in the gas stream.

The Redostat™ current method yielded reliable results only when ferric iron precipitation was minimized, either by working at very low pH below 0.6, or by minimizing the concentration of ferric iron present in solution at higher pH. At very low pH hydrogen evolution was promoted and a current efficiency of only about 80% was measured.

For the biological oxidation of ferrous iron, the Redostat™ current method also yielded excellent results. The rate of ferrous iron oxidation measured with the Redostat™ current was found to be in good agreement with that measured using the off-gas analysis method. The specific growth rate μ was measured at 35°C, pH 1.2, 5g/l of total iron and low ferric to ferrous iron ratios of 0.17, 0.51 and 1.65 (corresponding to 419, 452, and 482mV versus Ag/AgCl reference electrode) respectively. It is difficult to obtain data at such low ferric to ferrous iron ratios because of limitations of both batch and continuous cultures. The value of μ measured was decreasing with increasing ferric to ferrous iron ratio as suggested by many ferrous iron biological oxidation kinetic models. The modified Monod equation for product inhibition by ferric iron was used to describe the growth kinetics. A maximum specific growth rate of 0.12h^{-1} and a ratio $\frac{K_S}{K_i}$ of 0.28 were calculated. The literature values of μ_{max} are sufficiently close to the one calculated in this study under similar conditions, but the reported values of $\frac{K_S}{K_i}$ are much lower than the value that was calculated in this present study.

It was also found that the biomass specific ferrous iron and oxygen consumption rates $q_{Fe^{2+}}$ and q_{O_2} and the biomass yields on ferrous iron and oxygen $Y_{Fe^{2+}X}$ and Y_{O_2X} were changing with biomass concentration even though μ remained a constant for a particular ferric to ferrous

iron ratio. This phenomenon has not been previously described and could have significant implications for start-up of heaps.

Kinetic data was generated rapidly with the Redostat™ device. It took one day to complete one run which was characterized by a specific redox potential, whilst continuous culture usually takes several days to reach steady state. The Redox potential was kept constant within an acceptable range of +2mV and +4mV from the redox potential setpoint value for the abiotic and biological ferrous iron oxidation experiments respectively. The redox potential control can be improved for better ferrous and ferric iron concentrations control and longer runs by increasing the Redostat™ control gain.

Table of Contents

List of Figures

List of Tables

Nomenclature

a	Reaction Order with Respect to Ferrous Iron	-
$\mathbf{C^*}$	Concentration of Dissolved Oxygen at Saturation	[mol/l]
$\mathbf{C_N}$	Microbial Concentration	[Cell/ml]
C_{O_2}	Concentration of Dissolved Oxygen	[mol/l]
$\mathbf{C_S}$	Substrate Concentration	[mmol/l]
C_S^0	Substrate Concentration in the Feed	[mmol/l]
$\mathbf{C_X}$	Biomass Concentration	[mmol C/l]
D	Dilution Rate	$[h^{-1}]$
E	Redox potential	[mV]
$\mathbf{E^\#}$	Activation Energy	$[kj.mol^{-1}]$
$\mathbf{E_0}$	Standard Redox Potential	[mV]
F	Faraday Constant	[C]
I	Redostat™ Current	[A]
K	Kinetic Constant $\frac{K_S}{K_i}$	-
k	Kinetic Constant	$[s^{-1}$ or $mol^{-1}.s^{-1}]$
k	Equilibrium constant	[mol/atm.Kg of H_2O]
$\mathbf{k_0}$	Arrhenius Constant	$[mol^{-1}.s^{-1}]$
$\mathbf{k_d}$	Specific Death Rate	$[h^{-1}]$
$\mathbf{K_i}$	Ferric Iron Inhibition Coefficient	[mol/l]

$\mathbf{K_La}$	Oxygen Mass Transfer Coefficient	[s^{-1}]
$\mathbf{K_m}$	Michaelis-Menten Coefficient	[mol/l]
$\mathbf{K_S}$	Ferrous Iron Saturation Coefficient	[mol/l]
$\mathbf{m_S}$	Maintenance Coefficient on Substrate	[mmol Sub./mmol C.h]
$m_{Fe^{2+}}$	Maintenance Coefficient on Ferrous iron	[mmol Fe^{2+}/mmol C.h]
m_{O_2}	Maintenance Coefficient on Oxygen	[mmol O_2/mmol C. h]
$N_{K_2Cr_2O_7}$	Normality of $K_2Cr_2O_7$ Solution	[g-equ./l]
$\mathbf{P_g}$	Gassed Power	[W]
P_{O_2}	Oxygen Partial Pressure	[atm.]
Q	Redostat™ Intergrated Charge	[C]
$q_{Fe^{2+}}$	Biomass Specific Ferrous Iron Oxidation Rate	[mmol Fe^{2+}/mmol C.h]
q_{O_2}	Biomass Specific Oxygen Consumption Rate	[mmol O_2/mmol C.h]
$q_{O_2}^{max}$	Maximum Biomass Specific Oxygen Consumption Rate	[mmol O_2/mmol C.h]
R	Universal Gas Constant	[$j.mol^{-1}.K^{-1}$]
$-r_{bm}$	Rate of Ferrous Iron Oxidation Calculated with the Batch Method	[mol/l.s]
$-r_{CO_2}$	CO_2 Consumption Rate	[mmol/l.h]
$-r_{CO_2}^0$	Initial CO_2 Consumption Rate	[mmol/l.h]

$-r_{Fe^{2+}}$	Ferrous Iron Oxidation Rate	[mol/l.s or mmol/l.h]
$-r_{Fe^{3+}}$	Rate of Ferric Iron Reduction at the Redostat™ Cathode	[mol/l.s]
$-r_I$	Rate of Ferrous Iron Oxidation Calculated with the Redostat™ Current Method ($-r_I = -r_{Fe^{3+}}$)	[mol/l.s]
$-r_{O_2}$	Oxygen Consumption Rate	[mmol/l.h]
$-r_{O-gas}$	Rate of Ferrous Iron Oxidation Calculated with the Off-gas Analysis Method	[mol/l.s]
r_p	Rate of Product Formation	[mol/l.h]
r_P^{max}	Maximum Rate of Product Formation	[mol/l.h]
r_X	Biomass Growth Rate	[mmol C/l.h]
T	Temperature	[K or °C]
t	Time	[s or h]
$\mathbf{t_d}$	Cell Generation Time	[h]
U	Superficial Gas Velocity	[m/s]
V	Redostat™ Working Volume	[l]
$\mathbf{V_L}$	Liquid Volume	[m^3]
$\mathbf{V_S}$	Iron Solution Sample Volume	[ml]
$\mathbf{V_T}$	$K_2Cr_2O_7$ Titration Volume	[ml]
$Y_{Fe^{2+}X}$	Biomass Yield on Ferrous Iron	[mmol C/mmol Fe^{2+}]
Y_{O_2X}	Biomass Yield on Oxygen	[mmol C/mmol O_2]

$Y^{max}_{Fe^{2+}X}$	Maximum Biomass Yield on Ferrous Iron	[mmol C/mmol Fe^{2+}]
$Y^{max}_{O_2X}$	Maximum Biomass Yield on Oxygen	[mmol C/mmol O_2]
Y^{max}_{SX}	Maximum Biomass Yield on Substrate	[mmol C/mmol Sub.]
α	Constant	-
Φ	Fraction < 1	-
Φ_{in}	Feed Air Flow Rate	[mmol/h]
Φ_{out}	Off-gas Flow Rate	[mmol/h]
η	Redostat™ Current Efficiency	[%]
μ	Biomass Specific Growth Rate	[h^{-1}]
μ_{max}	Maximum Specific Growth Rate	[h^{-1}]
$[CO_2]_{in}$	CO_2 Molar Fraction in the Feed Air	-
$[CO_2]_{out}$	CO_2 Molar Fraction in the Off-gas	-
$[Fe^{2+}]_0$	Ferrous Iron Initial Concentration	[mol/l]
$[Fe]_T$	Total iron concentration	[mol/l]
$[Fe^{2+}]_{thres}$	Threshold Ferrous Iron Concentration	[mol/l]
$[O_2]_{in}$	Oxygen Molar Fraction in the Feed Air	-
$[O_2]_{out}$	Oxygen Molar Fraction in the Off-gas	-

Chapter 1. Introduction

1.1. Background

The continuing supply of metals to satisfy the world demand is of crucial significance. A considerable number of metals such as copper, zinc, nickel, cobalt, antimony, tin, lead, bismuth, and molybdenum are found as sulphides (Barrett et al., 1993). Sulphide minerals conventionally undergo roasting, smelting, or pressure oxidation for metal recovery.

Roasting and smelting generate sulphur dioxide as well as arsenic trioxide (if arsenopyrite is present), which are both of environmental concern. The use of additional emission control devices such as scrubbers to prevent pollution increases even more the capital and operating costs of these two techniques. Pressure oxidation is also an expensive metallurgical route since autoclaves are costly and require high level of operator training and skills. Therefore, the use of these conventional methods is justified only for concentrates which are economically produced from high-grade ores and whose metal value can support the processing cost.

The continuing depletion of high-grade mineral resources and the refractoriness of some ores have created a need for the development of new economically viable and environmentally safe processes for the treatment of lower-grade ores and ores that can not be handled by conventional technology to ensure the continued availability of a range of metals in the twenty-first century (Barrett et al., 1993; Torma, 1993).

Heap bioleaching is such a low-cost and environmentally favourable processing method and is applicable for low grade ores which cannot be economically concentrated and processed by conventional methods. Heap bioleaching significantly reduces production costs owing to lower energy requirements, lower labour costs, and lower reagent usage; diminishes capital costs due to simpler equipment and rapid construction and increases mineral reserves, because lower grade ores can be economically treated and varied mineral types can be processed. It also provides better environmental conditions and worker safety, because there are no toxic gas emissions such as sulphur dioxide and arsenic trioxide (Brierley, 2005).

Bioleaching is currently practiced on a commercial scale for pretreatment of refractory gold-bearing sulphide minerals (Table 1.1), recovery of copper from chalcopyrite concentrates and secondary sulphide ores such as chalcocite (Table 1.2) and the extraction of uranium from its oxide ore UO_2 (Brierley and Brierley, 2001; Akcil, 2004; Brierley, 2005; Watling, 2006). In 2003, the contribution of bioleaching to the production of copper, uranium and gold was estimated to be approximately 15%, 13% and 25% of the total world production, respectively (Akcil, 2004).

There is also considerable potential for bioleaching and pretreatment of a wide range of base metals and platinum-group metals. Microbial leaching has been shown at laboratory or pilot plant scale for the base metal sulphides of cobalt, gallium, molybdenum, nickel, zinc, and lead. Sulphide minerals occluding platinum-group metals (Pt, Rh, Ru, Pd, Os and Ir) can be microbially pretreated (Brierley and Brierley, 2001).

Table 1.1: Commercial Tank bioleaching plants treating gold concentrates (Brierley and Brierley, 2001, Acevodo, 2002, van Aswegen et al., 2007)

Plant	Concentrate treatment capacity (t/day)	Commissioned
Fairview, South Africa	35	1986
Sao Bento, Brazil	150	1990
Wiluna, Australia	158	1993
Ashanti, Ghana	1000	1994
Sansu, Ghana	1000	1994
Fosterville, Australia	211	2005
Suzdal, Kazakhstan	196	2005

Table 1.2: Commercial bioleaching of copper ores (Watling, 2006)

Region/mine	Operation reserves (tonne)	Ore processed (tonne/day)	Copper production (tonne/year)
Cerro Colorado, Chile 1993-	Heap bioleach $80x10^6$ at 1.4% Cu	Chalcocite, covellite $16x10^3$	$100x10^3$
Ivan zar, Chile 1994-	Heap bioleach $5x10^6$ at 2.5% Cu	Oxides/sulphides $1.5x10^3$	$12x10^3$
Punta del Cobre, Chile 1994-	Heap (bio)leach $10x10^6$ at 1.7% Cu	Oxides/sulphides	$7\text{-}8x10^3$
Quebrada Blanca, Chile 1994-	Heap/dump bioleach $85x10^6$ at 1.4% Cu, $45x10^6$ at 0.5% Cu	Chalcocite $17.3x10^3$	$75x10^3$
Andacollo, Chile 1996-	Heap/dump bioleach $32x10^6$ at 0.58% Cu	Chalcocite $15x10^3$	$21x10^3$
Dos Amigos, Chile 1996-	Heap bioleach 2.5%Cu	Chalcocite $3x10^3$	-
Zaldivar, Chile 1998-	Heap/dump bioleach $120x10^6$ at 1.4% Cu, $115x10^6$ at 0.4% Cu	Chalcocite $20x10^3$	$150x10^3$
Lomas Bayas, Chile 1998-	Heap/dump $41x10^6$ at 0.4% Cu	Oxide/sulphides $36x10^3$	$60x10^3$
Cerro Verde, Peru 1977-	Heap bioleach at 0.7% Cu	Oxide/sulphide $32x10^3$	$54.2x10^3$
Escondida, Chile	Heap bioleach $1.5x10^9$ at 0.3-0.7% Cu	Oxides, sulphides	$200x10^3$
Nifty Copper, Australia, 1998-	Heap bioleach 1.2% Cu	Oxides/chalcocite $5x10^3$	$16x10^3$
Whim Creek and Mons Cupri, Australia 2006-	Heap bioleach $900x10^6$ at 1.1% Cu, $6x10^6$ at 0.8% Cu	Oxides/sulphides	$17x10^3$
S&K Copper, Monywa, Myanmar, 1999-	Heap bioleach $126x10^6$ at 0.5% Cu	Chalcocite $18x10^3$	$40x10^3$
Morinci, Arizona 2001-	Mine for leach $3450x10^6$ at 0.28% Cu	Chalcocite, pyrite $75x10^3$	$380x10^3$
Phoenix deposit, Cyprus, 1996-	Heap (bio)leach $9.1x10^6$ at 0.78% Cu, $5.9x10^6$ at 0.31% Cu	Oxide/sulphide	$8x10^3$
Jinchuan Copper, China 2006-	$240x10^6$ at 0.63%	Chalcocite, covellite, enargite	$40x10^3$

1.2. Problem Statement

Tank bioleaching, which is used for sulphide concentrates, has made a lot of progress and a metal recovery of 95 to 98% is achievable after 5 days (Brierley, 2005) whereas heap bioleaching, which is used for low-grade sulphide whole ores, is still a developing technology. Its kinetics are still slow and the metal recovery limited (Petersen, 2003). Acid heap leaching of oxide minerals such as tenorite, cuprite, malachite, and chrysocolla might take hours to days but heap bioleaching of sulphide minerals such as chalcocite, covellite, bornite, and enargite takes months to years. A copper recovery typically ranging from 75 to 80% is achieved from 150 days (Watling, 2006) up to 2 years (Petersen and Dixon, 2007b) from bornite and chalcocite. Chalcopyrite, the most abundant copper sulphide which is generally low grade,

leaches at about one fifth the rate of chalcocite and its heap bioleaching takes years (Watling, 2006).

The key role of microorganisms in bioleaching is the facilitation of oxidation of ferrous iron to ferric iron, as given in equation 1.1. Ferric iron, in turn, leaches many sulphide minerals (Eq. 1.2).

$$2Fe^{2+} + \frac{1}{2}O_2 + 2H^+ \xrightarrow{microorganisms} 2Fe^{3+} + H_2O \quad (1.1)$$

$$2Fe^{3+} + MeS \rightarrow 2Fe^{2+} + Me^{2+} + S^0 \downarrow \quad (1.2)$$

It is believed that more metal values can be recovered in a shorter timeframe if the kinetics of ferrous iron biological oxidation (Eq. 1.1) are comprehensively understood since under certain conditions this bioleaching subprocess can be the overall rate controlling step of bioleaching (Hansford, 1997). Millions of tonnes of low-grade ore and copper-rich tailings await the development of an efficient and economic bioleach process for chalcopyrite (Watling, 2006).

A number of kinetic models of the biological oxidation of ferrous iron already exist, yet there is still a need to develop a comprehensive kinetic model which includes all the operating parameters such as pH, temperature, total iron concentration, etc., and which is applicable to heap bioleaching conditions.

Two different experimental methods are mainly used for the study of ferrous iron biological oxidation kinetics, namely batch and continuous culture techniques. Batch culture technique is characterized by a high initial concentration of ferrous iron which is depleted rapidly and in an uncontrolled manner. The changing conditions in batch culture directly effect the kinetic performance of iron oxidizing microorganisms (Boon et al., 1999a) and make the interpretation of data difficult.

Continuous culture technique is a more reliable technique as the experimental conditions can be kept constant throughout the all experiment. But only very high ferric to ferrous iron ratios (> 100), and corresponding potentials (E > 600 mV against Ag/AgCl 3M KCl electrode) can be investigated with this method because of wash-out behaviours at lower ferric to ferrous iron ratios or potentials. Also, this technique is time consuming; it takes days to complete an experiment for a given ferric to ferrous iron ratio. Lastly, the continuous culture technique might not reflect the real conditions prevailing within a heap bioleaching system as the heap is not really a continuous reactor. Some zones within the heap bed where the residence time is long enough can behave more like batch reactors where microorganisms oxidize ferrous iron reduced by the mineral particles and increase in number until a point of saturation.

To address these downsides of batch and continuous culture techniques **this work has evaluated the Redostat™ device which combines the speed of the batch culture technique with the controlled conditions of the continuous culture technique, for the study of ferrous iron biological oxidation kinetics**.

The Redostat™ device is conceptually a fed-batch reactor which has the potential to regenerate ferrous iron by reducing automatically and electrolytically ferric iron at a platinum cathode, thus keeping the redox potential constant within an acceptable range. At steady state, when the redox potential does not change, ferrous and ferric ions concentrations also remain constant according to the Nernst equation (Eq. 3.1). Also, this device will help obtain a better simulation of heap conditions at laboratory scale, with the cathode regenerating ferrous iron as the mineral would, and the microbial population increasing until some point of saturation like in the heap bed.

After the initial commissioning of the Redostat™ device, two series of experiments, abiotic and biological oxidations of ferrous iron were carried out in order to assess its performance as a faster, controllable and reliable experimental tool for the study of ferrous iron bio-oxidation kinetics. The kinetics of these two reactions were studied by using the Redostat™ current, off-gas analysis and batch methods. The kinetic data generated with the Redostat™ current method was compared to that obtained by using the other two established experimental methods. The

findings of this study and recommendations for future research are summarized in the conclusion and recommendations of this work.

Chapter 2. Literature Review

2.1. Bioleaching

2.1.1. Historical Background

Bioleaching has been practised since ancient times, although the principles governing it were unknown then. Galen, around 166 A.D., reported in his travel notes that in ancient Cyprus copper mines, cavities were excavated in mineral-bearing rock, permeable enough to let surface water percolate and become loaded with copper sulphate. Pregnant solution dripped from the roofs of these cavities and was collected in Roman amphorae before they were poured in ponds where copper sulphate was recovered by crystallization after water evaporation. Pliny, about a century earlier (23-79 A.D.), also reported in Book 34 of his Naturalis Historia that in situ copper-ore leaching was being carried out in the mines of Asturia, Gallacia, and Lusitania in Spain, for the production of solutions from which chalchantum (copper sulphate) was extracted (Rossi, 1990).

Rio Tinto mines in Spain were the first recorded large scale heap leaching operation for the production of copper where bioleaching played a major role in the eighteenth century. It was believed that the Rio Tinto ore or the Spanish climate had some obscure and mysterious quality as this technique appeared to work only at Rio Tinto for many years and not elsewhere, like in the south-western states of the U.S.A. where the leaching of low grade copper ore was attempted without any success. It was only after the discovery of *Acidithiobacillus ferrooxidans* in acid mine drainages from coal mines and its ability to oxidise both the sulphur and iron moieties of pyrite by Colmer et al. between 1950 and 1951, that the need arose to investigate the possibility of using this bacterium for the oxidation, therefore the solubilization, of other metal sulphides such as copper sulphides and molybdenite (Brierley, 1982; Rossi, 1990).

Bryner et al. and Bryner and Anderson, in 1954 and 1957 respectively, provided the evidence of the ability of *Acidithiobacillus ferrooxidans* to oxidise other metal sulphides. Their pioneering work marked the beginning of such an intensive research activity that already by

1966 Ducan et al. were able to publish a list of as many as nineteen metal sufides whose solubilization had been shown to be enhanced by *Acidithiobacillus ferrooxidans* by several researchers all over the world. Since then, the microorganism has been isolated from all the acid drainage waters flowing from orebodies, mines and dumps of low grade ore, as well as in all the old heaps from Rio to Fenice Capanne to Szomolnok, where leaching had been performed with its effective mediation for centuries. Thus a correlation was established between the presence of the bacterium and the dissolution of metals in copper leaching operations (Brierley, 1982; Rossi, 1990).

The discovery of *Acidithiobacillus ferrooxidans* and its properties marked the beginning of a new era (biohydrometallurgy) in the understanding of phenomena related to the formation of acid mine drainages and the leaching of sulphide minerals or bioleaching. Then in the mid-eighties there was a breakthrough in bioleaching practice when in Minera Pudahuel in Chile the first copper mine switched from a mixed acid and bacterial leaching to full heap bioleaching of an ore containing 1 to 2 % copper with a production of 14,000 tonnes of fine copper per year. Since the 1980s bioleaching have been developing increasingly (Brierley and Brierley, 2001; Acevedo, 2002; Akcil, 2004).

2.1.2. Definition and Mechanism

Bioleaching can be defined as the oxidation and dissolution of metal bearing minerals, especially sulphide minerals, by ferric iron as the leaching agent which is regenerated by certain types of iron oxidising microorganisms.

Ferric iron oxidizes the sulphide mineral MeS bearing the valuable metal to elemental sulphur and the targeted metal is either released into the leaching solution as a sulphate if it is a base metal such as copper or exposed for cyanidation in the case of occluded gold (Fig. 2.1). The ferrous iron produced by the ferric leaching (Eq. 2.1) is oxidized back to ferric iron by iron oxidising microorganisms (Eq. 2.2) so that the leaching can proceed in a cyclic way. The elemental sulphur produced by the ferric leaching (Eq. 2.1) can be oxidized to form sulphuric

acid by sulphur-oxidising microorganisms (Eq. 2.3) so that the mineral surface can remain exposed for further leaching.

$$2Fe^{3+} + MeS \rightarrow 2Fe^{2+} + Me^{2+} + S^0 \downarrow \quad (2.1)$$

$$2Fe^{2+} + \frac{1}{2}O_2 + 2H^+ \xrightarrow{microorganisms} 2Fe^{3+} + H_2O \quad (2.2)$$

$$S + \frac{3}{2}O_2 + H_2O \xrightarrow{microorganisms} H_2SO_4 \quad (2.3)$$

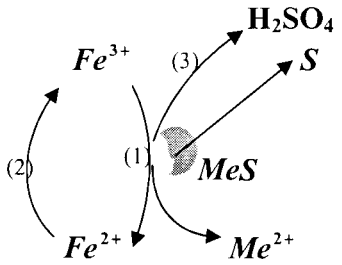

Figure 2.1: Bioleaching mechanism

For minerals such as oxides and carbonates, their metal values may be recovered by allowing the biological oxidation of pyrite (Eq. 2.4), to provide iron (III) and sulfuric acid solutions which solubilize the metal content. The solubilization reaction may also involve the oxidation of the metal to a higher oxidation state than it possessed in the mineral as in the bioleaching of uranium oxide ores (Eq. 2.5) (Barrett et al., 1993; Torma, 1993).

$$4FeS_2 + 15O_2 + 2H_2O \rightarrow 4Fe^{3+} + 8SO_4^{2-} + 4H^+ \quad (2.4)$$

$$UO_2 + Fe_2(SO_4)_3 \rightarrow UO_2SO_4 + 2FeSO_4 \quad (2.5)$$

2.1.3. Industrial Applications of Bioleaching

Bioleaching is an economical and environmentally favourable metallurgical route for the processing of sulphide minerals. The use of bioleaching for the production of metals significantly reduces the capital and production costs. It increases the mineral reserves as the low grade ores and refractory gold bearing sulphides, which are becoming more and more predominant nowadays, can be economically processed. It also offers better environmental

conditions as there are no toxic gas emissions such as sulphur dioxide or arsenic trioxide associated with it (Brierley, 2005). However, it is worth noting that in some cases conventional methods are preferable over bioleaching for the processing of mineral concentrates (Dreisinger, 2005).

As stated in the introduction, bioleaching is now exploited on an industrial scale for the production of copper from low grade sulphide ores (Table 1.2) and chalcopyrite concentrates (Brierley, 2005), the pre-treatment of refractory gold bearing sulphides (Table 1.1), and the production of uranium from its oxide ore UO_2 (Torma, 1993).

Bioleaching is also used on a commercial scale for the production of cobalt from a cobaltiferous pyrite concentrate in Uganda (Morin and D'Hugues, 2007). There is still considerable potential for bioleaching of the base metal sulphides of Pb, Zn, Co, Mo, Ga, and Ni, and of sulphide minerals occluding platinum-group metals. The next commercial application of base metal bioleaching appears to be for nickel. Billiton has developed the BioNIC® process as a biohydrometallurgical technology for extraction of nickel from low-grade sulphide ores but its commercialisation will depend on selective recovery of the nickel from the leach solution (Brierley and Brierley, 2001).

Different bioleaching techniques are industrially used depending on the grade or value of the ore to be processed.

2.1.4. Tank Bioleaching

Tank bioleaching is accomplished in highly engineered, aerated, continuously stirred tank reactors (Fig. 2.2). The tanks are made out of stainless steel, each as large as 1380 m^3, and equipped with agitators that maintain the finely ground sulphide mineral concentrate in suspension and ensure that oxygen is efficiently transferred to the microorganisms. Each tank is cooled to maintain the bioleach solution at the proper temperature for the microorganisms used (Brierley, 2005).

The mineral concentrate is added to acidified water containing NH_4^+ and PO_4^{3-} ions and fed continuously to the first tank in a series of tanks. Mineral concentrates move from the first-stage reactor(s) on a continuous basis through three to four continuous stirred tank reactors in series until the sulphide minerals are oxidized. This usually requires about a five-day residence time across the entire bioleaching circuit (Brierley, 2005).

If the metal is a base metal, such as Cu^{2+}, it dissolves when the mineral is oxidized according to reaction 2.1. The oxidized slurry exits the final reactor and undergoes solid/liquid separation, after which the solid is discarded and the liquid is processed (solvent extraction & electrowinning) to recover the metal (Brierley, 2005).

If the mineral concentrate is gold bearing, the liquid from the last-stage reactor is neutralized and stabilized for safe disposal and the solid is processed by cyanidation to recover the gold. When micrometer-sized gold particles are embedded within sulphide minerals, usually pyrite or arsenopyrite, the direct cyanidation of these ores leads to a very poor gold recovery of 0 to 30%. A sufficient oxidation of the sulphide matrix by bioleaching to liberate the embedded gold prior to cyanidation significantly increases the gold recovery (Brierley, 2005).

Metal recovery in continuous stirred tank reactors bioleach circuits are in the order of 95-98% (Brierley, 2005).

Figure 2.2: Continuous stirred tank bioleaching reactors, China (Unknown source)

The use of controlled conditions in continuous stirred tank reactors, such as temperature, pH, and concentrations, results in rapid and highly effective oxidation of sulphides. Since conditions are optimized for the microorganisms, numbers reach 10^9 to 10^{10} organisms per ml of solution. Copper and gold are recovered from chalcopyrite and sulfidic gold concentrates (Table 1.1) respectively by using tank bioleaching (Brierley, 2005).

Tank bioleaching is suitable for concentrates only since low grade ores which cannot be economically concentrated cannot cover the processing cost.

2.1.5. Heap Bioleaching

Low grade metal resources are becoming more and more predominant nowadays as high grade ores are becoming more and more depleted. These low grade resources cannot be economically processed by conventional methods or tank bioleaching because of the cost of concentration or their low metal value. Therefore a low cost processing method such as heap bioleaching is indispensable for low grade ores.

The ore is typically crushed to less than 19 mm and agglomerated with acidic water to bind finely ground rock into larger rock particles, hence improving air and solution distribution in

the heap. Agglomerated floatation tailings can also be used instead of the ore (Barrett et al., 1993). Large, slightly inclined soil pads are covered with plastic, and two arrays of perforated plastic pipes (one for air and the second for solution collection) are placed on the plastic. The ore is stacked 6-10 m deep on top of the plastic (Fig. 2.3). The heap is drip irrigated with the leaching solution and forced air is provided through the pipes under the crushed ore. Naturally occurring microorganisms proliferate, reaching 10^6 to 10^7 per gram of ore and per millilitre of solution (Brierley, 2005).

Temperatures in the heap generally stay within the range for mesophilic bacteria but in some gold bioheaps they can reach as much as 70°C. To accommodate this temperature rise all three groups of bioleaching microorganisms (mesophiles, moderate thermophiles, and extreme thermophiles) are used within the heap bed, with each group becoming active as its temperature range is achieved (Brierley, 2005). Heap heat balance is influenced by the heat generating potential of the ore (exothermic oxidation of sulfides), which is largely a function of pyrite content, and the ambient environmental conditions (climate), which govern the net rate of gain at the heap surface. On top of these two factors the thermal effects owing to the liquid and gas flows must be taken into account (Dixon, 2000).

Figure 2.3: Heap construction (Photo courtesy of Compania Minera Zaldivar)

Regardless of irrigation mode, the leaching solution within the heap bed is divided into two parts, the flowing liquid and the stagnant liquid (Fig. 2.4) (Petersen, 2003). The stagnant liquid is made up of the process solution filling up the intra-particle pores, intra-agglomerates pores and any liquid film clinging to the surface of agglomerates (stagnant films). It is affected by the physical properties of the solution as well as the shape, size and wettability of the particles.

The flowing liquid is the rest of the process solution flowing downward through the heap bed interstices as rivulets and films. This fraction is more likely to proceed through preferential discrete flowing channels between clusters of particles containing stagnant moisture. The flowing liquid phase depends primarily on the packing characteristics and to a lesser extent on the liquid physical properties, the liquid and gas flow rates. Bouffard and Dixon reported a ratio of stagnant to mobile liquid of approximately 5 to 6 (Bouffard and Dixon, 2001).

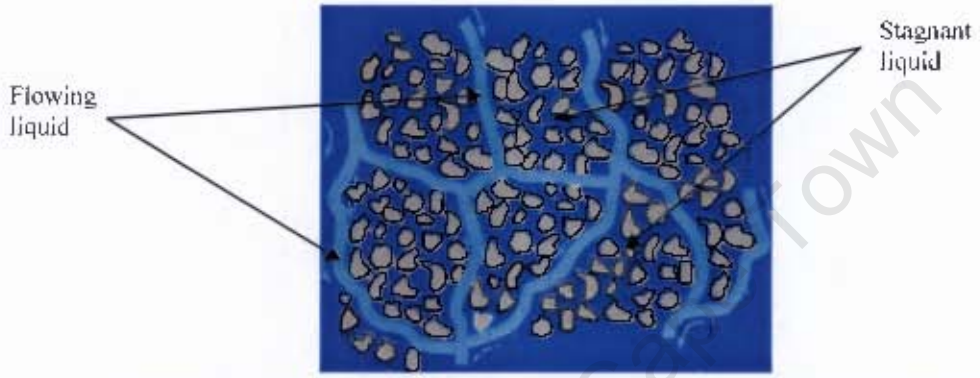

Figure 2.4: Solution distribution within the heap bed (Petersen, 2003)

The transport of reagents and reaction products within the heap bed is by advection in the flowing liquid and gas, and by diffusion at the gas/liquid interface, stagnant liquid /flowing liquid interface and through the stagnant liquid phase (Fig. 2.5). The reagents are brought by advection in the leaching solution and blown air, the carbon dioxide and oxygen are absorbed into the liquid phase and the dissolved reagents diffuse into and through the stagnant liquid to react with the mineral particles (Eq. 2.1, 2.3). The reaction products diffuse back into the flowing liquid and are transported by advection to the bottom of the heap bed where the pregnant solution is collected for electrowinning after proper purification process (solvent extraction) and the barren solution is recycled to the top of the heap for further leaching (Fig. 2.6). But if the valuable metal to be recovered is gold, the pretreated ore is neutralized with lime, and chemically leached, usually with a dilute cyanide solution to dissolve the gold (Bouffard and Dixon, 2001; Brierley, 2005; Petersen and Dixon, 2007a).

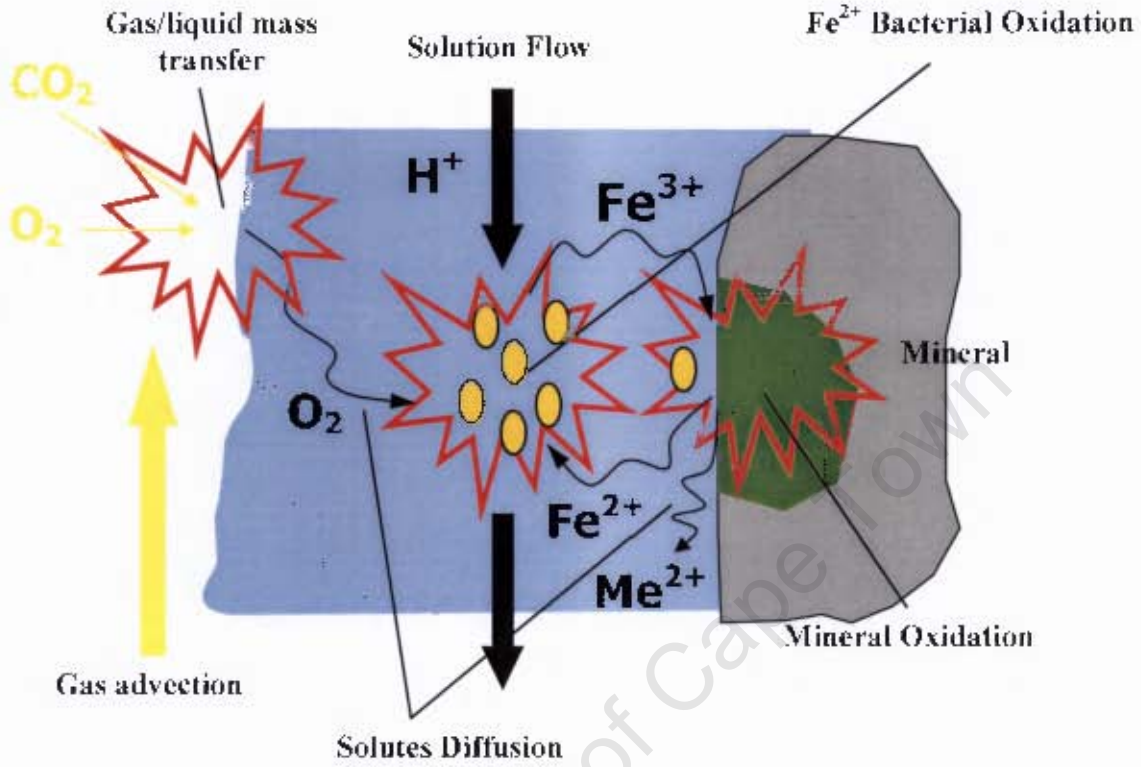

Figure 2.5: Reaction-transport network within the heap bed (Petersen and Dixon, 2007a)

Since the 1980s, heap bioleaching of the copper sulphide minerals Cu_2S and CuS has been widely practiced commercially for ores grading 0.5-1.5% Cu or occasionally higher (Table 1.2). Copper extraction of around 80% is achieved in 6 to 15 months (varies widely from place to place) (Watling, 2006; Petersen, 2007b). Heap bioleaching for pre-treatment of gold sulfidic ores has been practiced since the mid-1990s and it can take up to 1.5 years depending on the ore particle size and other factors. Gold recovery of 75-85% is achieved after heap bioleaching pre-treatment and cyanidation (Brierley, 2005).

When the ore grade is very low (lower than about 0.5% for copper ores) to justify beneficiation with conventional processes or heap bioleaching, dump or in-situ bioleaching are used as leaching techniques for the metal recovery. These techniques, similar in principles to heap bioleaching, are less efficient but more economical than heap bioleaching for the processing of

very low grade ores. A dump is a pile of waste materials or very low grade fragmented rocks whose size often exceeds 1m and the pile can be as high as 60m. Dumps are also irrigated with a leaching solution from the top like heaps but the microorganisms get their oxygen and carbon dioxide from natural convection of air caused by the temperature rise within the dump bed. For in-situ leaching, the leaching solution is applied to the permeable ore body without removing it from the ground. Dump leaching of copper and in-situ leaching of uranium and copper are established procedures (Barrett et al., 1993; Brierley, 2005).

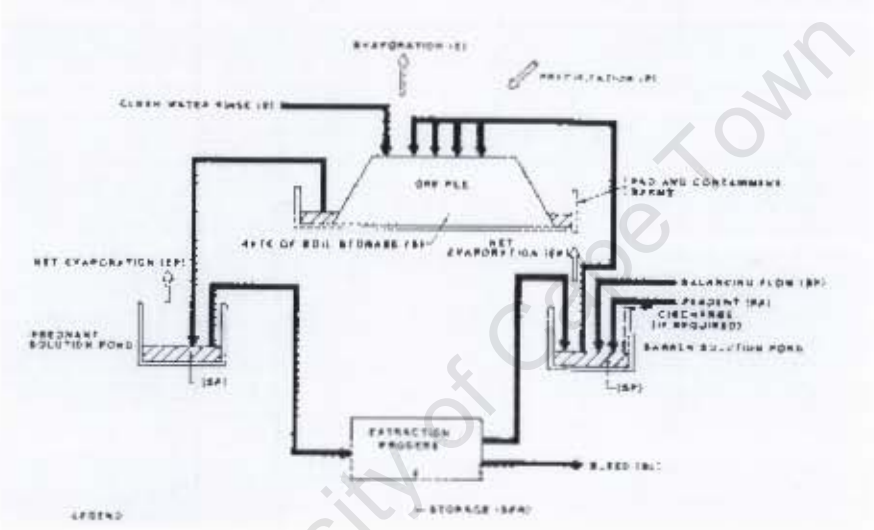

Figure 2.6: Heap leach process flow sheet (Bartlett, 1992)

Although heap bioleaching is an established metallurgical method for the recovery of copper and gold there is still a need to improve its kinetics. The overall rate of heap bioleaching depends on a long and complex chain of subprocesses such as diffusion of dissolved constituents, gas/liquid mass transfer, ferrous iron biooxidation, and mineral oxidation (Fig. 5.2). In general, the slowest of these determines the overall rate. It is believed that under certain conditions the biological oxidation of ferrous iron can be the overall rate-controlling subprocess of bioleaching (Hansford, 1997; Petersen and Dixon, 2007a).

2.2. Ferrous Iron Biological Oxidation

2.2.1. Iron-oxidizing Microorganisms

The microorganisms involved in the leaching of metals from ores obtain energy for reproduction and maintenance by oxidizing ferrous iron Fe^{2+}, and elemental sulphur S^0. These organisms require oxygen as their electron acceptor and carbon dioxide as their sole carbon source, obtained from air, and some nitrogen, potassium, phosphorus, and other macronutrients. The biomining organisms need a sulphuric acid environment of pH 2.5 to a lower pH limit of about 0.5 (Brierley, 2001).

There are three distinct groups of biomining organisms (Brierley, 2001):

1. mesophilic bacteria that live and reproduce at about 10-45°C;
2. moderately thermophilic (heat loving) bacteria that function at about 45-60°C;
3. and extremely thermophilic archaea, which grow in the 60-90°C range.

2.2.1.1. Mesophilic Bacteria

The most common iron-oxidizing microorganisms found in commercial bioleaching systems, at moderate temperatures below 40°C, are *Acidithiobacillus ferrooxidans, Leptospirillum ferriphilum* (previously thought to be *Leptospirillum ferrooxidans*) and *Leptospirillum ferrooxidans* (Rawlings et al., 1999; Coram and Rawlings, 2002; Romero et al., 2003; Watling, 2006).

Acidithiobacillus ferrooxidans are gram-negative nonsporulating rods (Fig. 2.7a), 0.5-0.6 μm wide by 1.0-2.0 μm long, with round ends, occurring singly or in pairs, rarely in chains (Fig. 2.7b). They are motile by means of a single polar flagellum and are found naturally in acid mine drainage waters of sulphide ore deposits, bituminous coal mines, and commercial bioleaching systems (Nemati et al., 1998; Rawlings et al., 1999). These bacteria grow on ferrous iron or sulphur and reduced sulphur compounds. According to MacIntosh and Stevens

et al., *Acidithiobacillus ferrooxidans* are able to fix atmospheric nitrogen to satisfy their nitrogen requirement. This property might explain the activity of *Acidithiobacillus ferrooxidans* in the absence of any other obvious nitrogen source (Barrett et al., 1993). They grow between 4°C and 40°C with an optimal temperature around 33°C. Their growth and the related oxidation rate decrease rapidly above the optimal temperature. The pH of the solution in which they can occur is within the range of 1.5 to 6.0 with an optimum between 2.0 and 2.5. They usually do not survive above a pH of 6.5 or below a pH of 1 (Nemati et al., 1998). The mean generation time quoted for growth of *Acidithiobacillus ferrooxidans* on ferrous iron, t_d (Eq. 2.35), is between 5 to 12 hours (Pronk and Johnson, 1993).

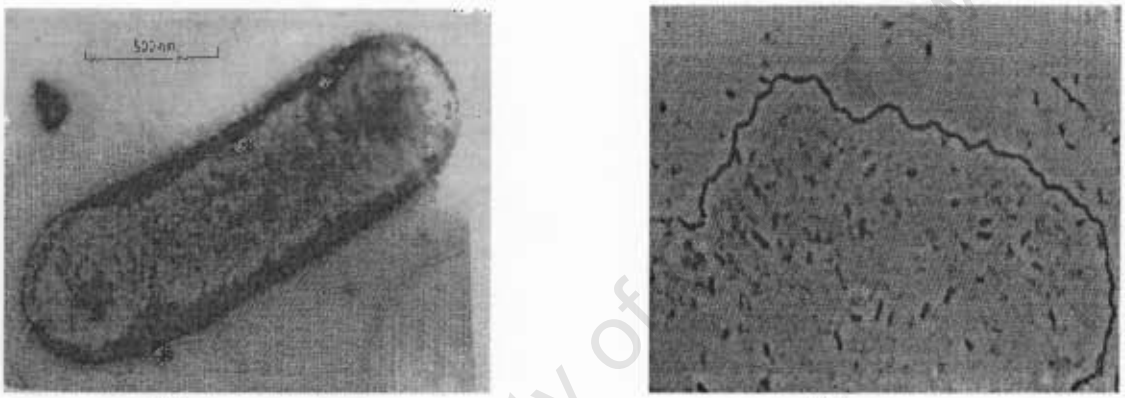

(a) (b)

Figure 2.7: Electron micrograph of a single (a) cell and a chain (b) of *Acidithiobacillus ferrooxidans* (Rossi, 1990)

Leptospirillum ferriphilum (*ferri*, iron; *philum*, loving) are small curved rod cells or spirilla, measuring 0.3 to 0.6 µm wide and 0.9 to 3.5 µm long. Cells are gram negative, spore forming, and motile by means of a single polar flagellum. Growth is aerobic and chemolithotrophic, with ferrous iron but not sulphur serving as the energy source. Optimum pH is 1.4 to 1.8 and temperature 30 to 37°C, with possible growth at 45°C (Coram and Rawlings, 2002).

Leptospirillum ferrooxidans are gram-negative, curved rod shaped or vibrioid bacteria (Fig. 2.8a), 0.9 to 1.1µm long by 0.2 to 0.4 µm wide. They can form longer spirals by joining vibrios at their ends (Fig. 2.8b). They are motile by means of a polar flagellum. Unlike *Acidithiobacillus ferrooxidans*, these bacteria can only oxidize ferrous iron and not sulphur;

this is why it is impossible for them to grow on sulphide minerals on their own. They grow in the temperature range of 15°C to less than 45°C (Coram et al., 2001) with an optimum around 35°C. The pH of the solution in which they can survive is within the range of 0.5 to 4.0 with an optimum of 1.2 to 2.0. The mean generation time quoted for growth on ferrous iron, t_g (Eq. 2.35), is between 10 to 15 hours (Rossi, 1990; Pronk and Johnson, 1993; Bosecker, 1997; Rawlings et al., 1999).

Leptospirillum species are widespread in ore deposits, in ore dumps, and in solutions produced in the process of copper leaching (Barrett et al., 1993; Brierley, 2001).

Acidithiobacillus ferrooxidans is considered to be more tolerant of low temperatures and less tolerant of high temperatures than is *Leptospirillum ferrooxidans*. This latter tolerates lower pH values and higher concentrations of ferric iron (higher redox potentials), uranium, molybdenum, silver, and sulphates than the first, but it is more sensitive to copper (Norris et al., 1987; Sand et al., 1992; Bosecker, 1997; Rawlings et al., 1999; Romero et al., 2003).

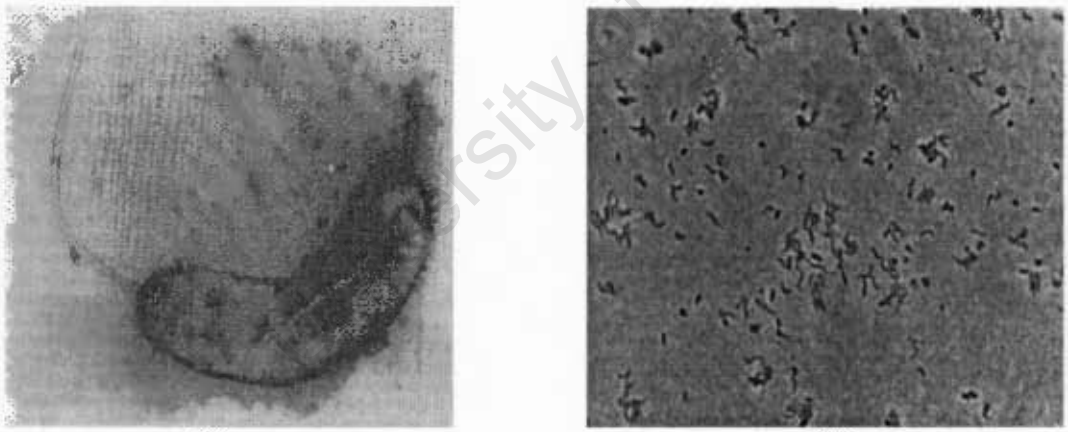

(a) (b)

Figure 2.8: Vibrio (a) and spirals (b) of *Leptospirillum ferrooxidans* (Rossi, 1990, Rawlings et al., 1999)

For temperatures exceeding 45°C the activity of *Acidithiobacillus ferrooxidans* and *Leptospirillum* species is strongly inhibited. The microbial oxidation of ferrous iron, beyond this temperature, is carried out by moderate (50°C to 60°C) and extreme thermophiles which can survive up to 90°C (Rossi, 1990; Brierley, 2001).

2.2.1.2. Moderately Thermophilic Bacteria

The existence of moderately thermophilic acidophilic bacteria in thermal springs and ore deposits was demonstrated by Le Roux et al., Brierly, J.A and Lockwood in the United States and by Golovacheva and Karavaiko in Russia. Some of moderately thermophilic bacteria have been classified as being members of the new genus *Sulfobacillus,* others are still known only by their code names. It is quite possible that some or even all the non-classified moderate thermophiles will be assigned to the genus *Sulfobacillus* when they have been fully characterized (Barrett et al., 1993).

The genus *Sulfobacillus* is composed of aerobic Gram-positive facultatively autotrophic extreme acidophilic eubacteria which are able to use iron (II), elemental sulphur and reduced sulphur compounds as energy sources. The bacteria of this genus are morphologically similar in that they consist of straight rods, 1μm in diameter by 5-10μm long, although other forms are sometimes observed (Barrett et al., 1993; Brierly, 2001).

The moderately thermophilic bacteria are found in the same types of natural environments as the mesophilic bacteria, becoming more abundant as the temperature increases (Brierly, 2001).

2.2.1.3. Extremely Thermophilic Archaea

Extremely thermophilic archaea have no rigid wall surrounding the microbial cell like other biomining bacteria, but have a membrane covered with an amorphous layer. They are facultative chemolithoautotrophs and grow under autotrophic, mixotrophic or heterotrophic conditions. Under autotrophic conditions they oxidize iron (II) and various sulphur substances to gain energy for reproduction and maintenance. They grow and reproduce in sulphuric acid environments approaching boiling temperatures with high dissolved metal content and low amounts of oxygen, carbon dioxide, ammonium, and phosphate. These organisms are 1-2μm in diameter spherical in shape. The cells are immotile and have no flagella (Barrett et al., 1993; Brierly, 2001).

Sulfolobus species belong to this class. *Sulfolobus*-like archaea have been found at higher temperatures such as the 70°C bioleach process for copper from chalcopyrite (Barrett et al., 1993).

The archaea dwell in the harshest conditions on Earth – very hot acid springs, volcanic zones, hot coal waste piles, deep oceans where sulphur gases vent, and hot biomining operations (Brierly, 2001).

2.2.2. Mechanism of Ferrous Iron Bio-oxidation

The electron transport chain in *Acidithiobacillus ferrooxidans*

During the microbial oxidation process, ferrous iron is the electron donor while oxygen is the electron acceptor. Electrons flow from ferrous iron (Eq. 2.6a) located outside the cell to oxygen in the cytoplasm (Eq. 2.6b) via an electron chain of redox proteins namely, rusticyanin and cytochromes (Fig. 2.9). The reduced oxygen is transformed into water. Therefore, the microbial oxidation reaction of ferrous iron can be split into two half reactions as follows (Rossi, 1990; Nemati et al., 1998):

$$2Fe^{2+} \rightarrow 2Fe^{3+} + 2e^{-} \quad (2.6a)$$

$$2e^{-} + \frac{1}{2}O_2 + 2H^{+} \rightarrow H_2O \quad (2.6b)$$

Sulphate ions seem to play an important role in the mechanism of ferrous iron oxidation as they act as an anionic stabilizer of the exa-aquated Fe^{2+} complex which serves as a direct substrate for the iron-oxidizing enzyme system. The electrons transfer and the pH gradient (i.e. acidic periplasm relative to a near neutral cytosol) cause a potential gradient ΔE across the cell membrane which becomes charged positively on the outer side and negatively on the inner. The migration of a proton across that potential gradient ΔE releases energy that is used for ATP synthesis, NAD(P) reduction for CO_2 fixation and mechanical work. When compared to the oxidation of glucose, that of ferrous iron does not yield much energy. 20.5 mol of Fe^{2+} would have to be oxidized to synthesize one mol of ATP and assimilate 1 mol of carbon, based

on the assumption that the bacterium requires 500.2 kj of energy to fix this much carbon at 100% efficiency. But efficiency values as low as 3.2% to as high as 30% have been reported. It is obvious therefore, that large quantities of iron must be oxidized by the bacterium to satisfy its energy requirement (Rossi, 1990; Nemati et al., 1998).

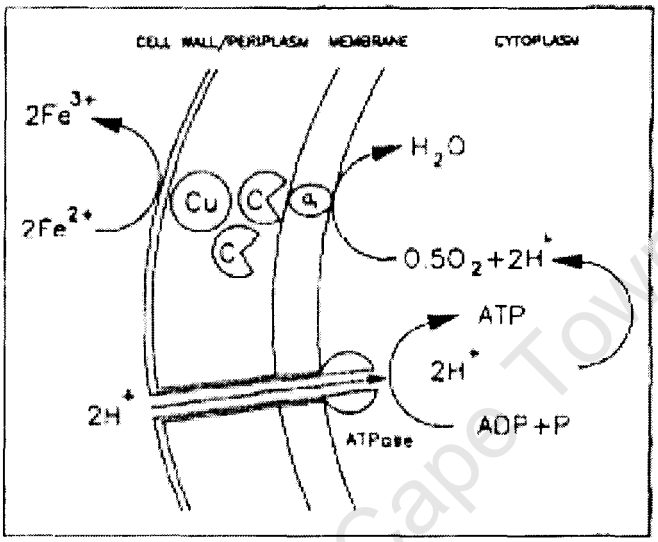

Figure 2.9: Fe^{2+} oxidizing chain of Acidithiobacillus ferrooxidans (after Ingledew and Houston). Cu refers to rusticyanin; C, cytochrome c; a_1, cytochrome a_1 (Nemati et al., 1998).

2.2.3. The Kinetics of Ferrous Iron Bio-oxidation

The rate of ferrous iron oxidation in aqueous solutions has been shown to be a function of the concentrations of ferrous iron, oxygen, and hydroxyl ions in solution. Some other anions besides hydroxyl ion are also known to affect the rate of the reaction. In acid solutions with pH below 2, the reaction usually shows no dependence on pH. McBain was the first to examine the kinetics of the oxidation reaction, and he obtained the following rate equation by experiments with sulphuric acid solutions:

$$-\frac{d[Fe^{2+}]}{dt} = k[Fe^{2+}]^2[O_2] \qquad (2.7)$$

The validity of equation (2.7) was confirmed later for sulphuric, nitric, and perchloric acids solutions (Tamura et al., 1976). Chmielewski and Charewicz (1984), Verbaan and Crundwell

(1986) also found second-order rate equations with respect to ferrous iron, which are given by equations 2.8 and 2.9 respectively, for the abiotic oxidation of ferrous iron in aqueous sulphuric acid solutions.

$$-r_{Fe^{2+}} = \frac{k[Fe^{2+}]^2[O_2]}{[H^+]^{0.36}} \tag{2.8}$$

$$-r_{Fe^{2+}} = k[Fe^{2+}]^2 P_{O_2} \tag{2.9}$$

where P_{O_2} is the oxygen partial pressure

However, it was found by some researchers that, when complexing anions such as Cl^- are introduced, the rate of Fe (II) oxidation by oxygen in aqueous sulphuric acid solutions is described by a first-order kinetic equation with respect to ferrous iron (Chmielewski and Charewicz, 1984).

The mediation of microorganisms in the oxidation of ferrous iron makes the rate of oxidation several orders of magnitude greater than the rate of abiotic oxidation of ferrous iron. The biological ferrous iron oxidation and microbial growth kinetics are related since biomass formation (Eq.2.10) is dependent on the energy released for carbon fixation, which in turn depends on the oxidation of ferrous iron.

$$CO_2, NH_4, H_2O \rightarrow CH_{1.8}O_{0.5}N_{0.2} \tag{2.10}$$

The right hand side term of equation (2.10) is a stoichiometric formula of bacteria which refers only to the organic part of biomass (Roels, 1983).

2.2.3.1. Biomass Yield on Ferrous Iron

It is the amount of carbon-moles of biomass produced per mole of ferrous iron consumed and it is given by:

$$Y_{Fe^{2+}X} = \frac{r_X}{-r_{Fe^{2+}}} \qquad [mol\ C / mol\ Fe^{2+}] \tag{2.11}$$

r_X is the rate of biomass production or growth rate.

Similarly the biomass yield on oxygen is given by:

$$Y_{O_2X} = \frac{r_X}{-r_{O_2}} \qquad [mol\ C / mol\ O_2] \tag{2.12}$$

2.2.3.2. Overall Reaction – Ferrous Iron Oxidation plus Microbial Growth

Since ferrous iron oxidation and growth are related the kinetics of the two reactions can be linked by combining equations (2.2) and (2.10) into one balanced equation (Eq. 2.13) (Boon, 1996).

$$CO_2 + 0.2\,NH_4^+ + \frac{1}{Y_{Fe^{2+}X}} Fe^{2+} + \left(\frac{1 - 4.2\,Y_{Fe^{2+}X}}{4Y_{Fe^{2+}X}}\right) O_2 + \left(\frac{1}{Y_{Fe^{2+}X}} - 0.2\right) H^+ \rightarrow$$

$$\left(\frac{1}{2Y_{Fe^{2+}X}} - 0.6\right) H_2O + \frac{1}{Y_{Fe^{2+}X}} Fe^{3+} + CH_{1.8}O_{0.5}N_{0.2} \tag{2.13}$$

In the overall reaction (Eq. 2.13), oxidation and growth are put together and it is much easier this way, by performing a degree of reduction balance over it (Boon, 1996) or by stoichiometry, to relate the rate of ferrous iron oxidation to the rate of biomass production and oxygen utilization (Eq. 2.14). The rate of carbon dioxide utilization is equal to the rate of biomass production since 1mole of CO_2 is consumed per carbon-mole of biomass produced (Eq. 2.13).

$$-r_{Fe^{2+}} = -4r_{O_2} - 4.2r_{CO_2} \tag{2.14}$$

Equation (2.14) is called the degree of reduction balance on ferrous iron.

2.2.3.3. Biomass Specific Ferrous Iron Oxidation Rate

The biomass specific ferrous iron oxidation rate is the amount of ferrous iron consumed per unit time and carbon-mole of biomass and it is given by (Boon, 1996):

$$q_{Fe^{2+}} = \frac{-r_{Fe^{2+}}}{C_X} \qquad [mol\ Fe^{2+} / mol\ C.h] \tag{2.15}$$

C_X is the concentration of biomass in the culture medium.

Similarly the biomass specific oxygen consumption rate is the number of moles of oxygen consumed per carbon-mole of biomass and unit time. It is given by (Boon, 1996):

$$q_{O_2} = \frac{-r_{O_2}}{C_X} \qquad [mol\ O_2 / mol\ C.h] \tag{2.16}$$

2.2.3.4. Pirt Equation

This is another equation relating the rate of ferrous iron oxidation to the growth rate. It also accounts for the energy used by microorganisms for growth and maintenance.

The Pirt Equation (Pirt, 1982), for growth on ferrous iron, is given by:

$$-r_{Fe^{2+}} = \frac{r_X}{Y^{max}_{Fe^{2+}X}} + m_{Fe^{2+}} C_X \tag{2.17}$$

The maintenance coefficient on ferrous iron $m_{Fe^{2+}}$ is defined as the amount of ferrous iron that is required per unit of time to maintain one carbon-mole of biomass and the maximum biomass yield on ferrous iron $Y^{max}_{Fe^{2+}X}$ is the maximum amount of biomass that can be produce per mole of ferrous iron consumed (van Scherpenzeel et al., 1998).

The Pirt equation can also be expressed in terms of $q_{Fe^{2+}}$ (Eq. 2.18) or $Y_{Fe^{2+}X}$ (Eq. 2.19) by dividing equation (2.17) by C_X or r_X respectively.

$$q_{Fe^{2+}} = \frac{\mu}{Y^{max}_{Fe^{2+}X}} + m_{Fe^{2+}} \quad (2.18)$$

μ is the specific growth rate.

$$\frac{1}{Y_{Fe^{2+}X}} = \frac{1}{Y^{max}_{Fe^{2+}X}} + \frac{m_{Fe^{2+}}}{\mu} \quad (2.19)$$

The maintenance coefficient and the maximum biomass yield are constants for a certain microorganism growing on a certain substrate. Thus, the Pirt equation only applies if a linear relation exists between the rates of ferrous iron oxidation and microbial growth. The applicability of the Pirt equation can be examined by using $q_{Fe^{2+}}$ or $Y_{Fe^{2+}X}$. If the Pirt equation applies, $q_{Fe^{2+}}$ versus μ (Eq. 2.18) and $\frac{1}{Y_{Fe^{2+}X}}$ versus $\frac{1}{\mu}$ (Eq. 2.19) are both straight lines (Fig. 2.10-2.11).

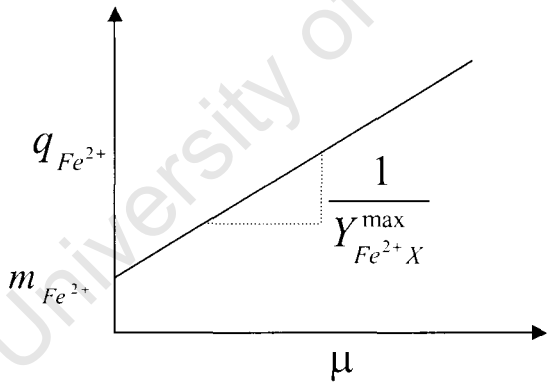

Figure 2.10: $q_{Fe^{2+}}$ versus μ graph

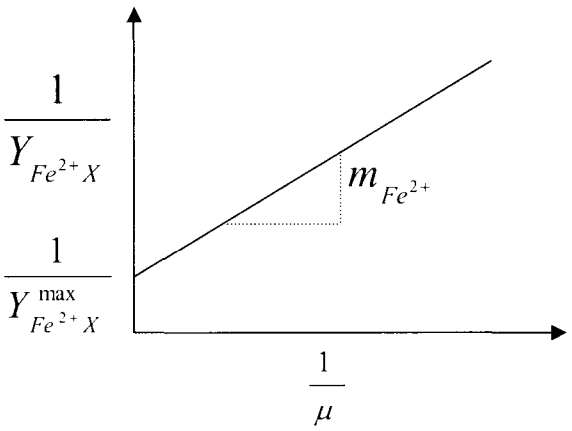

Figure 2.11: $\frac{1}{Y_{Fe^{2+}X}}$ **versus** $\frac{1}{\mu}$ **graph**

Equation (2.18) or (2.19) can be used graphically to determine the values of the maximum biomass yield and maintenance coefficient on ferrous iron (Fig. 2.10-2.11). From these two equations it is obvious that the biomass specific ferrous iron oxidation rate and the actual biomass yield depend on the specific growth rate μ.

Similarly, the Pirt equation relates the oxygen consumption rate to the bacterial growth rate and the maintenance requirements of bacteria growing on ferrous iron:

$$-r_{O_2} = \frac{r_X}{Y^{max}_{O_2X}} + m_{O_2} C_X \qquad (2.20)$$

In this equation, $Y^{max}_{O_2X}$ is the maximum yield of biomass on oxygen and m_{O_2} is the maintenance coefficient of biomass on oxygen. These two parameters are determined graphically by plotting the biomass specific oxygen consumption rate versus μ (Eq. 2.21) or the reciprocal of the actual yield of biomass on oxygen versus the reciprocal of the specific growth rate (Eq. 2.22).

Then, by dividing equation (2.20) by C_X or r_x the Pirt equation becomes equations (2.21) or (2.22) respectively.

$$q_{O_2} = \frac{\mu}{Y_{O_2X}^{max}} + m_{O_2} \tag{2.21}$$

$$\frac{1}{Y_{O_2X}} = \frac{1}{Y_{O_2X}^{max}} + \frac{m_{O_2}}{\mu} \tag{2.22}$$

If the Pirt equation applies the maximum yield of biomass on ferrous iron can be related to the maximum yield of biomass on oxygen by means of the degree of reduction balance:

$$Y_{O_2X}^{max} = \frac{4Y_{Fe^{2+}X}^{max}}{1 - 4.2Y_{Fe^{2+}X}^{max}} \tag{2.23}$$

and the maintenance coefficient on ferrous iron can also be related to the amount of oxygen used for maintenance:

$$m_{O_2} = \frac{m_{Fe^{2+}}}{4} \tag{2.24}$$

2.2.3.5. Ferrous Iron Bio-oxidation Kinetic Models

It has been shown that the growth of microorganisms on ferrous iron depends on different factors such as temperature, pH, concentrations of ferric and ferrous iron, concentrations of toxic ions, dissolved oxygen, carbon dioxide, etc. Mathematically, this relation is written as follows (Nemati et al., 1998):

$$\mu = f\left(T, pH, [Fe^{3+}], [Fe^{2+}], [M^{n}], [O_2], [CO_2], \ldots\right) \qquad [h^{-1}] \tag{2.25}$$

The specific growth rate μ shows how quickly growth is taking place in a particular environment, and $[M^n]$ is the concentration of toxic ions in the medium.

Substantial effort has been made to model the kinetics of ferrous iron bio-oxidation using one of the following equations as the starting point (Breed and Hansford, 1999):

- The Michaelis-Menten equation

$$r_p = \frac{r_p^{max} C_S}{K_m + C_S} \tag{2.26}$$

- The Monod equation

$$\mu = \frac{\mu_{max} C_S}{K_S + C_S} \tag{2.27}$$

- Or the logistic equation (G. Rossi, 1990)

$$\frac{dC_X}{dt} = \mu_{max} C_X (1 - \alpha C_X) \tag{2.28}$$

r_p is the rate of product formation, r_P^{max} the maximum rate of product formation, μ_{max} the maximum specific growth rate, C_S the limiting substrate concentration, K_m and K_S the Michaelis and Monod constants respectively, and α is a constant.

To date a number of kinetic models for ferrous iron bio-oxidation have been proposed (Nemati et al., 1998; Ojumu et al., 2006). These models can be broadly classified as either Michaelis-Menten/Monod (Eq. 2.29-2.31) or empirical based. Michaelis-Menten based models assume that the rate limiting reaction can be described using the traditional enzyme kinetics whereas empirical models use tools such as the logistic equation (Eq. 2.28) to model the kinetics.

Lacey and Lawson (1970) used the Monod equation (Eq. 2.27) to describe the kinetics of ferrous iron oxidation in batch culture. Jones and Kelly (1983) modified the Monod equation to account for ferric iron inhibition (Eq. 2.29) and Bradlock et al. (1984) introduced the concept of a threshold ferrous iron oxidation below which growth does not occur (Eq. 2.30).

$$\mu = \frac{\mu_{\max}}{1 + \frac{K_S}{[Fe^{2+}]} + \frac{K_S}{K_i}\frac{[Fe^{3+}]}{[Fe^{2+}]}} \tag{2.29}$$

$$\mu = \frac{\mu_{\max}}{1 + \frac{K_S}{[Fe^{2+}] - [Fe^{2+}]_{thres}}} \tag{2.30}$$

K_S and K_i are substrate (ferrous iron) saturation and ferric iron inhibition constants respectively.

Boon et al. proposed a rate equation (Eq. 2.31) incorporating both ferric iron inhibition from Kelly and Jones and a threshold value from Braddock et al (Hansford, 1997, Boon et al., 1999a)

$$q_{O_2} = \frac{q_{O_2}^{\max}}{1 + \frac{K_S}{[Fe^{2+}] - [Fe^{2+}]_{thres}} + \frac{K_S}{K_i}\frac{[Fe^{3+}]}{[Fe^{2+}] - [Fe^{2+}]_{thres}}} \tag{2.31}$$

$q_{O_2}^{\max}$ is the maximum biomass specific oxygen utilization rate.

And if the Pirt equation applies (Eq. 2.21) and the maximum specific growth and oxygen consumption rates coincide (Eq. 2.32) a specific growth rate equation (Eq. 2.33) can be derived from equation (2.31).

$$q_{O_2}^{\max} = \frac{\mu_{\max}}{Y_{O_2X}^{\max}} + m_{O_2} \tag{2.32}$$

$$\mu = \frac{\mu_{\max} + m_{O2} Y_{O_2X}^{\max}}{1 + \frac{K_S}{[Fe^{2+}] - [Fe^{2+}]_{thres}} + \frac{K_S}{K_i}\frac{[Fe^{3+}]}{[Fe^{2+}] - [Fe^{2+}]_{thres}}} - m_{O_2} Y_{O_2X}^{\max} \tag{2.33}$$

Hansford (1997) developed a simple rate equation (Eq. 2.34), which well approximates the kinetics of ferrous iron bio-oxidation, by neglecting the ferrous iron saturation term and the threshold ferrous iron concentration in equation 2.31.

$$q_{O_2} = \frac{q_{O_2}^{max}}{1 + K\frac{[Fe^{3+}]}{[Fe^{2+}]}} \tag{2.34}$$

where $K = \frac{K_S}{K_i}$

Although the kinetics of the microbial oxidation of ferrous iron has been modelled the challenge still remains in incorporating the influence of other parameters such as temperature, pH, toxic ions, concentrations of dissolved oxygen and carbon dioxide etc. and in extending the applicability of these models to heap bioleaching operating conditions (Nemati et al., 1998; Ojumu et al., 2006). Therefore, the study of the kinetics of ferrous iron bio-oxidation is still in progress using different experimental techniques.

2.2.4. Current Experimental Techniques for the Study of Ferrous Iron Bio-oxidation Kinetics

This section is dealing with some experimental methods that are currently used to understand the kinetics of ferrous iron bio-oxidation for bioleaching purposes. All these methods consist of growing iron oxidizing microorganisms on ferrous iron in an experimental vessel.

2.2.4.1. Microbial Growth Kinetics

When microorganisms are cultivated under favourable conditions such as optimum temperature and pH, water, oxygen and nutrients availability, they grow exponentially. The iron-oxidizing microorganisms have their optimum growth temperature either between 20°C

and 50°C for mesophiles and moderate thermophiles or above 50°C for extreme thermophiles and their optimum pH are around 2. They are chemolithoautotrophs which grow on ferrous iron.

If C_N is the concentration of cells at a time t the growth equation is as follows:

$$\frac{dC_N}{dt} = \mu C_N \tag{2.35}$$

As sometimes it is quite difficult to count individual cells in a culture, growth can be expressed in terms of biomass which is an easier parameter to measure. Then equation (2.35) becomes:

$$\frac{dC_X}{dt} = r_X = \mu C_X \tag{2.36}$$

In practice, when cultivating microorganisms, they do not immediately multiply exponentially after inoculation. The growth process passes through these following successive phases represented by the sigmoid curve below (Fig. 2.12):

- The lag phase
- The exponential phase
- The stationary phase
- The death phase or phase of decline

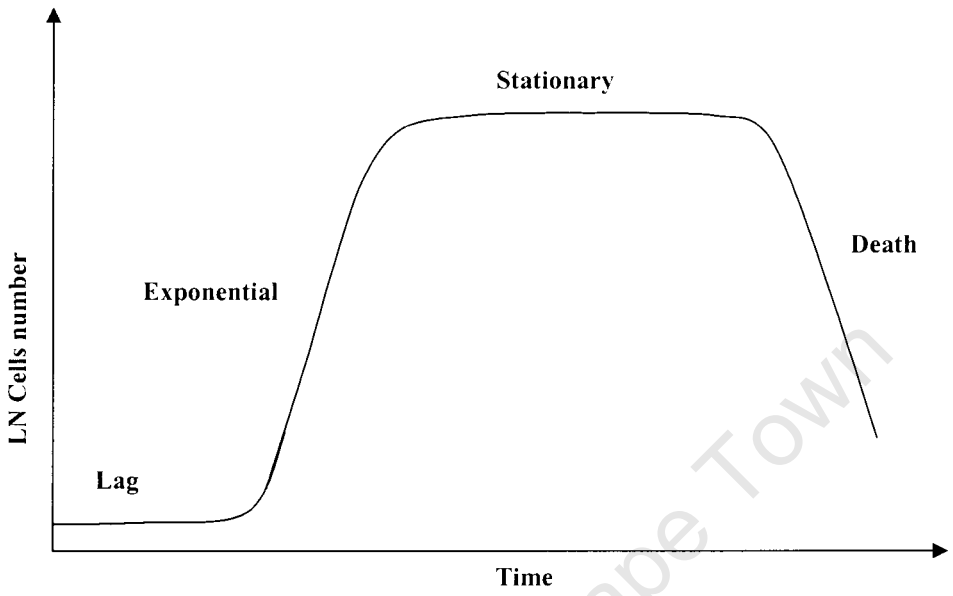

Figure 2.12: Microbial growth curve

The lag phase is characterized by an absence of significant cell multiplication and an adaptation of microorganisms to the new environment. Its duration can range from a few minutes to several hours and even days (for *Acidithiobacillus ferrooxidans* (Rossi, 1990)). For a certain type of microorganism, the length of this phase depends chiefly on the growth conditions and the state of the inoculum (size and physiology). The lag phase is shortest where growth conditions are good and the inoculum is large and consists of actively growing cells. Poor growth conditions, a small inoculum or cells taken from a previous culture in lag, stationary or death phase will result in a longer lag in this new culture (Rossi, 1990).

After the lag phase, the exponential phase starts where microorganisms grow exponentially according to equation (2.35) or (2.36). The slope of the portion of the curve (Fig. 2.12) representing this phase gives the specific growth rate μ. Growth, during this phase, is also characterized by the cell generation time which is defined as the mean time between one cell division and the next for all the cells in a given culture and it is given by (Rossi, 1990):

$$t_d = \frac{\ln 2}{\mu} \tag{2.37}$$

The growth rate is influenced by the growth conditions and the type of microorganism. If exponential phase cells are removed from a nutritionally poor medium to a nutritionally rich medium a short lag phase will occur but the subsequent growth rate will be observed to be faster than before the transfer (so-called shift up). Conversely, if exponential phase cells are moved from a nutritionally rich growth medium to a nutritionally poor growth medium, there will be a longer lag phase as cells need to switch on metabolic pathways not previously utilised. The subsequent growth rate will then be observed to be slower than before the transfer (so-called shift down).

The stationary phase takes place when the microbial population no longer grows. During this phase there is either no cell division or equality between the growth rate and the death rate due to the depletion of nutrients, changes in pH, formation of toxic metabolites, etc.

The last phase, phase of decline, occurs when the death rate becomes greater than the growth rate resulting in a decrease of the microbial population.

The batch and continuous culture techniques, used to investigate ferrous iron bio-oxidation kinetics, pass at least through the first two growth phases.

2.2.4.2. Batch Culture Technique

A batch culture is characterised by a microbial population growing in a medium until the supply of nutrients is depleted. There is no fresh feed to compensate what microorganisms have consumed and all the products of the metabolic process remain in the culture. This accumulation of metabolites in the culture can lead to inhibition effects on growth.

Since there are no fresh feed and disposal of toxic metabolites in a batch culture, microorganisms cannot grow indefinitely. The growth process (net increase in microbial

population) stops as soon as there is insufficient substrate to sustain it or once the concentration of toxic products cannot be tolerated by the microorganisms any more. At this stage the batch culture can be either in a stationary phase where the growth rate is equal to the death rate or in a phase of decline where the death rate is greater than the growth rate (see Eq. 2.39).

Batch culture is an unsteady state technique where the concentrations of substrate and biomass in the medium are changing with the time as shown in the following Biomass and Limiting Substrate Mass Balance equations respectively:

$$\frac{dC_S}{dt} = -\mu C_X \frac{1}{Y_{SX}^{max}} - m_S C_X \tag{2.38}$$

$$\frac{dC_X}{dt} = \mu C_X - k_d C_X \tag{2.39}$$

k_d is the specific death rate.

Boon et al. (1999a) studied ferrous iron bio-oxidation kinetics in batch cultures. The first hours of the experiment show a disagreement between the values of the specific growth rate μ measured using the off-gas analysis method (mu batch curve in fig. 2.13) and those calculated (mu cal. curve in fig. 2.13) using the kinetic model (Eq. 2.33). According to equation 2.33, at low ratios of $\frac{[Fe^{3+}]}{[Fe^{2+}]}$ or high ferrous iron concentration in the initial phase of the batch culture experiment, μ_{max} would occur, but the measured specific growth rate increases until a maximum is reached after some hours. Boon et.al (1999a) propose that this dynamic behaviour of the growth kinetics is caused by "major changes in the anabolic system" which can occur under changing external conditions. Therefore, during this dynamic phase of the batch system, the specific growth rate μ cannot be described by the rate equation for competitive product inhibition (Eq. 2.33).

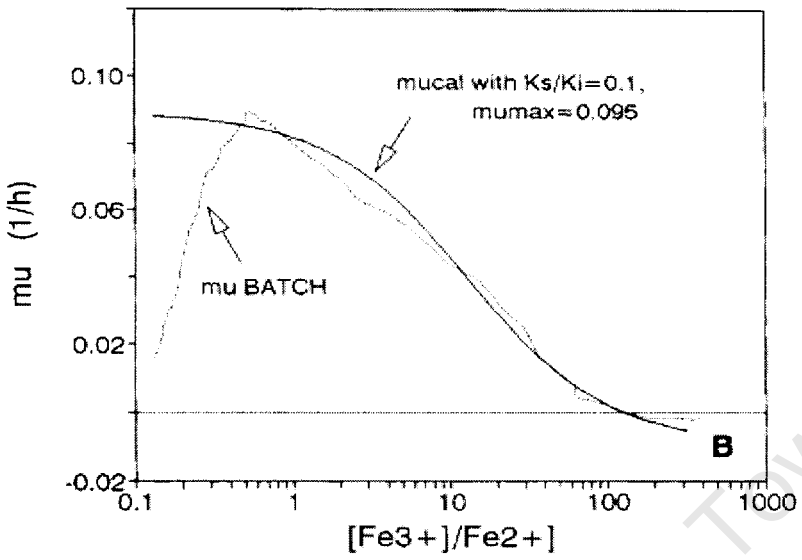

Figure 2.13: μ versus $[Fe^{3+}]/[Fe^{2+}]$ in batch culture (Boon et al., 1999a)

After the dynamic phase, where growth and oxidation are said to be uncoupled, a rapid pseudo-steady state takes place and the two curves in figure 2.13 coincide. This only occurs during the last hours of the batch experiment and at this stage the ratio $[Fe^{3+}]$ / $[Fe^{2+}]$ changes so quickly that sometimes it is much more difficult to monitor its effects (Boon et al., 1999a).

It has been shown that the batch culture technique is inappropriate to quantify the effect of total iron, toxic metal ions and pH on the steady state kinetics of ferrous iron bio-oxidation. The values of the kinetic parameters $q_{O_2}^{\max}$, $\mu_{\max}$, and $\frac{K_S}{K_i}$ generated with this technique are not always consistent with those measured using a continuous culture under similar conditions (Boon et al., 1999a, Boon et al., 1999b).

To accommodate these problems a continuous technique (chemostat) or a fed-batch culture, where the substrate depletion is compensated, can be used. Unfortunately, the latter method is not suitable for bioleaching studies when the feed added to regenerate ferrous iron contains some chemical (reductant) that can interfere with the bacteria (Harvey and Crundwell, 1997).

2.2.4.3. Continuous Culture Technique (Chemostat)

In a continuous culture the microbial growth is maintained in the exponential growth phase (Fig. 2.12) for as long as possible by compensating the consumption of substrate with a permanent fresh feed and eliminating the metabolic products in a continuous overflow (Fig. 2.14). When steady state is reached the concentration of biomass and substrate remain constant. And the mass balance equations are written as follows:

- Biomass mass balance

$$\frac{dC_X}{dt} = -DC_X + \mu C_X - k_d C_X \tag{2.40}$$

$$\Rightarrow D = \mu \quad (at\ steady\ state\ and\ k_d \approx 0) \tag{2.41}$$

- Substrate mass balance

$$\frac{dC_X}{dt} = D C_S^0 - D C_S - \mu C_X \frac{1}{Y_{SX}^{max}} - m_S C_X \tag{2.42}$$

$$\Rightarrow C_X = \frac{D (C_S^0 - C_S)}{(D \frac{1}{Y_{SX}^{max}} + m_S)} \qquad at\ steady\ state \tag{2.43}$$

D is the dilution rate which is the flow rate F divided by the volume of the continuous culture V and C_S^0 the concentration of substrate in the feed.

From equation 2.43 the relation between D and C_X is plainly shown, so the growth of microorganisms C_X in a continuous culture can be controlled by adjusting the concentration of substrate in the feed C_S^0 and the dilution rate. If Monod kinetics (Eq. 2.27) apply the concentration of substrate in the culture medium C_S at steady-state, is a function of D only, i.e.

it does not depend on C_S^0 (Eq. 2.44). The dilution rate is used in continuous culture to set the ratio ferric to ferrous iron at a desired value. It can only vary in a certain range of values. When D becomes too large the culture will be washed out and as a result the concentration of the substrate in the feed becomes equal to its value in the overflow and no reaction takes place any more. This is why D should always be kept below its critical value.

$$C_S = \frac{K_S\, D}{\mu_{max} - D} \tag{2.44}$$

The continuous culture as a steady state technique is the most reliable experimental method for the study of ferrous iron bio-oxidation kinetics. However, this method is time-consuming and limited to high potentials (Boon et al., 1999b). The residence time $\frac{1}{D}$ for continuous cultures typically ranges from 10 to 150hours and steady state is only assumed after 3 residence times. Therefore, to generate a set of data at different residence times like in figure 2.14, where the residence time varied between 10 and 100h (Breed and Hansford, 1999), if one takes a step of 10 hours between two successive residence times it will take 450h (about 19days) (Eq. 2.45) and 1650h (about 2 months) (Eq. 2.46) to get 5 and 10 datapoints respectively.

$$\mathbf{\Delta t = 10*3 + 20*3 + 30*3 + 40*3 + 50*3 = 450h} \tag{2.45}$$

$$\mathbf{\Delta t = 10*3 + 20*3 + 30*3 + 40*3 + 50*3 + 60*3 + 70*3 + 80*3 + 90*3 + 100*3 = 1650h} \tag{2.46}$$

Therefore, there is a need to develop a faster method for ferrous iron bio-oxidation kinetics studies. The method that Boon et al. developed by terminating the feed of a continuous culture of *Acidithiobacillus ferrooxidans* thus changing it into a batch system cannot be unfortunately applicable to kinetic measurements with *Leptospirillum ferrooxidans* because its very short duration (couple of minutes for this case) will make it very inaccurate (Boon et al., 1999b).

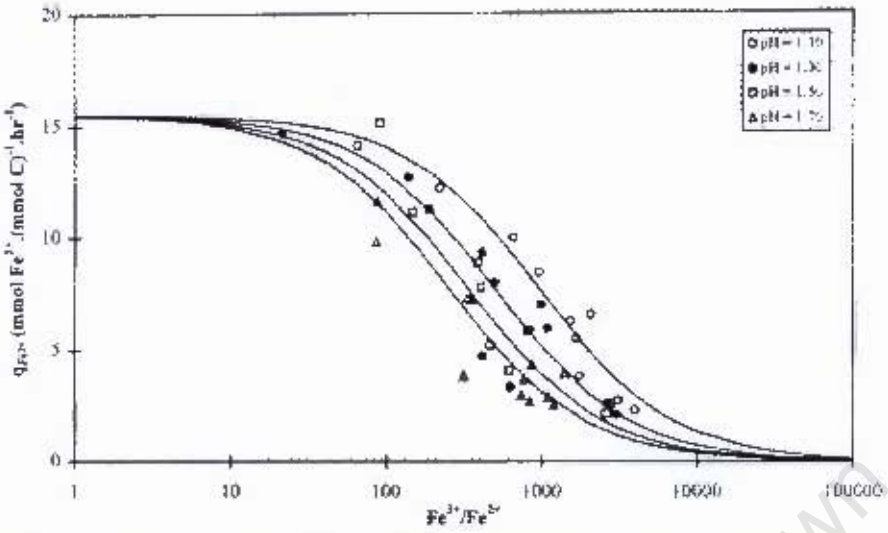

Figure 2.14: Actual experimental data from continuous culture for 0.01<D<0.1 (Breed and Hansford, 1999)

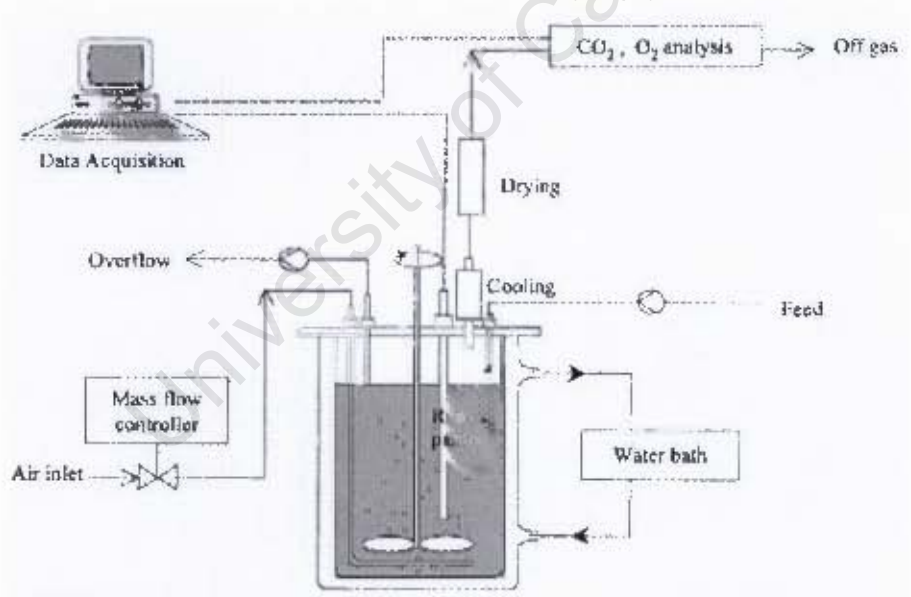

Figure 2.15: Schematic representation of a continuous culture bioreactor (Breed and Hansford, 1999)

Chapter 3. Experimental

3.1. Apparatus *(Anonymous, 2005)*

This work has used the Redostat™ device (Fig. 3.1) as the experimental tool for the measurement of the abiotic and biological oxidation kinetics of ferrous iron. The Redostat system is made up of 5 main components which are the Redostat controller, cell and components, waterbath, uninterruptible power supply, and stirrer motor.

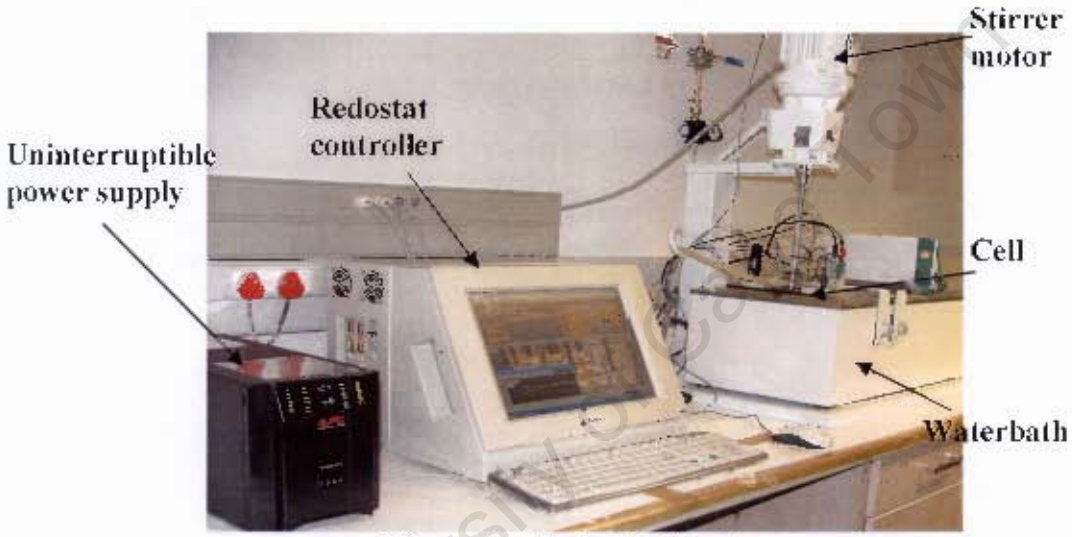

Figure 3.1: Redostat™ system

The Redostat™ cell is subdivided into two compartments, the working and counter compartments, separated by a cationic membrane (Fig. 3.2). The working compartment is that part of the Redostat cell where the oxidation of ferrous iron was taking place and the counter compartment only contained a solution of sulphuric acid which is indispensable for current flow between the cathode and anode. The volumes of the two solutions were 3.3 and 4 litres respectively. The volume of sulphuric acid solution in the counter compartment was larger because a higher level of liquid was required in the counter compartment to prevent the migration or diffusion of ions, due to the concentration gradient, from the working compartment to the counter compartment.

The solution of ferrous iron was agitated by a 90 degrees blade impeller powered by an electric motor spinning at a maximum speed of 500rpm. The air inlet was arranged at the end of the impeller shaft to insure an even distribution of the compressed air blown into the solution. The air flowrates varied between 300 and 450ml/min for the abiotic and biological oxidation of ferrous iron.

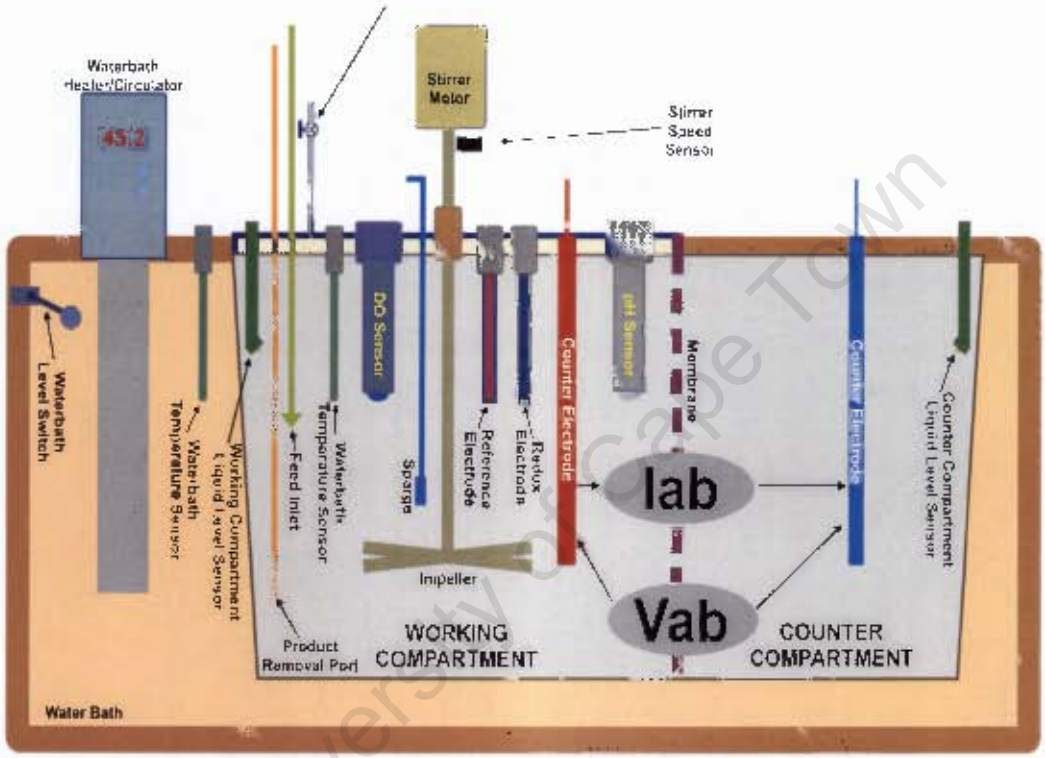

Figure 3.2: Schematic representation of the Redostat™ cell

The working compartment is equipped with different types of probes for easier monitoring of the experiments (Fig. 3.2). All the experimental conditions are displayed numerically or graphically on the controller screen throughout the all experiments (Fig. 3.3). A waterbath is used to heat up the cell to the desired temperature which was measured to one decimal place by the working compartment temperature probe. The biological oxidation of ferrous iron was studied at 35°C whilst the abiotic oxidation was studied at 41.4, 51, 60 and 68°C respectively.

Two liquid level sensors, one for the working compartment and the other for the counter compartment, helped monitor the levels of the two solutions to prevent any unexpected solution dry out which can be detrimental for the experiments and the equipment itself. A

condenser maintained at 2°C by a cooler was mounted at the off gas port of the working compartment in order to reduce to a minimum the loss of solution by evaporation.

The pH of the reacting ferrous iron solution was continuously measured online with a Hanna HI 61014 pH electrode.

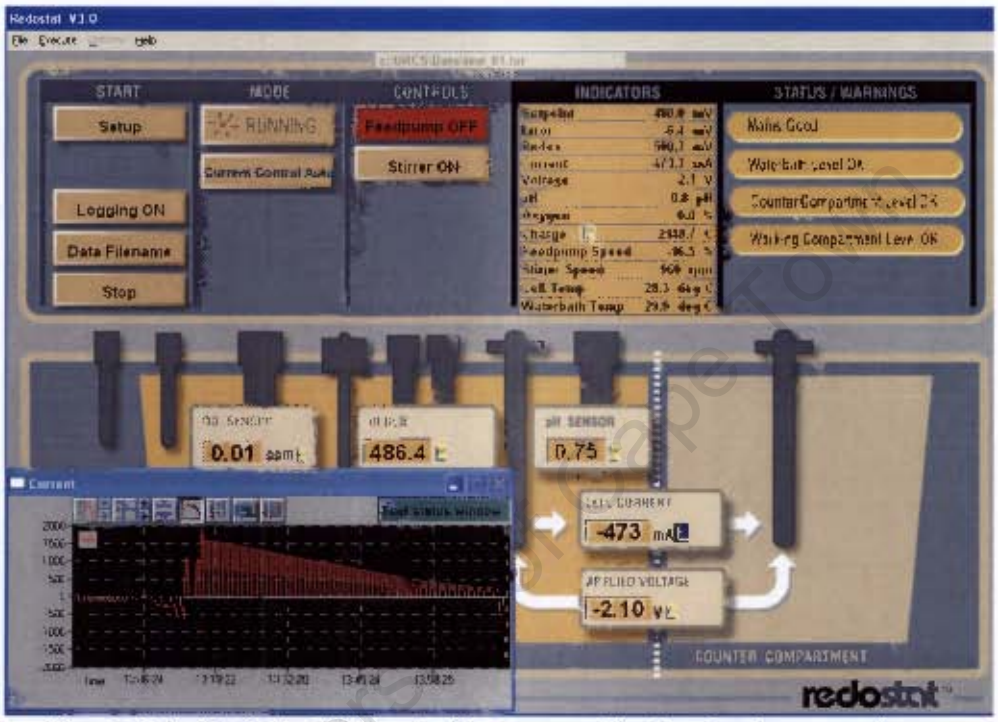

Figure 3.3: Redostat™ Controller screen display during experiment

The solution redox potential was also measured online by using a Metrohm 6.0301.100 platinum electrode and a Metrohm 6.0726.107 silver-silver chloride reference electrode. A calibration of these electrodes showed that there is a linear relationship between the redox potential measured and the logarithm of ferric to ferrous iron ratio (Fig. 3.4) according to the Nernst equation (Eq. 3.1). The redox potential was kept constant within a range of +2mV and +4mV from the setpoint, which is considered acceptable, for all the abiotic and biological oxidation of ferrous iron experiments respectively.

$$E = E_0 + \frac{R\,T}{F} \ln \frac{[Fe^{3+}]}{[Fe^{2+}]} \qquad (3.1)$$

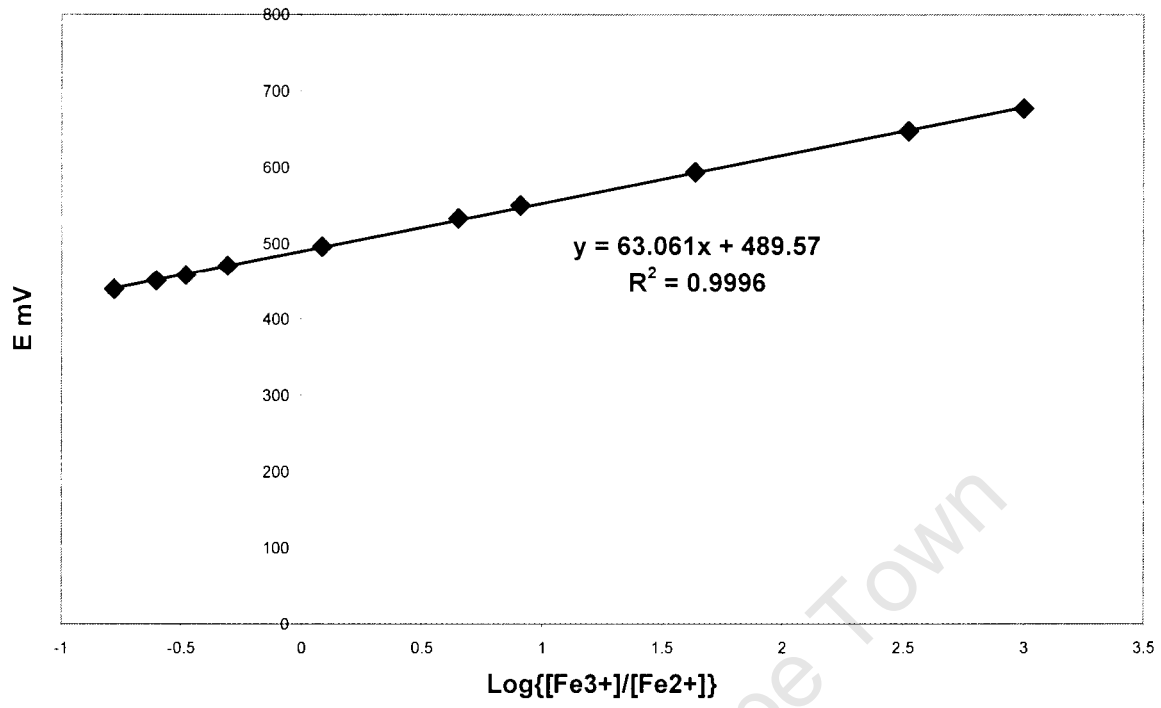

Figure 3.4: Redox probes calibration curve at 35°C and pH 1.3

The fundamental redox potential control in the Redostat™ device is achieved through reducing electrolytically at the cathode the ferric ions generated by the oxidation of ferrous iron (Eq. 3.2) and at the anode in the counter compartment water is decomposed so that the resulting protons can migrate as an electrolytic current to the working compartment through the cationic membrane to ensure electric neutrality (Eq. 3.3).

$$2Fe^{3+} + 2e^{-} \rightarrow 2Fe^{2+} \qquad cathodic \quad reduction \tag{3.2}$$

$$H_2O \rightarrow 2H^{+} + \frac{1}{2}O_2 + 2e^{-} \qquad anodic \quad oxidation \tag{3.3}$$

$$2Fe^{3+} + H_2O \rightarrow 2Fe^{2+} + 2H^{+} + \frac{1}{2}O_2 \tag{3.4}$$

Theoretically, protons generated by the decomposition of water should replace the protons consumed in the working compartment by the oxidation of ferrous iron (Eq. 2.2) and thus keeping the pH constant. The cathodic and anodic half reactions can be replaced by one

reaction (Eq. 3.4) which is the opposite of the ferrous iron oxidation reaction (Eq. 2.2). Therefore, the Redostat™ system reverses equation 2.2 to maintain the redox potential constant.

The intensity of the electrolytic current "I" applied by the Redostat™ device is directly proportional to the difference between the setpoint value and the actual value of the redox potential, the so-called redox potential error, the control gain, and inversely proportional to the deadband. In the present study the Redostat™ device was operated at its maximum control gain of 200 to get the greatest current possible for a better control of ferrous and ferric iron concentrations. Poor results were obtained at lower control gains, especially for the biological oxidation of ferrous iron experiments since this reaction is much faster. The deadband is the interval between the redox potential setpoint value and the actual redox potential value where the Redostat™ controller applies no current into the cell. A deadband of 0 to 0.2mV wide was used in our experiments in order to maintain better control of the redox potential.

The Redostat™ current is applied automatically and periodically every time that the redox potential error measured by the Redostat™ controller is greater than the deadband.

The Redostat™ timebase counter gives the duration of one current cycle. It varies from zero to 100 counts and one count or base clock is equivalent to a specific length of time. The base clock used for the present study was 500ms. This time is limited by the communications between internal measurement and control components. During a cycle the current is switched on and off and the redox potential is measured when the current is interrupted and the solution homogenized. All these operations are done automatically by the Redostat™ controller.

For the abiotic oxidation of ferrous iron, a timebase counter of 50 counts or 25s was used (Fig. 3.5). Then, the current was on for the first 20 counts or 10s and between the 20^{th} count and the 40^{th} count the current was off. It was switched on again at the 40^{th} and stayed on for the rest of the cycle. The redox potential was measured at the 30^{th} count or 15^{th} s of each cycle after the solution was homogenized for 10counts or 5s. Thus, for a current cycle of 25s, the current was applied for 15s only and the remaining 10s were used for solution homogenization and redox

potential measurement. This setting is equivalent to 14.4 hours of current application and 9.6 hours of current interruption per day.

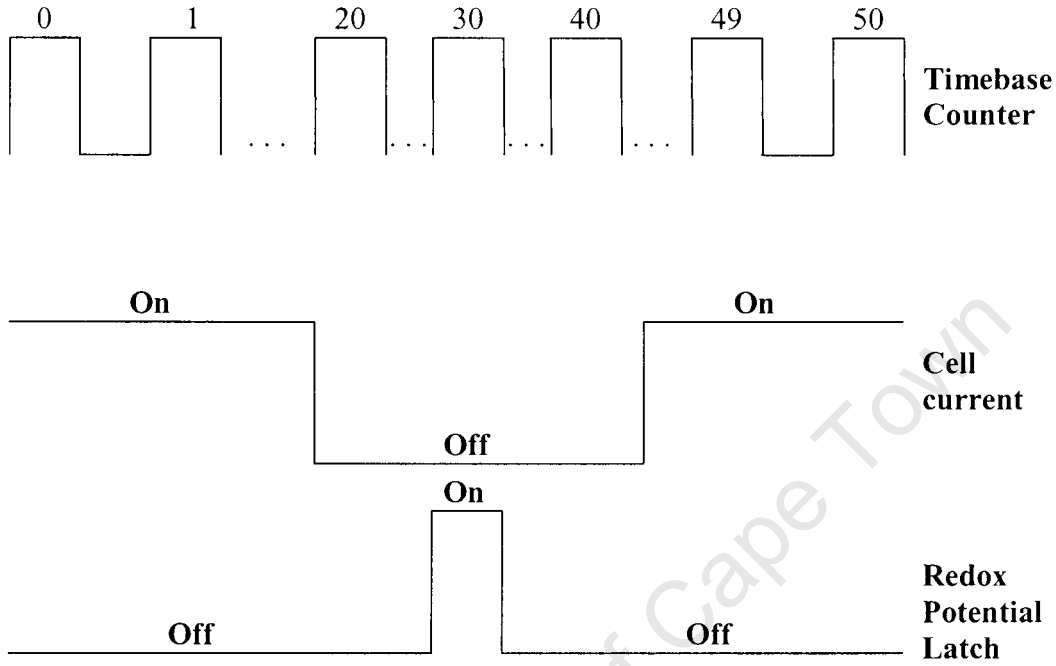

Figure 3.5: Redostat™ current cycle

The Redostat™ setting was changed to 100 counts and the period of current interruption shortened to 15 counts rather than 20 counts for the biological oxidation of ferrous iron. This was done to allow reduction of more ferric ions per cycle than it could be done with the previous setting, as the biological oxidation of ferrous iron is much faster than the abiotic oxidation. Then, the current was on for the first 20 counts or 10s and off between the 20^{th} and the 35^{th} count. It was switched on again at the 35^{th} count for the remainder of the cycle. The redox potential was still measured at the 30^{th} count or 15^{th} s of each cycle. For this new setting, the current was applied for 85 counts or 42.5s and interrupted for 7.5s when the solution was homogenized and the redox potential measured. This is equivalent to 20.4 hours of current application and 3.6 hours of current interruption a day.

The experimental conditions or data such as temperature, pH, current "I", integrated charge, etc., for each experiment were automatically saved in a text file which could be easily read into an Excel spreadsheet. The Redostat™ system was connected to an uninterruptible power supply to prevent any data loss due to any unexpected power failure.

3.2. Chemicals and Microorganism

Analytical-grade reagents were used for all the experiments. For the abiotic oxidation of ferrous iron, solutions 0.21M $FeSO_4.7H_2O$ adjusted at pH below 0.6 with 98% H_2SO_4 were used. Different concentrations of ferrous iron were then obtained by oxidising ferrous iron with the Redostat™ current. Once the desired concentration of ferrous iron was achieved, the experiment was then carried out at constant redox potential or ferrous iron concentration. At pH 1.1 another approach was used to get different concentrations of ferrous iron without producing much ferric iron since it was difficult to control the redox potential at high pH and concentration of ferric iron (>2g/l) due to jarosite precipitation. Each experiment was then started with a lower concentration of $FeSO_4.7H_2O$ of about 0.11M and this was gradually increased by staged addition of $FeSO_4.7H_2O$ until a final concentration of ferrous iron of about 0.21M was obtained (Tables A.2-A.5 in appendix A). After each addition of $FeSO_4.7H_2O$, which corresponded to a new ferrous iron concentration, the Redostat™ device was run at constant potential to generate kinetic data. Small amounts of $Fe_2(SO_4)_3$ .xH_2O were occasionally used for this second approach.

A strain *Leptospirillum ferriphilum* from Gamsberg (South Africa) was used for the biological oxidation of ferrous iron experiments. The ferrous iron growth media were inoculated with 10% v/v inoculums obtained from a continuous culture of *Leptospirillum ferriphilum* growing on ferrous iron. The growth media consisted of 5g/l Fe^{2+} got from $FeSO_4.7H_2O$, 1.11g/l K_2SO_4, 0.53g/l $(NH_4)_2HPO_4$, 1.83g/l $(NH_4)_2SO_4$ and 10ml/l Vishniac trace element solution (Vishniac et al., 1957) adjusted to pH 1.2 using 98% H_2SO_4. This growth medium composition was determined in previous studies with *Leptospirillum* species (Breed and Hansford, 1999; Dempers et al., 2003). As for the abiotic oxidation, different ferric to ferrous iron ratios were obtained by oxidising ferrous iron with the Redostat™ current prior to inoculation. It is worth

noting that an independent experiment was carried out for each ferric to ferrous iron ratio. No attempt was made to maintain sterile conditions.

3.3. Experimental Methods

This study was based on the comparison of the kinetic measurements of ferrous iron oxidation using the Redostat™ current with other recognized experimental methods such as the batch method and the off-gas analysis method in order to validate the Redostat system as a faster and more controllable experimental tool for the study of ferrous iron biological oxidation kinetics.

3.3.1 Redostat™ Current

Since the Redostat current "I" is used to reduce the ferric ions produced by the oxidation of ferrous iron in order to maintain the concentrations of ferrous and ferric iron constant, the oxidation rate of ferrous iron $-r_{Fe^{2+}}$ (Eq. 2.2) is equal to the rate of electrolytic reduction of ferric iron $-r_{Fe^{3+}}$ (Eq. 3.4) at steady state, providing that ferric iron precipitation and hydrogen evolution are negligible. $-r_{Fe^{3+}}$ is given by equation 3.5 which is derived from the Faraday equation.

$$-r_{Fe^{3+}} = -r_{Fe^{2+}} = -\frac{dQ}{dt} * \frac{1}{96500 * V} \qquad [mol.l^{-1}.s^{-1}] \tag{3.5}$$

$$\frac{dQ}{dt} = -I \tag{3.6}$$

Q is the amount of charge required to reduce a certain mass of ferric iron and V is the working volume of the Redostat™ cell.

The current "I" (Eq. 3.6) is a constant in the case of abiotic oxidation of ferrous iron at steady state since $-r_{Fe^{2+}}$ does not change at steady state. Thus, "I" is calculated by dividing the amount of charge consumed ΔQ to keep the concentration of ferrous iron constant by the interval of time Δt required to complete the experiment.

For the biological oxidation of ferrous iron "I" is a variable since $-r_{Fe^{2+}}$ increases with the increasing microbial population and "I" is calculated as the first derivative of the charge consumed Q with respect to time "$-\frac{dQ}{dt}$". The function $Q = f(t)$ was obtained by polynomial interpolation of the Q versus time data which were automatically recorded by the Redostat™ controller for each run. These data were fitted with a polynomial function since the rate of ferrous iron biological oxidation is an exponential function that can be expanded as a polynomial function according to the Maclaurin series (Eq. 3.7).

$$f(x) = \sum_{n=0}^{\infty} \frac{f^{(n)}(0)}{n!} x^n = f(0) + \frac{f'(0)}{1!} x + \frac{f''(0)}{2!} x^2 + \ldots \qquad \text{(Eq. 3.7)}$$

where f(x) is a function of x and $f^{(n)}$ its nth derivative with respect to x

3.3.2. Batch Method

This method was used for the abiotic ferrous iron oxidation kinetics study only. It consisted of oxidising ferrous iron in the Redostat™ cell without any control of the redox potential of the solution like in an ordinary batch reactor and determining the concentration of ferrous iron with time. The kinetic data obtained in this way was then analysed using the integral method of analysis. This method consists of guessing a particular form of rate equation and, after appropriate integrations and mathematical manipulations, predicting that the plot of a certain concentration function versus time should yield a straight line (Levenspiel, 1972). For a first order kinetic equation, $-\ln[Fe^{2+}]$ versus time is a straight line (Fig. 3.6) as shown by equation 3.8 and for a second order kinetic equation, $\frac{1}{[Fe^{2+}]}$ versus time is also a straight line (Fig. 3.7) as shown by equation 3.9. Equations 3.8 and 3.9 can be easily derived from the differential first and second-order rate equations of ferrous iron abiotic oxidation (Levenspiel, 1972). $[Fe^{2+}]_0$ and $[Fe^{2+}]$ are the concentrations of ferrous iron at times zero and t respectively.

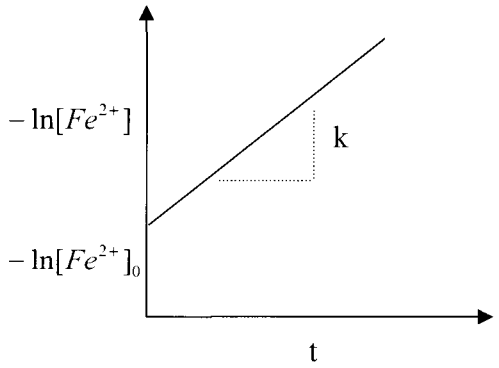

Figure 3.6: First-order kinetic equation plot

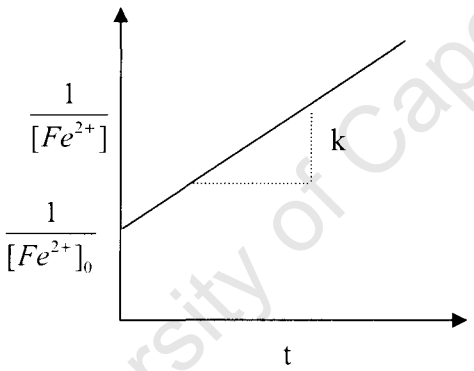

Figure 3.7: Second-order kinetic equation plot

$$-\ln[Fe^{2+}] = k\ t - \ln[Fe^{2+}]_0 \tag{3.8}$$

$$\frac{1}{[Fe^{2+}]} = k\ t + \frac{1}{[Fe^{2+}]_0} \tag{3.9}$$

Therefore, the rate of ferrous iron oxidation was calculated by using the kinetic constant k in the correct kinetic equation of ferrous iron oxidation which were both obtained from the integral analysis of batch data.

3.3.3. Off-gas Analysis Method

The concentrations of oxygen and carbon dioxide in the feed and the off-gas of the Redostat™ device were measured with a Hartmann & Braun Advance Optima Magnos 6 paramagnetic oxygen analyzer and a Hartmann & Braun Advance Optima Uras 4 nondispersive infrared carbon dioxide analyzer respectively. The oxygen analyzer uses the paramagnetic behaviour of oxygen, i.e. the characteristic of oxygen molecules to be drawn into areas of higher field strength in a nonhomogeneous magnetic field, for the measurement of oxygen concentration whilst the carbon dioxide analyzer uses the infrared radiation absorption of CO_2 (Lamber-Beer law) for the measurement of CO_2 concentration. These concentrations were measured offline using samples collected in an inflatable bag for the abiotic oxidation of ferrous iron and online for the biological oxidation of ferrous iron.

CO_2 and O_2 concentrations are used for the determination of the rates of oxygen and carbon dioxide consumptions (Eq. 3.11-3.12). These rates are necessary for the determination of ferrous iron oxidation rate (Eq. 2.14), biomass growth rate, and biomass specific growth rate.

Based on the stoichiometry of the oxidation of ferrous iron (Eq. 2.2) the rate of ferrous iron abiotic oxidation can be determined in term of oxygen consumption rate as follow:

$$-r_{Fe^{2+}} = -4r_{O_2} \tag{3.10}$$

The rate of oxygen consumption is given by:

$$-r_{O_2} = \frac{\Phi_{in}[O_2]_{in} - \Phi_{out}[O_2]_{out}}{V} \tag{3.11}$$

Φ_{in} and Φ_{out} are the flow rates [mol / unit time] of the feed air and the off gas respectively. $[O_2]_{in}$ and $[O_2]_{out}$ are the concentrations (molar fractions) of oxygen in the feed and off gases respectively and V is the Redostat™ cell volume.

For the biological oxidation of ferrous iron, equation 3.9 becomes equation 2.14 as this reaction is accompanied with carbon dioxide consumption. Omitting the rate of carbon dioxide consumption in equation (2.15) causes an error of about 5% in the calculation of the rate of

ferrous iron biological oxidation (Boon, 1996, Boon et al., 1998). The rate of carbon dioxide consumption is given by:

$$-r_{CO_2} = \frac{\Phi_{in}[CO_2]_{in} - \Phi_{out}[CO_2]_{out}}{V} \tag{3.12}$$

$[CO_2]_{in}$ and $[CO_2]_{out}$ are the concentrations (molar fractions) of carbon dioxide in the feed and off gases respectively. The flow rate of the reference gas was determined by using a bubble flow meter and that of the off gas was obtained by using either the nitrogen balance (Eq. 3.13) (Boon, 1996) or a bubble flow meter.

$$\Phi_{out} = \Phi_{in} * \frac{1-[O_2]_{in}-[CO_2]_{in}}{1-[O_2]_{out}-[CO_2]_{out}} \tag{3.13}$$

The biomass specific growth rate μ was determined using equation (3.17) which can be derived from equations 2.36 as shown below.

The derivative of both sides of equation (2.36) with respect to time gives:

$$\frac{dr_x}{dt} = \mu \frac{dC_x}{dt} \tag{3.14}$$

$$\frac{dC_x}{dt} = r_x = -r_{CO_2} \quad \text{(Boon, 1996, Boon et al., 1997)} \tag{3.15}$$

Then $$\frac{d(-r_{CO_2})}{dt} = -\mu\, r_{CO_2} \quad \Rightarrow \quad \frac{d(-r_{CO_2})}{-r_{CO_2}} = \mu\, dt \tag{3.16}$$

The integration of both sides of equation (3.16) gives:

$$-r_{CO_2} = -r^0_{CO_2} e^{\mu t} \tag{3.17}$$

According to equation 3.17 the biomass specific growth rate μ is the power coefficient of the exponential function of biomass growth rate versus time.

3.4. Experimental Procedures And Analytical Method

3.4.1. Abiotic Oxidation Of Ferrous Iron Experiments At Very Low pH

Solutions of 12 g/L of ferrous iron were prepared by dissolving 209.11g of $FeSO_4.7H_2O$ in 3.5L of distilled water and the pH was adjusted below 0.6 using 98% H_2SO_4. Solutions of sulphuric acid were also prepared at a pH of 1.2 by diluting a 98% H_2SO_4 solution with distilled water and they were meant to be used in the counter compartment of the Redostat™ cell. Once the solutions were prepared the next steps were carried out as follow:

1. 3.3L of ferrous iron solution and 4L of sulfuric acid solution, prepared as mentioned above and measured with a 2 liters measuring cylinder, were used in the working compartment and counter compartment respectively. A larger volume of solution was used in the counter compartment because a higher level of liquid is required in that compartment to prevent diffusion of ions from the working compartment to the counter compartment due the concentration gradient

2. The Temperature of the Redostat™ cell was set at 60°C by using a waterbath in which the Redostat™ cell sits

3. Compressed air was blown into the working compartment at a flow rate of 300 to 320ml/min which was measured with a bubble flowmeter

4. The solution of ferrous iron in the working compartment was agitated at a speed of 500rpm by a vertical blade impeller powered by an electric motor to facilitate, dispersion of dissolved components and ensure solution homogeneity

5. Once the solution reached the working temperature of 60°C, the Redostat™ device was set to run at constant potential under automatic redox control mode. Each run was characterized by a given concentration of ferrous iron, and different concentrations of ferrous iron needed for the Redostat™ current and off-gas analysis methods were obtained by oxidizing ferrous iron with the Redostat™ current. It can be seen from figure 3.4 that different ferric to ferrous iron ratios can be achieved by simply changing the Redostat™ redox potential setpoint value and thus forcing the Redostat™ device to oxidize or reduce ferrous or ferric iron until the desired Redox potential is achieved

6. The concentration of ferrous iron was measured by titration with a $K_2Cr_2O_7$ solution at steady state for each run

7. Experimental measurements were done at steady state when the temperature, pH, and redox potential were constant. For the Redostat™ current method the necessary data, integrated charge Q versus time, were automatically recorded every 63s by the Redostat™ controller throughout each run. For the off-gas analysis method, a sample of the Redostat™ off-gas was collected with an inflatable bag and analyzed with the gas analyzer to determine the concentration of CO_2 and O_2 for each run. The feed air was analyzed online. For the batch method, the Redostat™ device was run under uncontrolled mode like an ordinary batch reactor with the same solution of ferrous iron used for the two other methods, and the concentration of ferrous iron was titrated at different times as it was decreasing. It is worth noting here that the batch method was carried out last and the concentration of ferrous iron was brought back to its initial value of 12 g/L by using the Redostat™ current before the start of the batch method. The kinetic data obtained were then processed as described in section 3.3.

This approach used here to get different concentrations of ferrous iron by oxidizing ferrous iron is not an easy one, since it produces ferric iron which starts to precipitate as jarosite (Eq. 3.18 (Daoud et al., 2006)) once its concentration exceeds a certain value (>2g/L). When this happens, it becomes difficult to operate the Redostat™ device at a constant potential, since the

potential starts dropping instead of increasing and thus ruining the experiment. Reliable results were only obtained at very low pH (<0.6) where ferric iron precipitation is minimized. For higher pH values a second approach was used where ferric iron precipitation was kept to a minimum by minimizing the concentration of ferric iron in solution.

$$3Fe^{3+} + M^{+} + 2HSO_4^{-} + 6H_2O \rightarrow MFe_3(SO_4)_2(OH)_6 \downarrow + 8H^{+} \quad (3.18)$$

$$M^{+} = K^{+}, Na^{+}, NH_4^{+}, or\ H_3O^{+}$$

3.4.2. Abiotic Oxidation Of Ferrous Iron Experiments At pH 1.1

Another approach was used for the abiotic oxidation of ferrous iron experiments, since the first one was significantly affected by jarosite precipitation if the pH is not set to the right value. This new approach consisted of keeping the concentration of ferric iron to a minimum to minimize ferric iron precipitation. A solution of lower concentration of ferrous iron of about 6g/L (0.11M) was firstly prepared for each experiment by dissolving $FeSO_4.7H_2O$ in distilled water and the pH was adjusted at 1.1 using 98% H_2SO_4 and the solution of sulfuric acid at pH 1.2 to be used in the counter compartment was also prepared as indicated previously. Once the two solutions were prepared the next steps were carried out as follow:

1. 3.3L of the ferrous iron solution and 4L of the sulfuric acid solution, measured with a 2 liters measuring cylinder, were used in the working compartment and counter compartment respectively. Each run was characterised by a given ferrous iron concentration which was kept constant by setting the Redostat™ device under automatic redox potential control mode once the working temperature was reached. The first run at a particular temperature was carried out with the solution of lower concentration of ferrous iron mentioned above. Different concentrations of ferrous iron for the following runs were then obtained by adding more and more $FeSO_4.7H_2O$ into the initial solution. At each temperature 4 to 5 runs were carried out (Tables A.2-A.5 in appendix A).

2. The Temperature of the Redostat™ cell was set at 41.4, 51, 60, and 68°C respectively by using a waterbath in which the Redostat™ cell sits

3. Compressed air was blown into the working compartment at a flow rate of 300 to 320ml/min which was measured with a bubble flowmeter

4. The solution of ferrous iron in the working compartment was agitated at a speed of 500rpm by a right blade impeller powered by an electric motor to facilitate dissolved components diffusion and ensure solution homogeneity

5. The concentration of ferrous iron was measured by titration with a $K_2Cr_2O_7$ solution at steady state for each run

6. Experimental measurements were done at steady state when the temperature, pH, and redox potential were constant. For the Redostat™ current method the necessary data, integrated charge Q versus time, were automatically recorded by the Redostat™ controller throughout each run. For the off-gas analysis method, a sample of the off-gas was collected with a balloon and analyzed with the gas analyzer to determine the concentration of CO_2 and O_2 for each run. The feed air was analyzed online. For the batch method the Redostat™ device was run under uncontrolled mode like an ordinary batch reactor with the same solution of ferrous iron used for the two other methods and the concentration of ferrous iron was titrated at different times as it was decreasing with time. The kinetic data obtained were then processed as described in section 3.3.

5g of $Fe_2(SO_4)_3 .xH_2O$ (≈1g/l Fe^{3+}) were added to 3.3L of the initial solution of lower concentration of ferrous iron for the experiments carried out at 51, 60, and 68°C, as it was unsure if the Redostat™ device can perform well without a considerable concentration of ferric iron. It was later found that the performance of the Redostat is not affected by the amount of ferric iron present in solution, since the experiment carried out at 41.4°C without any ferric iron added to the initial solution yielded similar results. It is worth noting that ferric iron was

also produced by the oxidation of ferrous iron and some of it was accumulated during the first phase of each experiment where the Redostat™ device was operated without any redox potential control because the working temperature was not achieved yet. Ferric iron might have also come from impurities of the chemicals used since no chemical is 100% pure. Although ferric iron was present in the solutions used, its concentration was kept to a minimum by only using $FeSO_4.7H_2O$ to change the concentration of ferrous iron required for different runs.

3.4.3. Biological Oxidation of Ferrous Iron Experiment

For the biological oxidation of ferrous iron experiment growth media of the following composition were prepared: 5g/L Fe^{2+} from $FeSO_4.7H_2O$, 1.11g/L K_2SO_4, 0.53g/L $(NH_4)_2HPO_4$, 1.83g/L $(NH_4)_2SO_4$ and 10ml/L Vishniac trace element solution (Vishniac et al., 1957) adjusted to pH 1.2 using 98% H_2SO_4. This growth medium composition as mentioned earlier was established in previous studies with *Leptospirillum* species (Breed and Hansford, 1999; Dempers et al., 2003). Once the growth medium was prepared the next steps were carried out as follows:

1. 4L of sulphuric acid solution at pH 1.2 prepared as in the two previous cases and 3.3L of the growth medium, measured with a 2 liters measuring cylinder, were used in the counter and working compartments respectively

2. The Redostat™ cell was set at 35°C by using a waterbath in which it sits

3. Compressed air was blown into the working compartment at a flow rate of 446.4ml/min which was measured with a bubble flowmeter

4. The solution of ferrous iron in the working compartment was agitated at speed of 500rpm by a right blade impeller powered by an electric motor to facilitate dissolved components diffusion and ensure solution homogeneity

5. Once the solution reached the working temperature of 35°C the Redostat™ was set to run at a constant potential under automatic redox control mode. The growth medium was then inoculated with 330 ml of a *Leptospirillum ferriphilum* inoculum obtained from an exponentially growing continuous culture of *Leptospirillum ferriphilum*. An equivalent volume of 330ml of the growing medium was removed from the working compartment before inoculation in order to keep a working volume of 3.3liters in the working compartment. Each run was characterized by a given ferric to ferrous iron ratio, and different ferric to ferrous iron ratios were obtained by oxidizing ferrous iron with the Redostat™ current prior to inoculation. It can be seen from figure 3.4 that different ferric to ferrous iron ratios can be achieved by simply changing the Redostat™ redox potential setpoint value and thus forcing the Redostat™ device to oxidize or reduce ferrous or ferric iron until the desired Redox potential is reached

6. The concentrations of ferrous and total iron were measured by titration with a $K_2Cr_2O_7$ solution at steady state for each run

7. Experimental measurements were done at steady state when the temperature, pH, and redox potential were constant. For the Redostat™ current method the necessary data, integrated charge Q versus time, were automatically recorded every 63s by the Redostat™ controller throughout each run. For the off-gas analysis method, the concentrations of oxygen and carbon dioxide were measured online logged on a computer every half an hour throughout each run. The kinetic data were then processed as indicated in section 3.3.

3.4.4. Analytical Method

The ferrous iron concentration was determined by titration with potassium dichromate 0.025 or 0.05N. The concentration of Ferric iron was calculated as the difference between the total iron concentration and the ferrous iron concentration (Eq. B.3 in appendix B). To get the total iron concentration, all the ferric ions were reduced to ferrous iron with stannous chloride prior to the titration with potassium dichromate. Potassium dichromate solutions were prepared using

distilled water and dry mass of potassium dichromate which was kept in the oven. Barium diphenylamine sulphonate was used as the indicator. The analytical procedure is given in appendix B.

Chapter 4. Results and Discussion

Two series of experiments were carried out with the Redostat™ system in order to assess its performance as a more controllable and faster experimental tool for the study of ferrous iron biological oxidation kinetics comparatively to ordinary batch and continuous cultures. These experiments consisted of oxidizing ferrous iron in the presence and absence of *Leptospirillum ferriphilum*. Kinetic data were generated with the Redostat™ current and two other recognized experimental methods viz., the batch method (abiotic oxidation only) and the off-gas analysis method. These kinetic data were compared and interpreted in the light of the relevant literature review compiled for this work.

4.1. Abiotic Ferrous Iron Oxidation

All the abiotic ferrous iron oxidation experiments were carried out at pH below 2, where it has been shown that the pH has a negligible effect on the kinetics (Tamura et al., 1976; Chmielewski and Charewicz, 1984). The concentration of dissolved oxygen was assumed to be constant and equal to its saturation value for each experiment since the rate of the abiotic oxidation of ferrous iron is very small at the pH and temperatures used in this present study. This assumption can be scientifically supported by considering equation 4.1 which is the oxygen mass balance equation at steady state. When the rate of ferrous iron oxidation $-r_{Fe^{2+}}$ is small the right hand side of equation 4.1 becomes small as well and this situation can suggest that the concentration of dissolved oxygen is almost equal to its saturation value C^* since the other terms of the equation are constant for a given temperature and oxygen partial pressure (see Appendix C for C* and C_{O2} calculation).

$$k_L a\,(C^* - C_{O_2}) = -\frac{1}{4}\, r_{Fe^{2+}} \tag{4.1}$$

$$C^* \approx C_{O_2} \Leftrightarrow -r_{Fe^{2+}} \text{ is small} \tag{4.2}$$

where k_La is the oxygen mass transfer coefficient, C^* the concentration of dissolved oxygen at saturation, and C_{O_2} the actual concentration of dissolved oxygen.

Therefore, under these conditions the rate equation of the abiotic oxidation can be written as a function of ferrous iron concentration only (Eq. 4.3).

$$-r_{Fe^{2+}} = k\,[Fe^{2+}]^a \tag{4.3}$$

where k is a constant, and a the kinetic order with respect to ferrous iron.

4.1.1. Oxidation at very low pH

The pH was primarily kept below 0.6 to minimize jarosite precipitation (Eq. 3.18) which is strongly dependent on the pH, ferric iron concentration, temperature and some other ions concentrations such as K^+, NH_4^+, and Na^+ concentrations (Daoud et al., 2006).

The rates of ferrous iron oxidation measured as indicated in section 3.3 were analyzed to see if they are consistent with equation 4.3, which suggests that $\ln(-r_{Fe^{2+}})$ versus $\ln[Fe^{2+}]$ should yield a straight line whose slope is equal to "a" and offset equal to $\ln k$ (Eq. 4.4).

$$\ln(-r_{Fe^{2+}}) = \ln k + a\ln[Fe^{2+}] \tag{4.4}$$

A linear interpolation of the of the Redostat™ current and off-gas data shows that they are in good agreement with equation 4.4, which was derived from the ferrous iron oxidation rate equation (Eq. 4.3), since the corresponding R^2 are close to 1 (Fig. 4.1). The consistency of the batch data reported in figure 4.1 can not be examined with equation 4.4 since they have been calculated by using equation 4.3 where k and "a" had been determined a priori with the integral method as indicated in section 3.3.2.

The consistency of the batch data was examined by using the integral method of analysis which is explained in section 3.3.2. It was found that these data verify the first-order kinetic

equation of ferrous iron oxidation, which suggests that $-\ln[Fe^{2+}]$ versus time is a straight line (Eq. 4.5), since the R^2 obtained is close to 1 (Fig. 4.2).

$$-\ln[Fe^{2+}] = k\,t - \ln[Fe^{2+}]_0 \qquad (4.5)$$

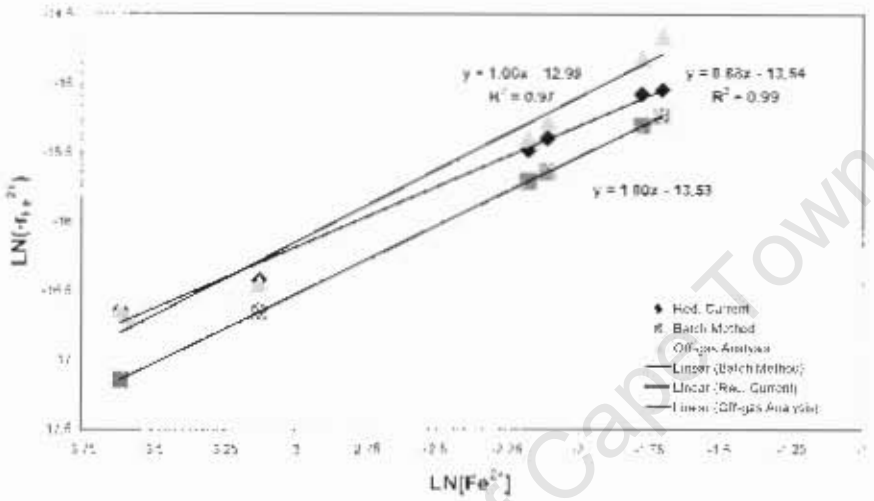

Figure 4.1: Ferrous iron oxidation rate at 60°C, pH < 0.6, and 0.21M of total iron

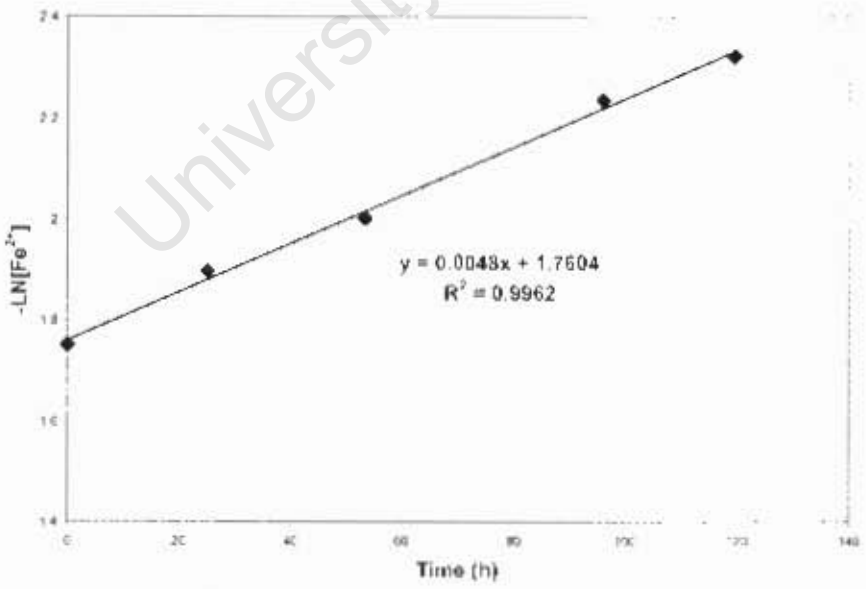

Figure 4.2: Batch kinetic data of the ferrous iron oxidation at 60°C, pH<0.6, and $[Fe]_{total}$~0.21M

A first-order kinetic equation with respect to ferrous iron was found with all the three methods (Table 4.1). This first order kinetics with respect to ferrous iron was obtained because of chloride ions contamination caused by leakage from the reference electrode, which was filled with 3M lithium chloride electrolyte. A number of researchers have shown that in the presence of complexing anions such as Cl^- the rate of ferrous iron oxidation by oxygen in aqueous sulphuric acid solution is described by a first order kinetic equation (Chmielewski and Charewicz, 1984). After fixing the leakage problem (which resulted from the height of the electrolyte in the electrode) the order of the reaction was no longer unity as it will be shown in the following section.

Table 4.1
Ferrous iron oxidation kinetic data at 60°C, pH<0.6, and $[Fe]_{total}$=0.21M

	Off-gas Analysis Method	Redostat Current Method	Batch Method
k (s^{-1})	$2.29x10^{-06}$	$1.32x10^{-06}$	$1.33x10^{-06}$
a	1.06	0.88	1
R^2	0.974	0.989	0.9962

The kinetic constant calculated with the Redostat current is in excellent agreement with the one calculated by using the batch method (Table. 4.1). The off-gas analysis method generated a kinetic constant which is greater than the other two. The small variation between the feed air and the off-gas oxygen concentrations caused by the slow rate of the abiotic oxidation of ferrous iron can be the reason why the off-gas analysis kinetic data are not similar to the ones obtained with the Redostat™ current and batch methods. The kinetic constants were determined by plotting equation 4.4 (Fig. 4.1) for the Redostat™ current and Off-gas analysis methods. For the batch method equation 4.5 was plotted (Fig. 4.2) for the determination of k according to the integral method of analysis of batch kinetic data.

The batch method was used as a reference for the calculation of the Redostat™ current efficiency η, which is the fraction of the Redostat current that actually reduces ferric ions, since it is an accurate and more direct method comparatively to the off-gas analysis method. η was then calculated by dividing the rate of ferrous iron oxidation obtained from the batch method

$-r_{bm}$ by the rate of ferrous iron oxidation calculated with the Redostat™ current $-r_I$ ($-r_I = -r_{Fe^{3+}}$). It can be seen from figure 4.1 that $-r_I$ is greater than $-r_{bm}$ and this suggests that more current was used than what was required to reduce ferric iron in order to keep the redox potential constant. Therefore, a current efficiency of about 80% was calculated (Table A.1 in appendix A). This situation can be the result of hydrogen evolution at the cathode (Eq. 4.6) which thus consumes a fraction of the Redostat™ current "I".

$$H^+ + e^- \rightarrow \frac{1}{2} H_2 \uparrow \tag{4.6}$$

4.1.2. Oxidation in presence of low concentration of ferric iron and at pH 1.1

The Redostat™ system did not perform well for concentration of ferric iron of about 2g/L or greater due to ferric iron precipitation (Eq. 3.18). Reliable results were only obtained at very low pH, which requires a considerable amount of sulfuric acid, otherwise the redox potential would drop instead of increase, as one would expect in case of ferrous iron oxidation. The decrease of the redox potential can be attributed to the fact that the rate of ferric iron precipitation was greater than the rate of ferrous iron oxidation and thus ferric ions were removed from solution faster than they were produced (Eq. 4.10). Hence, in order to keep the redox potential constant, the Redostat™ device was oxidizing ferrous iron automatically. Of course this was detrimental to the experiments because ferrous iron concentration was decreasing instead of remaining constant as desired.

Therefore, to minimize jarosite precipitation at higher pH, another experimental approach was sought. Minimizing the concentration of ferric ions present in solution was found to be the best workable.

The rate of ferrous iron oxidation calculated with the off-gas analysis method $-r_{O-gas}$, and $-r_I$ are in good agreement with the rate equation of the abiotic oxidation of ferrous iron (Eq. 4.3)

since straight lines with high values of R^2 were obtained by plotting equation 4.4 with these data (Fig. 4.3-4.6). The off-gas analysis method did not give reliable results at 41.4°C, probably due to the very slow ferrous iron oxidation kinetics at that temperature which resulted in minimal O_2 concentration changes in the off-gas. The batch data were used in figures 4.3 to 4.6 just for comparison, as mentioned in the previous section. The integral method (see section 3.3.2) revealed that the batch data can be described by a second order-kinetic equation (Eq. 4.7) which yielded with these data straight lines with high values of R^2 (Fig. 4.7).

$$\frac{1}{[Fe^{2-}]} = k\,t + \frac{1}{[Fe^{2+}]_0} \qquad (4.7)$$

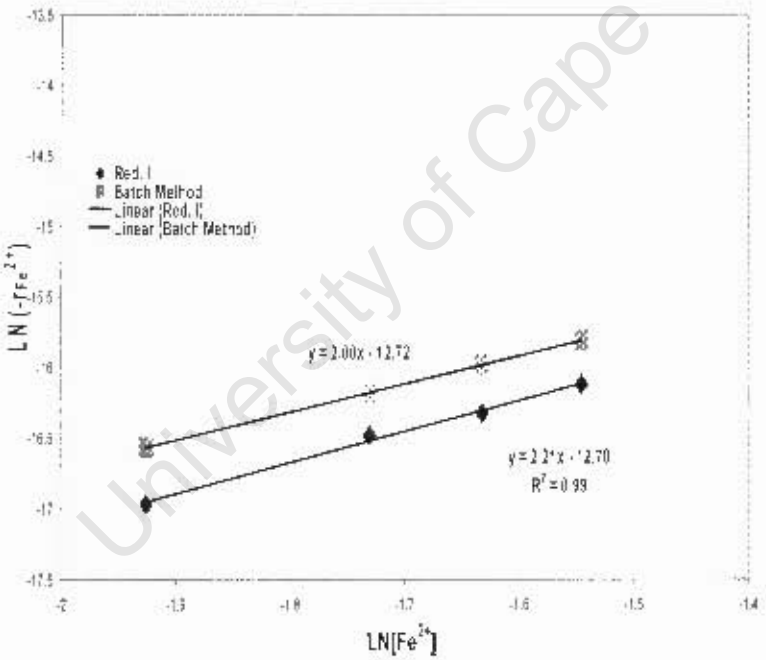

Figure 4.3: Ferrous iron oxidation rate at 41.4°C and pH =1.1

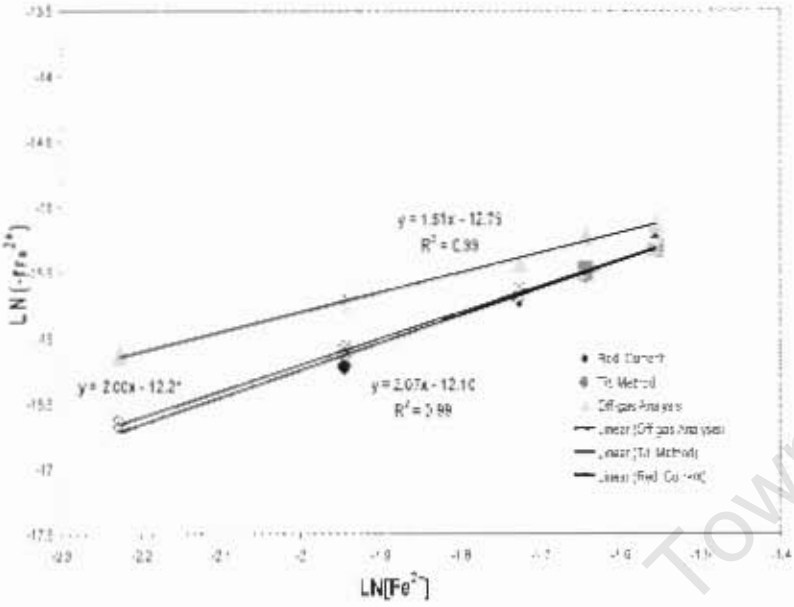

Figure 4.4: Ferrous iron oxidation rate at 51°C and pH =1.1

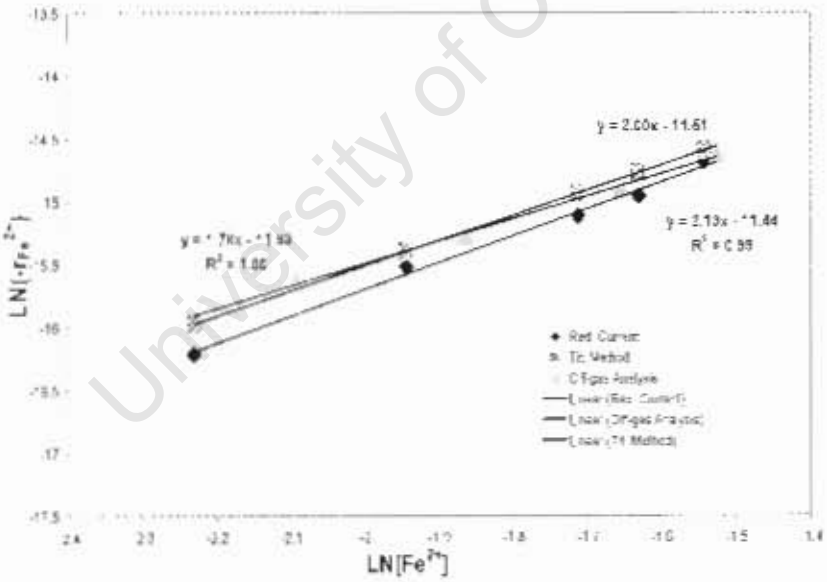

Figure 4.5: Ferrous iron oxidation rate at 60°C and pH =1.1

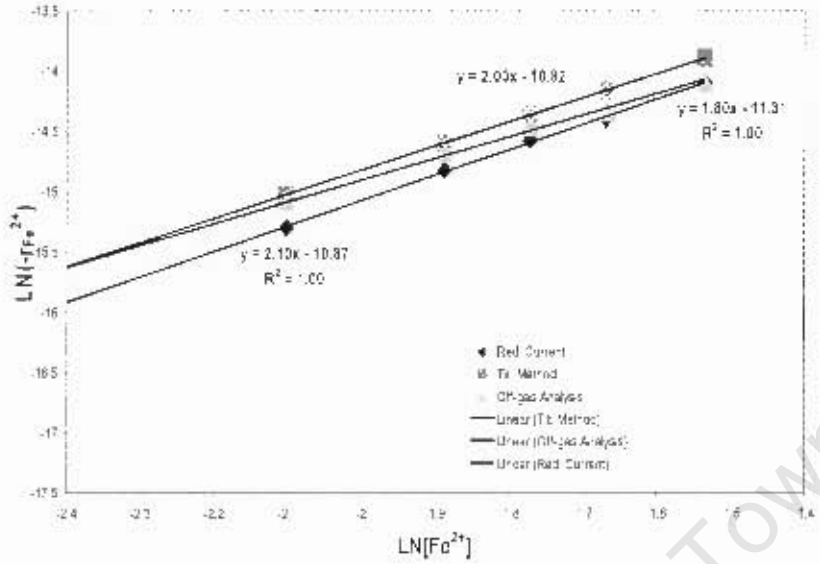

Figure 4.6: Ferrous iron oxidation rate at 68°C and pH =1.1

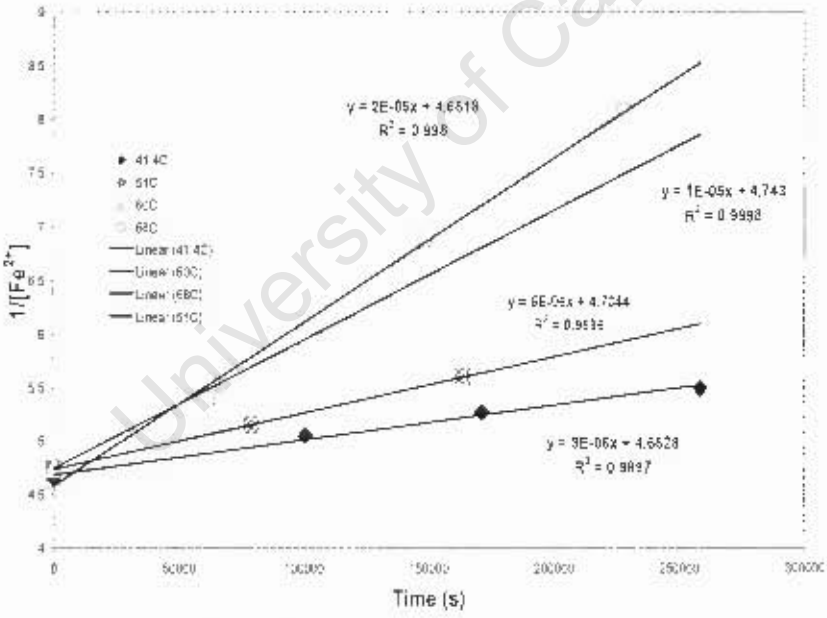

Figure 4.7.: Batch kinetic data of ferrous iron oxidation at 41.4-68°C and pH=1.1

A second order kinetic equation with respect to ferrous iron was found with all the three methods (Tables 4.2-4.5). The kinetic order of the reaction was determined by plotting equation 4.4 for the Redostat™ current and off-gas analysis methods (Fig. 4.3-4.6) but for

batch method the order of the reaction was determined by using the integral method described in section 3.3.2 (Fig. 4.7). Proper measures were taken for this second series of abiotic oxidation of ferrous iron experiments to avoid any contamination of Cl^- and it is reported in the literature that the rate of ferrous iron oxidation in a pure aqueous sulphuric acid solution follows a second-order kinetic equation (Tamura et al., 1976; Chmielewski and Charewicz, 1984).

The kinetic constants calculated with the batch method by plotting equation 4.7 (Fig. 4.7) are in excellent agreement with those calculated with the Redostat™ current method by plotting equation 4.4 (Fig. 4.3-4.6) as shown in tables 4.2 to 4.5. The off-gas analysis kinetic constants are a little bit different from the others, probably because of inaccuracies in the gas analysis due to small concentration changes.

Table 4.2
Ferrous iron oxidation kinetic data at 41.4°C and pH=1.1

	Redostat Current Method	Batch Method
k	3.06×10^{-06}	3.00×10^{-06}
a	2.21	2
R^2	0.99	0.9897

Table 4.3
Ferrous iron oxidation kinetic data at 51°C, pH=1.1

	Off-gas Analysis Method	Redostat Current Method	Batch Method
k	2.78×10^{-06}	5.57×10^{-06}	5.00×10^{-06}
a	1.51	2.07	2
R^2	0.99	099	0.9996

Table 4.4
Ferrous iron oxidation kinetic data at 60°C and pH=1.1

	Off-gas Analysis Method	Redostat Current Method	Batch Method
k	6.59×10^{-06}	1.07×10^{-05}	1.00×10^{-05}
a	1.78	2.13	2
R^2	0.9965	0.99	0.9998

Table 4.5
Ferrous iron oxidation kinetic data at 68°C and pH=1.1

	Off-gas Analysis Method	Redostat Current Method	Batch Method
k	1.23×10^{-05}	1.89×10^{-05}	2.00×10^{-05}
a	1.80	2.10	2
R^2	0.9979	0.9987	0.998

The kinetic constants calculated for this second series of abiotic oxidation of ferrous iron experiments are in good agreement with the Arrhenius equation (Eq. 4.8) since nice linear interpolations were obtained by plotting equation 4.9 with these data (Fig. 4.8).

$$k = k_0 \exp(-\frac{E^{\#}}{R\,T}) \tag{4.8}$$

$$\ln k = \ln k_0 - \frac{E^{\#}}{R}\,\frac{1}{T} \tag{4.9}$$

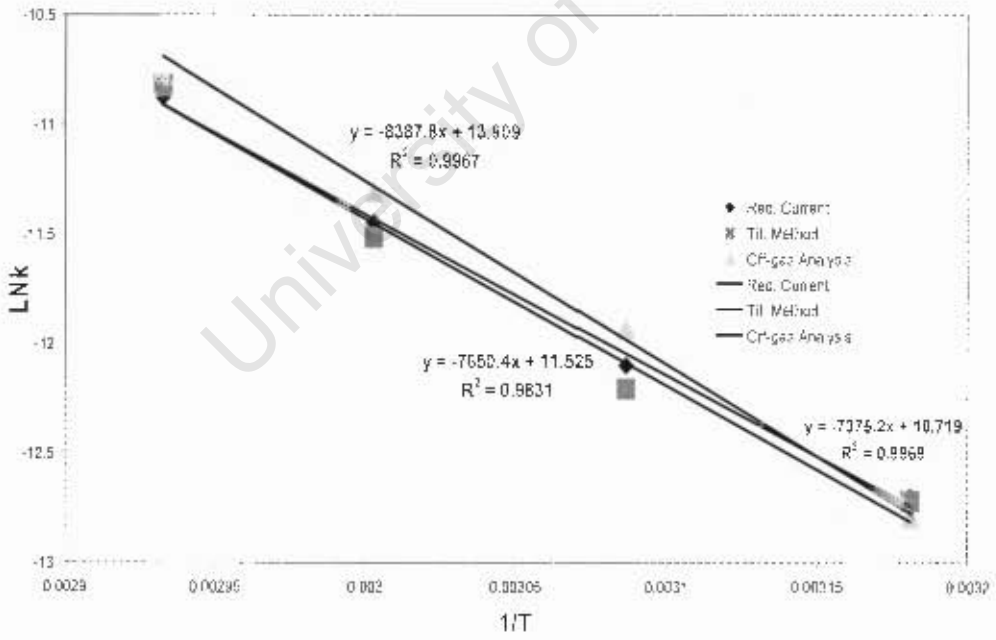

Figure 4.8: Arrhenius plot 314.4-341K

The activation energies measured by plotting equation 4.9 (Fig. 4.8) are in excellent agreement between the Redostat™ current and batch methods (Table 4.6). The off-gas analysis method also generated an activation energy that is of similar order, but slightly higher.

The values of the activation energy calculated in this study are in good agreement with the range of activation energies reported in the literature (Table 4.6).

Table 4.6
Ferrous iron oxidation activation energy

	Off-gas Analysis Method	Redostat Current Method	Batch Method	Chmielewski and Charewicz, 1984 313-408K	Verbaan and Crundwell, 1986 298-358K
$E^{\#}$ (kj.mol^{-1})	69.74	61.32	63.61	56.90	68.60

It was noticed that at pH 1.1 $-r_I$ is no longer greater than $-r_{bm}$ (Fig. 4.3-4.6) as observed at very low pH. $-r_I$ is in fact smaller than $-r_{bm}$ and the current efficiency measured for these experiments is greater than 1 (Tables A.2-A.5 in appendix A). This suggests that the amount of ferric iron reduced by the Redostat current "I" is less than what was produced by the oxidation of ferrous iron for the same length of time. Jarosite formation can be a plausible explanation to this situation. Equation 4.10 is the ferric iron mass balance equation at steady state where the left hand side term accounts for $-r_I$, the first right hand side term is the actual rate of ferrous iron oxidation and the last right hand side term is the rate of ferric iron precipitation.

$$-\frac{dQ}{dt} * \frac{1}{96500 * V} = -\frac{d[Fe^{2+}]}{dt} - \left(-\frac{d[Fe^{3+}]_j}{dt}\right) \tag{4.10}$$

It can be seen from equation (4.10) that when ferric iron precipitation is appreciable what usually occurs at higher pH and temperatures, the rate of ferric iron reduction at the cathode decreases since the rate of ferrous iron oxidation is a constant at steady state. It can also be understood from equation (4.10) that when the rate of ferric ions precipitation is greater than the rate of ferrous iron oxidation the sign of $-r_I$ changes. As mentioned earlier, this situation

was encountered at higher pH and ferric iron concentrations where the Redostat™ current changed the direction and started oxidizing ferrous ions to keep the Redox potential constant.

4.2. The Bacterial Oxidation of Ferrous Iron

The bacterial oxidation of ferrous iron was studied at 5g/L of total iron, pH 1.2 and low ferric to ferrous iron ratios of 0.17, 0.51, and 1.65 (Corresponding to redox potentials of 419, 452 and 482 mV against Ag/AgCl reference electrode) respectively. At these low ratios it is difficult to obtain any reliable data in batch cultures because of the dynamic behaviour (Boon et al., 1999a) and in continuous cultures because of bacteria wash out as discussed in sections 2.2.4.2 and 2.2.4.3.

The kinetic data were measured by using the Redostat current "I" and off-gas analysis methods only, since the batch method is not applicable to this kind of experiments. It was assumed that there is no gas-liquid mass transfer limitation since the rates of ferrous iron oxidation and oxygen consumption were increasing without flattening out (Fig. 4.13-4.15) (see Appendix C).

The rates of carbon dioxide and oxygen consumptions against time, measured as indicated in section 3.3.3, are given in figures 4.9 to 4.11. It can be seen from these figures that $-r_{CO_2}$ and $-r_{O_2}$ are increasing exponentially with time as it could have been predicted from equation (3.17). The abnormally low and high values of $-r_{O_2}$ measured at the sixteenth hour (Fig. 4.9) can probably be due to a wrong measurement of oxygen concentrations which could be caused by the oxygen analyzer. The trend of $-r_{CO_2}$, which is equivalent to the biomass growth rate $-r_X$ (Boon et al., 1998), against time is consistent with the theory of exponential growth of bacteria. Exponential growth was noticed after different lengths of time from the inoculation for the three different ferric to ferrous iron ratios since the duration of the lag phase that follows inoculation depends on many factors such as the growth conditions and the state of the inoculum (Rossi, 1990). The pH variation of the inoculum can be the reason why exponential growth was not observed after the same length of time for the three different runs.

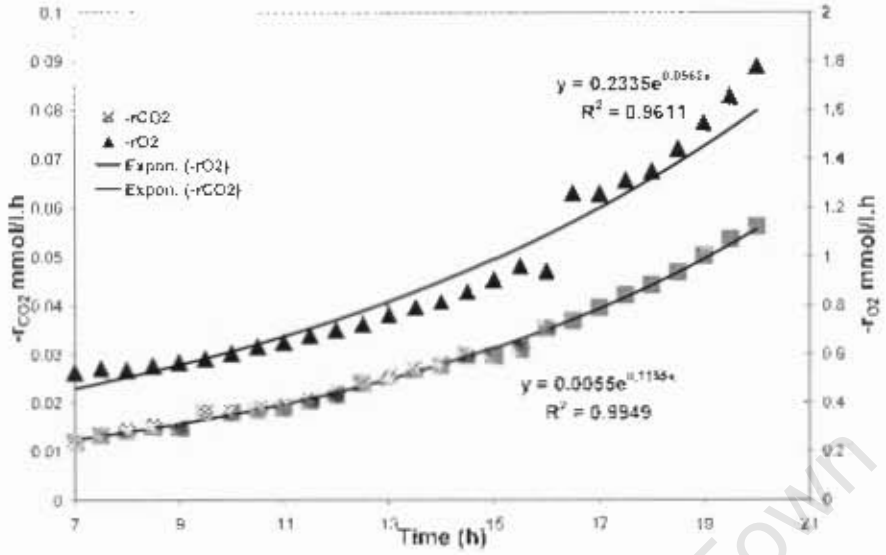

Figure 4.9: CO_2 and O_2 consumption rates at E = 419 mV or $\frac{[Fe^{3+}]}{[Fe^{2+}]} = 0.17$

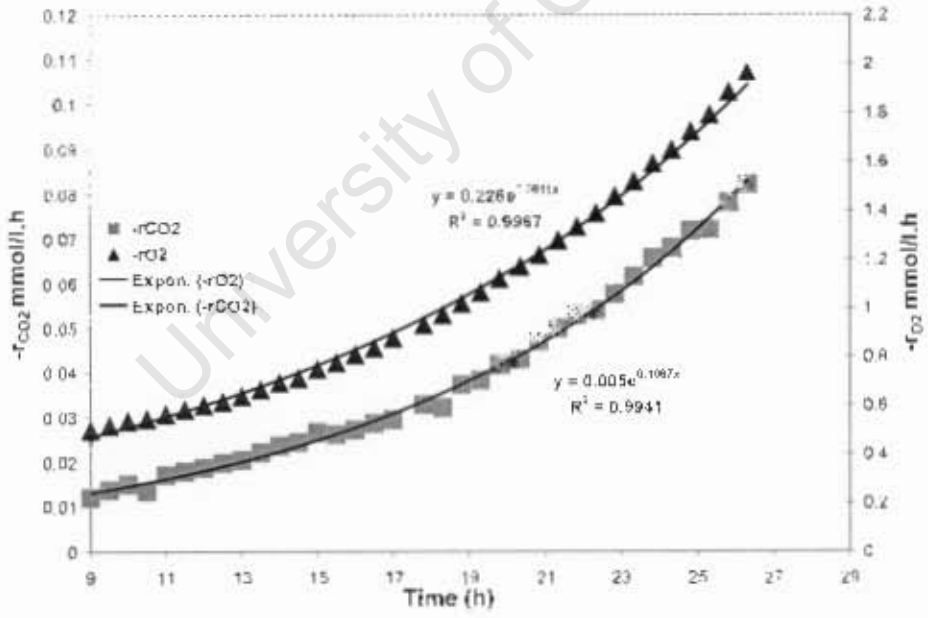

Figure 4.10: CO_2 and O_2 consumption rates at E = 452 mV or $\frac{[Fe^{3+}]}{[Fe^{2+}]} = 0.51$

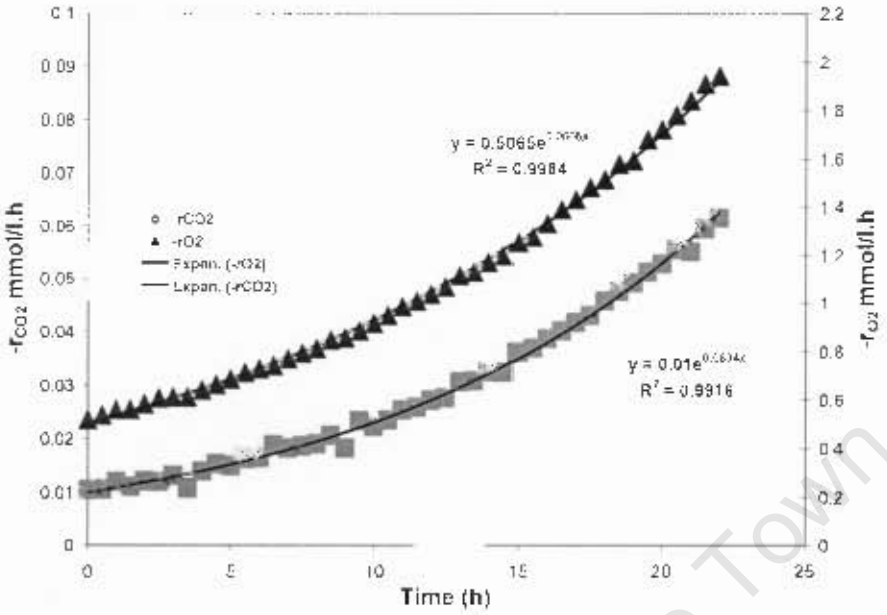

Figure 4.11: CO_2 and O_2 consumption rates at E = 482 mV or $\frac{[Fe^{3+}]}{[Fe^{2+}]} - 1.65$

The different values of the specific growth rate μ (Table A.6 in appendix A) were determined by fitting the data of r_{CO_2} against time with an exponential function as suggested by equation 3.17 and equating the coefficient of the power of this function to the specific growth rate. The specific growth rate thus measured was found to decrease with increasing ferric to ferrous iron ratio as suggested by many growth kinetic models (Eq. 2.29 and 2.33) probably due to substrate (ferrous iron) depletion and ferric iron inhibition. The modified Monod equation for product inhibition by ferric iron, where the saturation term $\frac{K_S}{[Fe^{2+}]}$ has been neglected (Eq. 4.11), was used to describe the growth kinetics in this present study. The values of the maximum growth rate μ_{max} and the constant K ($=\frac{K_S}{K_i}$) (Table 4.7) were measured by plotting equation 4.12, which is the reciprocal of equation 4.11, with the values of the specific growth rate measured (Fig. 4.12).

Values of 0.1024 and 0.1043 h^{-1} for the maximum specific growth rate of *Leptospirillum ferrooxidans* at pH 1.10 and 1.30 respectively have been reported in the literature (Breed and Hansford, 1999). It is worth noting here that *Leptospirillum ferriphilum* was previously thought to be *Leptospirillum ferrooxidans* (Coram and Rawlings, 2002). These literature values are close to the maximum specific growth rate of *Leptospirillum ferriphilum* calculated in this study at pH 1.2 (Table 4.7), but the reported values of K are much lower than the value that was calculated in this present study.

$$\mu = \frac{\mu_{max}}{1 + \frac{K_S\,[Fe^{3+}]}{K_I\,[Fe^{2+}]}} \tag{4.11}$$

$$\frac{1}{\mu} = \frac{1}{\mu_{max}} + \frac{K_S}{\mu_{max}\,K_I}\frac{[Fe^{3+}]}{[Fe^{2+}]} \tag{4.12}$$

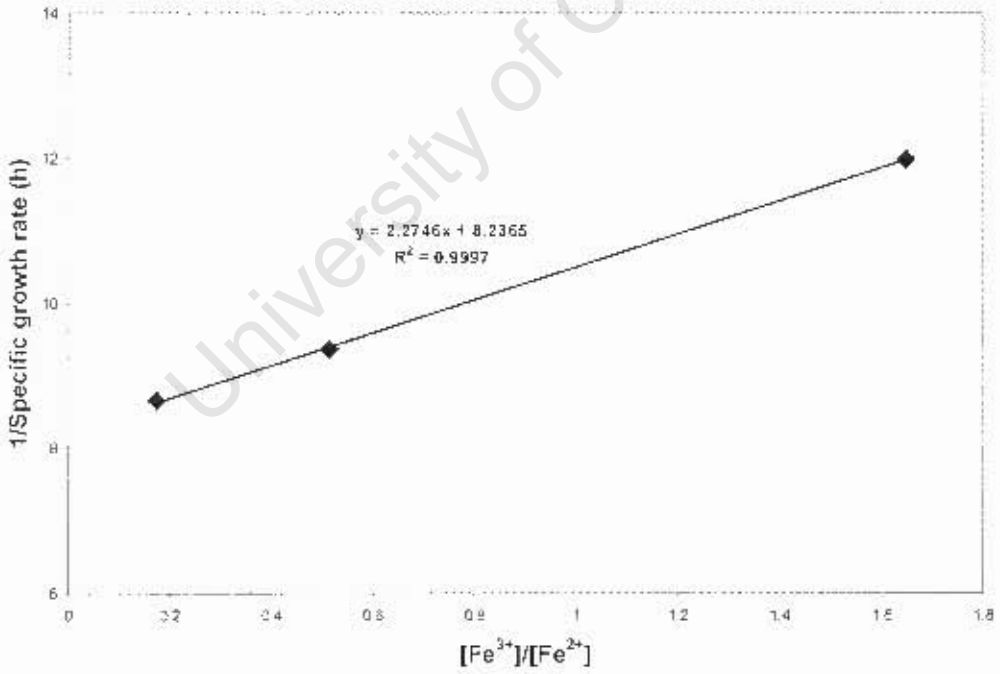

Figure 4.12: Double Reciprocal plot of the modified Monod equation for product inhibition by ferric iron

Table 4.7
Growth kinetics parameters

pH	μ_{max} h^{-1}	K	R^2
1.2	0.12	0.28	0.9997

$-r_{O-gas}$ (Eq. 2.14) increased exponentially with time (Fig. 4.13-4.15) since $-r_{CO_2}$ and $-r_{O_2}$ are exponential functions of time (Fig. 4.9-4.11). $-r_I$ also followed closely the same trend since the two rates are supposed to be equal at contant redox potential. The kinetic data of the rate of ferrous iron bacterial oxidation were fitted with polynomial functions because an exponential function can be expanded as a polynomial function of a certain power (Eq. 3.7).

It was noticed that the redox potential error ΔE was continuously increasing with time for each run probably because of the low Redostat™ control gain which was at its maximum value (200) for this study. The Redostat™ control gain dictates the intensity of current that should be applied for a given ΔE measured by the Redostat™ controller and when the current applied is not enough, ΔE becomes larger and larger with time because more ferric ions are produced than what are reduced by the current. This situation can be clearly seen from figures 4.14 and 4.15 where the rate of ferric iron reduction at the Redostat™ cathode $-r_I$ is slightly lower than the rate of ferrous iron oxidation $-r_{O-gas}$. In this case, the concentration of ferrous iron decreases with time.

A redox potential error of 4mV maximum was tolerated in this study and it resulted in a decrease of ferrous iron concentration of 0.3g/l (calculated by titration) over a period of 20 to 24 hours for each run. An integral calculation of the areas below the two curves (Fig. 4.13-4.15), which are the numbers of moles of ferric iron either reduced by the Redostat™ current ($\int -r_I dt$) or produced by the biological oxidation of ferrous iron ($\int -r_{O-gas} dt$), also showed a decrease of ferrous iron concentration for each run (Eq. 4.13-4.15). The decrease of ferrous iron concentration calculated by integration (Eq. 4.13-4.15) is almost equal to what was calculated with titration except in the first case (Eq. 4.13) probably due to the limited accuracy of the data measured at that potential.

Ferric iron precipitation is unlikely to be a problem here since the Redox potential was increasing with time for each run and no appreciable decrease of total iron concentration was noticed.

A higher Redostat™ control gain (>200) is required to keep the concentration of ferrous iron constant within an acceptable range for a longer period of time than a day, as it was the case in this present study.

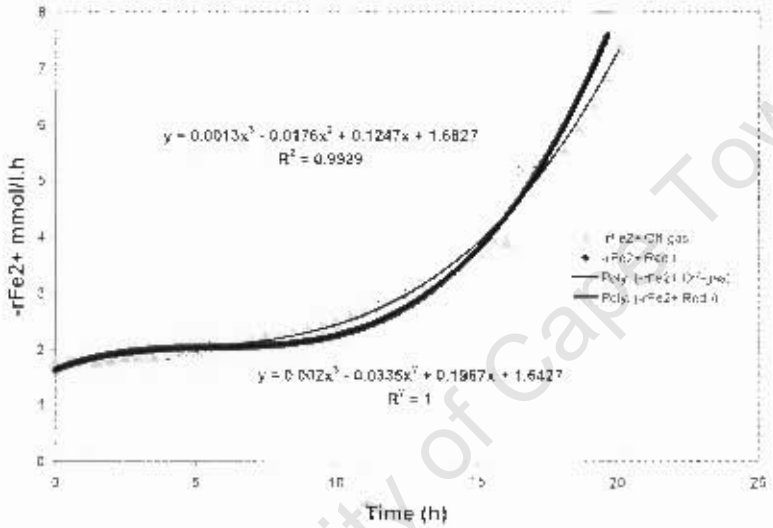

Figure 4.13: Rate of ferrous iron biological oxidation measured with the off-gas and Redostat™ current methods at 419mV

$$\Delta[Fe^{2+}] = \int_{0}^{20} \{-r_1 - (-r_{O-gas})\}\, dt = -0.8mmol/l = -0.045g/l \qquad (4.13)$$

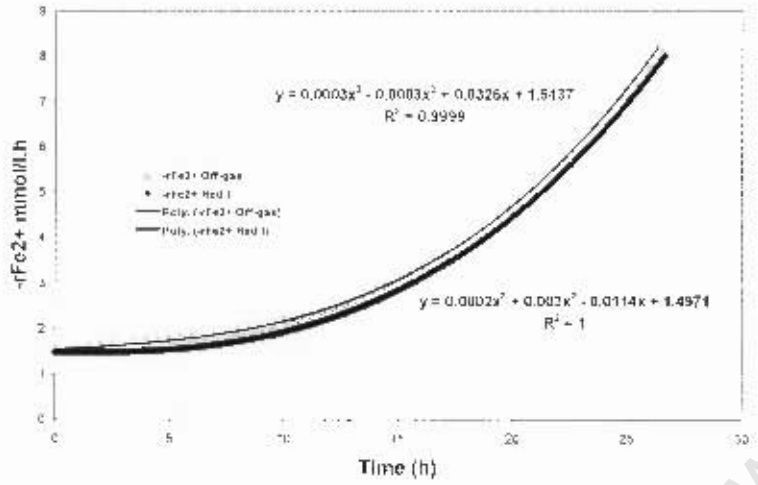

Figure 4.14: Rate of ferrous iron biological oxidation measured with the off-gas and Redostat™ current methods at 452mV

$$\Delta[Fe^{2+}] = \int_{0}^{26.3} [-r_f - (-r_{O-gas})]\, dt = -8.39 mmol/l = -0.47 g/l \qquad (4.14)$$

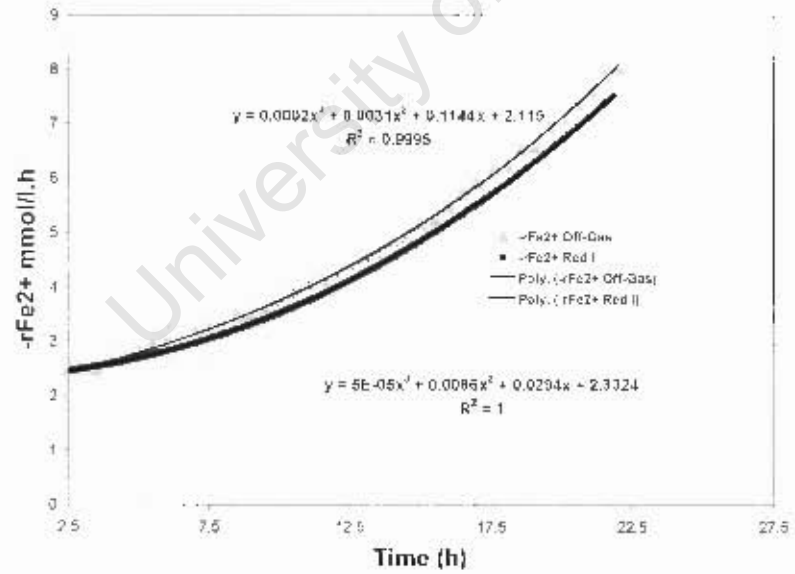

Figure 4.15: Rate of ferrous iron biological oxidation measured with the off-gas and Redostat™ current methods at 482mV

$$\Delta[Fe^{2+}] = \int_{2.25}^{22.8} [-r_f - (-r_{O-gas})]\, dt = -5.93 mmol/l = -0.33 g/l \qquad (4.15)$$

It was found that the biomass specific ferrous iron and oxygen consumption rates $q_{Fe^{2+}}$ and q_{O_2} and the biomass yields on ferrous iron and oxygen $Y_{Fe^{2+}X}$ and Y_{O_2X} were changing with the biomass concentration, although μ remained a constant for a particular ferric to ferrous iron ratio. This shows that, if equations 2.18-2.19 and 2.21-2.22 still apply the maintenance coefficient or the maximum yield or both are not constant with changing biomass concentration. $q_{Fe^{2+}}$ and q_{O_2} were decreasing with increasing biomass concentration (Fig. 4.16-4.18) and a similar situation was noticed in continuous culture where a high value of $q_{Fe^{2+}}$ was measured at low biomass concentration and low value of $q_{Fe^{2+}}$ at high biomass concentration (T.V. Ojumu, personal communication). C_X in continuous culture can be set by the concentration of ferrous iron in the feed (Eq. 2.43). $Y_{Fe^{2+}X}$ and Y_{O_2X} were increasing with increasing biomass concentration (Fig. 4.19-4.21).

The decrease of the specific rates $q_{Fe^{2+}}$ and q_{O_2} with increasing biomass concentration can be attributed to the fact that more and more bacteria are competing for the same amount of substrate (ferrous iron) and oxygen. This situation may result in an equilibrium state where there is not enough substrate or oxygen and thus stopping the bacterial growth. The fact that microorganisms grow much faster at higher biomass concentrations (Eq. 2.35-2.36) could be an explanation as to why the biomass yield increases with increasing biomass concentration.

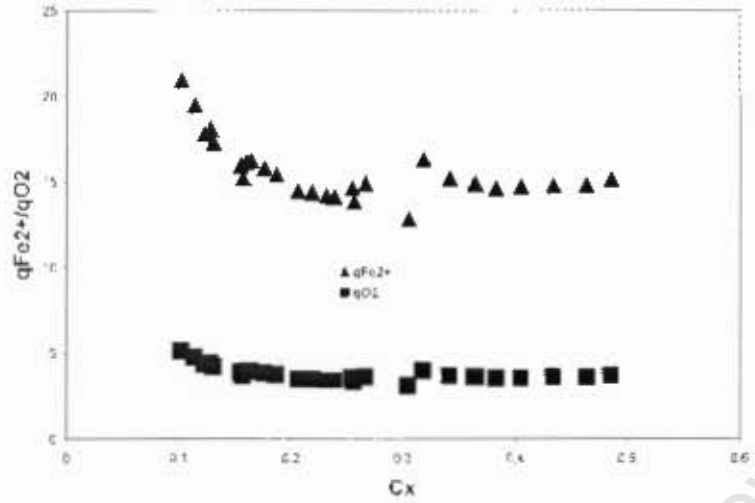

Figure 4.16: Specific ferrous iron and oxygen consumption rates at 419 mV

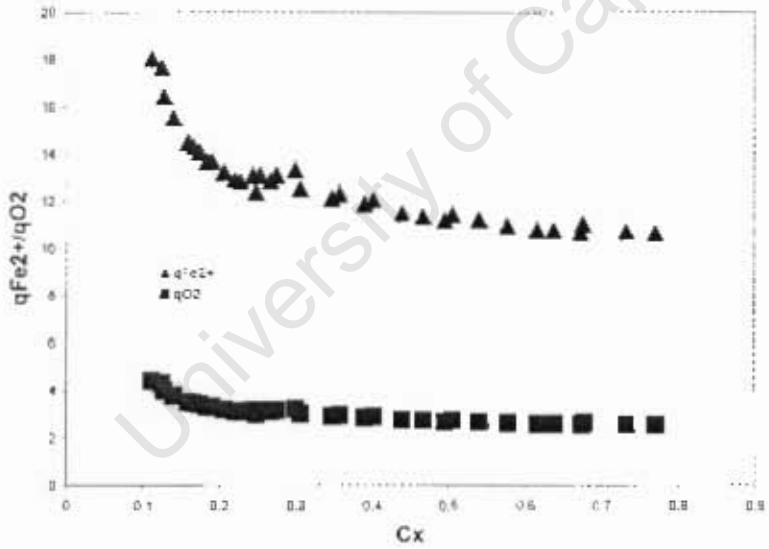

Figure 4.17: Specific ferrous iron and oxygen consumption rates at 452 mV

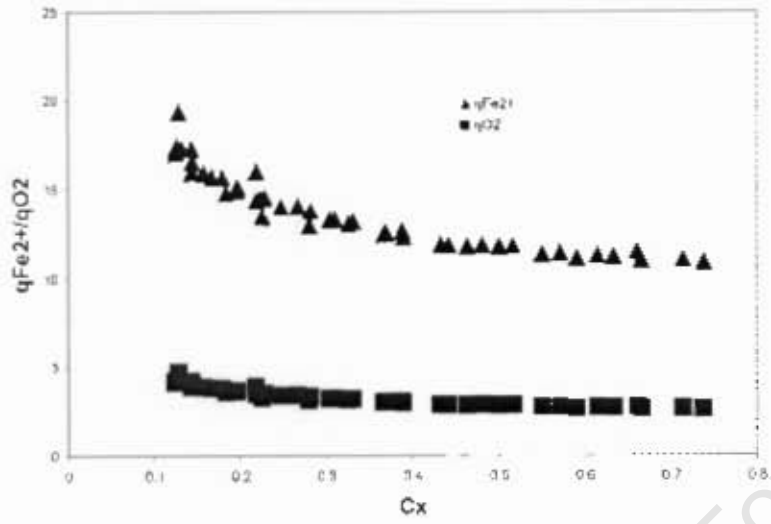

Figure 4.18: Specific ferrous iron and oxygen consumption rates at 482 mV

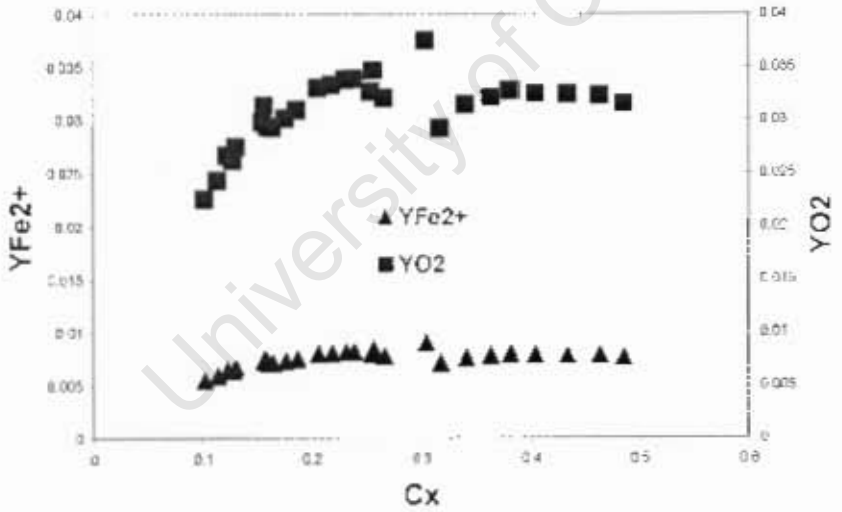

Figure 4.19: Biomass yield on ferrous iron and oxygen at 419 mV

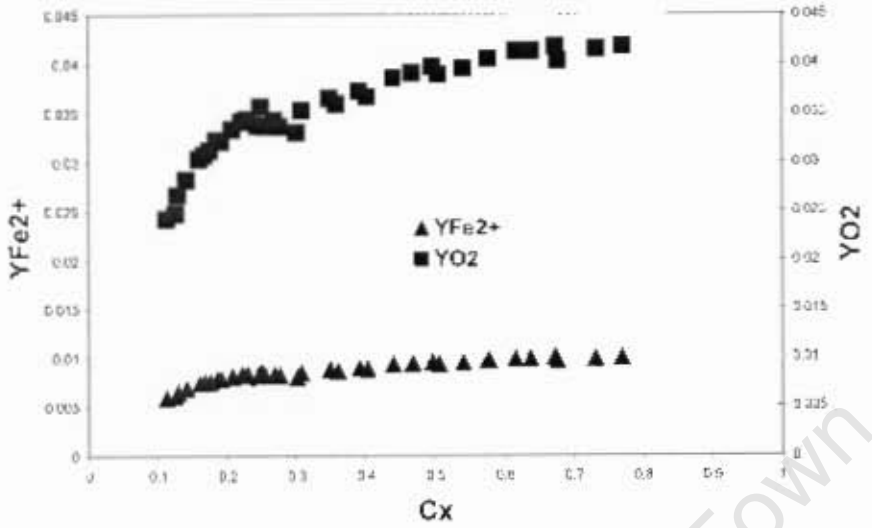

Figure 4.20: Biomass yield on ferrous iron and oxygen at 452 mV

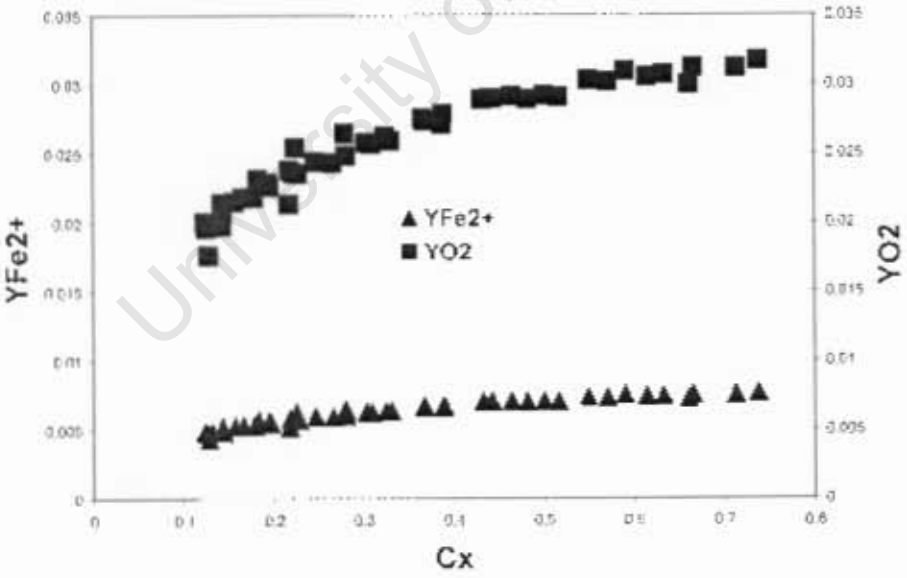

Figure 4.21: Biomass yield on ferrous iron and oxygen at 482 mV

4.3. Evaluation of the Redostat™ Device

The measurement of ferrous iron oxidation rate with the Redostat™ current is based on the fact that at steady state (constant redox potential) the rate of ferrous iron oxidation $-r_{Fe^{2+}}$ is equal to the rate of ferric iron reduction at the cathode if there is no ferric iron precipitation (Eq. 4.10). This implies that all the ferric iron produced by the oxidation reaction is electrolytically reduced back to ferrous iron thus keeping the concentrations of ferrous and ferric iron constant. Since reliable ferrous iron oxidation rates were generated with the Redostat™ current it can be confidently stated that the Redostat™ system keeps the concentrations of ferrous and ferric iron constant within an acceptable range.

Jarosite precipitation has to be reduced to a minimum in order to obtain good results with the Redostat™ device since the precipitation of ferric iron reduces the rate of ferric iron reduction at the Redostat™ cathode $-r_I$ (4.10). A lower $-r_I$ causes a decrease of ferrous iron concentration since more ferric iron is produced than what is reduced by the Redostat™ current. And when ferric iron precipitation is faster than ferrous iron oxidation, the sign of $-r_I$ changes (Eq. 4.10) and the Redostat™ device starts oxidizing ferrous iron in order to keep the potential constant. Jarosite precipitation can be limited by carefully choosing the right experimental conditions (T, pH, $[Fe^{3+}]$, etc.). A very low pH can promote hydrogen evolution at the Redostat™ cathode.

The quality of the results generated with the Redostat™ system also depends on the Redostat™ settings. A slow rate of oxidation requires a small current but fast reactions require larger currents to keep the redox potential constant. The Redostat™ current is determined by the control gain.

The Redostat™ system helps save time especially for the biological oxidation of ferrous iron experiments. To complete one run which is characterized by a particular redox potential or ferric to ferrous iron ratio it only takes 20 to 24 hours maximum whilst with continuous culture reactors a minimum of three times the residence time is indispensable to achieve steady state. And only long residence times (>10hours) corresponding to high ferric to ferrous iron are

achievable in continuous cultures. Minima of 19 days and 2months were estimated for the generation of 5 and 10 datapoints respectively in continuous culture (see section 2.2.4.3). Each datapoint was generated at a particular redox potential or ferric to ferrous iron ratio.

Chapter 5. Conclusion and Recommendations

For the abiotic oxidation of ferrous iron, it was found that the kinetic data generated with the Redostat™ current is in good agreement with that generated with the batch method. Activation energies of 61.32 and 63.61kj.mol^{-1} were calculated in the temperature range of 41.4 to 68°C and pH 1.1. These values are consistent with the activation energy values reported in the literature. A value of 69.74kj.mol^{-1} was calculated by using the off-gas analysis method. This slightly higher value was probably due to the low measurement accuracy of this method for low variations of oxygen concentration in the gas stream.

For the biological oxidation of ferrous iron experiments, the Redostat™ current method also yielded excellent results. The rate of ferrous iron oxidation measured with the Redostat™ current was found to be in good agreement with that measured using the off-gas analysis method. The value of μ measured was decreasing with increasing ferric to ferrous iron ratios as suggested by many ferrous iron biological oxidation kinetic models. A maximum specific growth rate of 0.12h^{-1} and a ratio $\frac{K_S}{K_i}$ of 0.28 were calculated. The literature values of μ_{max} are close enough to the one calculated in this study under similar conditions, but the reported values of $\frac{K_S}{K_i}$ are much lower than the value that was calculated in this present study.

It was also found in this study that the biomass concentration has an effect on the biomass specific ferrous iron and oxygen consumption rates and the biomass yields on ferrous iron and oxygen. This phenomenon has not been previously described and could have significant implications for start-up of heaps.

This study has revealed that the Redostat™ device can be successfully used as an experimental tool for the study of ferrous iron oxidation at constant potential or ferric to ferrous iron ratio provided that ferric ions precipitation is kept to a minimum. However, a higher Redostat™ control gain (>200) is required for the biological oxidation of ferrous iron in order to keep the

concentrations of ferrous and ferric iron constant within an acceptable range for a longer period of time than a day, as it was the case in this present study.

The Redostat™ device offers a quicker and more direct way of determining the rate of ferrous iron oxidation and allows to investigate the oxidation of ferrous iron at very low ferric to ferrous iron, where it is difficult to obtain kinetic data in batch and continuous cultures because of the dynamic behaviour in batch cultures and bacteria wash out in continuous cultures.

A lot of time is saved when the kinetics of ferrous iron bio-oxidation is studied in the Redostat™ device since it only takes one day (Fig. 4.9-4.11 and 4.13-4.15) to measure all the kinetic variables ($q_{Fe^{2+}}, q_{O_2}, \mu, Y_{Fe^{2+}X}, Y_{O_2X}, and\ C_x$) at a particular ferric to ferrous iron ratio whilst continuous cultures can run for days or even weeks to obtain the same kinetic data. It is worth noting here that for the determination of C_x there is no need to know the initial biomass concentration like in ordinary batch cultures (Boon, 1996) since C_x can be easily calculated from equation 2.36 where r_x and μ are known from equations 3.12 and 3.17 respectively.

Further research is needed about the effect of biomass concentration on the kinetics of ferrous iron bio-oxidation as this can shed more light on the oxidation of ferrous iron in heap where some zones behave like batch cultures operating at constant potential. And the Redostat™ unit is the experimental tool of choice for this kind of research since it can easily and successfully simulate these zones.

References

Acevedo, F., Present and future of bioleaching in developing countries, EJB Electronic Journal of Biotechnology, Vol.5 No.2, Issue of August 15, 2002. Available from internet at http://www.ejb.org/content/vol5/issue2/issues/01/index.html

Akcil, A., Potential bioleaching developments towards commercial reality: Turkish metal mining's future, Minerals Engineering 17 (2004) 477-480

Anonymous, Redostat™ User Manual, Danntech Precision instruments (Pty) Ltd. 2005

Barrett, J., M.N. Hughes, G.I. Karavaido and P.A. Spencer, Metal Extraction By Bacterial Oxidation Of Minerals, Ellis Horwood Limited, 1993, p. 1-55, 151-152

Bartlett, Robert W., Solution Mining, Leaching and Recovery of Materials, Gordon and Breach Science Publishers, 1992, p. 68

Boon, M., C. Ras, J. J. Heijnen, The ferrous iron oxidation kinetics of *Thiobacillus ferrooxidans* in batch cultures, Appl Microbiol Biotechnol (1999a) 51: 813-819

Boon, M., K.Ch.A..M. Luyben, J.J. Heijnen, The use of on-line off-gas analyses and stoichiometry in the bio-oxidation kinetics of sulphide minerals, Hydrometallurgy 48 (1998) 1-26

Boon, M., T.A. Meeder, C. Thone, C. Ras, J.J. Heijnen, The ferrous iron oxidation kinetics of *Thiobacillus ferrooxidans* in continuous cultures, Appl Microbiol Biotechnol (1999b) 51: 820-826

Boon, M., Theoretical and Experimental Methods in the Modeling of Bio-oxidation Kinetics of Sulphide Minerals, PhD thesis, Department of Biochemical Engineering, Delft University of Technology, 1996, p. 153-245

Bosecker, K., Bioleaching: metal solubilization by microorganisms, FEMS Microbiology Reviews 20 (1997) 591-604

Bouffard, S.C. and David G. Dixon, Investigative study into the hydrodynamics of heap leaching processes, Metall. Mater. Trans. B, 32B (2001), 763-776.

Braddock, J., Luong, H.V., and Brown, E.J., Appl. Environ. Microbiol., 48 (1984), 48-55

Breed, A.W. and Hansford, G.S., Effect of pH on ferrous-iron oxidation kinetics of Leptospirillum ferrooxidans in continuous culture, Biochemical Engineering Journal 3 (1999) 193-201

Brierley, C.L., "Bioleaching", in AccessScience@McGraw-Hill, http://www.accessscience.com, DOI 10.1036/1097-8542.082525, last modified: September 19, 2005. Visited on 2006/12/21

Brierley, C.L., "Biomining", in AccessScience@McGraw-Hill, http://www.accessscience.com, DOI 10.1036/1097-8542.YB010220, last modified: October 9, 2001. Visited on 2007/01/08

Brierley, C.L., Microbiological Mining, Scientific American, August 1982, p. 44-54

Brierley, J.A. and C.L. Brierley, Present and future commercial applications of biohydrometallurgy, Hydrometallurgy 59 (2001) 233-239

Chmielewski, T. and Witold A. Charewicz, The Oxidation of Fe(II) In Aqueous Sulphuric Acid Under Oxygen Pressure, Hydrometallurgy, 12 (1984) 21-30

Coram, N.J. and Douglas E. Rawlings, Molecular Relationship between Two Groups of the Genus Leptospirillum and the Finding that Leptospirillum Ferriphilum sp. nov. Dominates South African Commercial Biooxidation Tanks That Operate At 40^0C, Applied And Environmental Microbiology, Feb. 2002, p. 838-845

Dempers, C.J.N., A.W. Breed, and G.S. Hansford, The kinetics of ferrous-iron oxidation by *Acidithiobacillus ferrooxidans* and *Leptospirillum ferrooxidans*: effect of cell maintenance, Biochemical Engineering Journal 16 (2003) 337-346

Dixon, D.G., Analysis of heat conservation during copper sulphide heap leaching, Hydrometallurgy 58 (2000) 27-41

Dreisinger, D., Copper Leaching From Primary Sulphides: Options for Biological and Chemical Extraction of Copper, in: Proceedings of the 16th International Biohydrometallurgy Symposium 2005, edited by Susan T.L. Harrison, Douglas E. Rawlings and Jochen Petersen, p. xli-li

Hansford, G.S., Recent Developments in Modelling the Kinetics of Bioleaching, in: Biomining: Theory, Microbes and Industrial processes, edited by Douglas E. Rawlings. © Springer- Verlag and Landes Bioscience (1997) p. 153-175

Harvey, P.I. and F.K. Crundwell, Growth of *Thiobacillus ferrooxidans*: a Novel Experimental Design for Batch Growth and Bacterial Leaching Studies, Applied and Environmental Microbiology, July 1997, p. 2586-2592

Jeffrery, G.H., Basset, J., Mendham, J. and Denney, R.C., Vogel's Textbook of Quantitative Chemical Analysis, 5th edition, Longman Scientific and Technical, New York, 1989

Jones, C.A., Kelly, D.P., J. Chem. Tech. Biotechnol., 33B (4) (1983), 241-261

Lacey, D.T., Lawson, F., Biotechnol. Bioeng., 12 (1970), 29-50

Levenspiel, O., Chemical Reaction Engineering, Second Edition, Wiley International Edition, 1972, p. 41-86

Morin, Dominique Henri Roger and Patrick D'Hugues, Bioleaching of a Cobalt-Containing Pyrite in Stirred Reactors: a Case Study from Laboratory Scale to Industrial Application, in: Biomining, edited by Douglas E. Rawlings and D. Barrie Johnson, © Springer-Verlag Berlin Heidelberg 2007, p. 35-55

Nemati, M., S.T.L. Harrison, G.S. Hansford, C. Webb, Biological oxidation of ferrous sulphate by *Thiobacillus ferrooxidans*: a review on the kinetic aspects, Biochemical Engineering journal 1 (1998) 171-190

Norris, P.R., Barr, D.W., and Hinson D., Iron and Mineral Oxidation by Acidophilic Bacteria: Affinity for Iron and Attachment to Pyrite, in: Biohydrometallurgy Proc. Int. Symp., eds. Norris P.R., Kelly D.P., Warwick 1987, p. 43-59

Ojumu, T.V., J. Petersen, G.E. Searby and G.S. Hansford, Areview of rate equations proposed for the microbial ferrous iron oxidation with a view to application to heap bioleaching, Hydrometallurgy 83 (2006) 21-28

Petersen, J., Introduction to Heap Leach Practice and Theory, Hydrometallurgy Masters Course-UCT June/July 2003

Petersen, J. and David G. Dixon, Modeling and Optimization of Heap Bioleach Processes, in: Biomining, edited by Douglas E. Rawlings and D. Barrie Johnson, © Springer-Verlag Berlin Heidelberg 2007a, p. 153-176

Petersen, J. and David G. Dixon, Principles, Mechanisms and Dynamics of Chalcocite Heap Bioleaching, in Microbial Processing of Metal Sulfides, E.Donati, W. Sand (eds.), Springer Verlag, Berlin, 2007b, ISBN 978-1-4020-5588-1, p. 193-218.

Pirt, S.J. 1982, Maintenance energy: A general model for energy limited and energy sufficient growth. Arch.Microbiol. 133: 300-302

Pronk, J.T. and Johnson D.B., Oxidation and Reduction of Iron by Acidophilic Bacteria; Geomicrobiology Journal 10, 1993, p. 153-171

Rawlings, D.E., Tributsch, H., and Hansford, G.S., Reasons why '*Leptospirillum*'-like species rather than *Thiobacillus ferrooxidans* are the dominant iron-oxidizing bacteria in many commercial processes for the biooxidation of pyrite and related ores, Microbiology (1999), 145, 5-13

Roels, J.A., Energetics and Kinetics in Biotechnology. Amsterdam: Elsevier Biomedical Press, 1983

Romero, J., Carolina Yanez, Monica Vasquez, Edward R.B. Moore, Romilio T. Espejo, Characterization and identification of an iron-oxidizing, *Leptospirillum*-like bacterium, present in the high sulphate leaching solution of a commercial bioleaching plant, Research in Microbiology 154 (2003) 353-359

Rossi, G., Biohydrometallurgy/Giovanni Rossi.- Hamburg; New York [u.a.]: McGraw-Hill, 1990 p. 1-157, 236-244, 390-441

Sand, W., Rohde, k., Sobotke, B., and Zenneck, C., Evaluation of Leptospirillum ferrooxidans for leaching, Applied and Environmental Microbiology, Jan. 1992, Vol. 58: 85-92

Tamura, H., Katsumi Goto and Masaichi Nagayama, Effect of Anions on the Oxygenation of Ferrous Ion in Neutral Solutions, J. inorg. Nucl. Chem., 1976, Vol. 38, p. 113-117

Torma, A.E., Mineral Bioprocessing, Biomine'93, Australian Mineral Foundation, 1993, p. 1-1 to 1-10

Tromans, Desmond, Modeling Oxygen Solubility in Water and Electrolyte Solutions, Ind. Eng. Chem. Res. 2000, 39, 805-812

van Aswegen, Pieter C., Jan van Niekerk, and Waldemar Olivier, The BIOX™ Process for the Treatment of Refractory Gold Concentrates in: Biomining, edited by Douglas E. Rawlings and D. Barrie Johnson, © Springer-Verlag Berlin Heidelberg 2007, p. 1-33

van't Riet, Ind. Eng. Chem. Proc. Des. Dev., 18, 357, 1979

van Scherpenzeel, D.A., Boon, M., Ras, C., Hansford, G.S., and Heijnen, J.J., Kinetics of Ferrous Iron Oxidation by *Leptospirillum* Bacteria in Continuous Cultures, Biotechnol. Prog. 1998, 14, 425-433

Verbaan, B. and Crundwell, F.K., An electrochemical Model for the Leaching of Sphalerite Concentrate, Hydrometallurgy 16 (1986) p. 345-359

Vishniac, W. and M. Santer, The Thiobacilli. Bacterial Revs. 21 (1957) 195-213

Watling, H.R., The bioleaching of sulphide minerals with emphasis on copper sulphides – A review, Hydrometallurgy 84 (2006) 81-108

Appendix A

Kinetic Data

Table A.1
Ferrous iron oxidation rate at 60°C, pH<0.6, and $[Fe]_{total}$=0.21M

$[Fe^{2+}]$ M	$-r_{O-gas}$	$-r_I$	$-r_{bm}$	η
0.18	$4.31x10^{-07}$	$2.93x10^{-07}$	$2.42x10^{-07}$	0.83
0.17	$3.67x10^{-07}$	$2.84x10^{-07}$	$2.25x10^{-07}$	0.79
0.12	$2.33x10^{-07}$	$2.07x10^{-07}$	$1.62\ x10^{-07}$	0.78
0.11	$2.06x10^{-07}$	$1.89x10^{-07}$	$1.51x10^{-07}$	0.80
0.04	$7.16x10^{-08}$	$7.38x10^{-08}$	$5.87x10^{-08}$	0.80
0.03	$5.96x10^{-08}$	$5.96x10^{-08}$	$3.60x10^{-08}$	0.60

$-r_{O-gas}$: Ferrous iron oxidation rate calculated with the off-gas analysis method

$-r_I$: Ferrous iron oxidation rate calculated with the Redostat current "I"

$-r_{bm}$: Ferrous iron oxidation rate calculated with the batch method

η is the Redostat current efficiency which is the fraction of the Redostat current that actually reduces ferric ions.

Table A.2
Ferrous iron oxidation rate at 41.4°C and pH=1.1

[Fe2+] M	$-r_I$	$-r_{bm}$	η
0.15	$4.27x10^{-08}$	$6.37x10^{-08}$	1.5
0.18	$6.94x10^{-08}$	$9.43x10^{-08}$	1.36
0.20	$8.15x10^{-08}$	$1.15x10^{-07}$	1.41
0.21	$9.99x10^{-08}$	$1.36x10^{-07}$	1.37

Table A.3
Ferrous iron oxidation rate at 51°C, pH=1.1

[Fe2+] M	$-r_{O-gas}$	$-r_I$	$-r_{bm}$	η
0.11	$9.88x10^{-08}$	$5.81x10^{-08}$	$5.83x10^{-08}$	1.00
0.14	$1.46x10^{-07}$	$9.05x10^{-08}$	$1.02x10^{-07}$	1.13
0.18	$1.98x10^{-07}$	$1.52x10^{-07}$	$1.58x10^{-07}$	1.04
0.19	$2.44x10^{-07}$	$1.83x10^{-07}$	$1.87x10^{-07}$	1.02
0.21	$2.68x10^{-07}$	$2.33x10^{-07}$	$2.23x10^{-07}$	0.96

Table A.4
Ferrous iron oxidation rate at 60°C and pH=1.1

[Fe2+] M	$-r_{O-gas}$	$-r_{I}$	$-r_{b\,m}$	η
0.11	$1.30\text{x}10^{-07}$	$9.09\text{x}10^{-08}$	$1.56\text{x}10^{-07}$	1.27
0.14	$1.99\text{x}10^{-07}$	$1.82\text{x}10^{-07}$	$2.05\text{x}10^{-07}$	1.27
0.18	$3.11\text{x}10^{-07}$	$2.72\text{x}10^{-07}$	$3.26\text{x}10^{-07}$	1.20
0.20	$3.76\text{x}10^{-07}$	$3.19\text{x}10^{-07}$	$3.84\text{x}10^{-07}$	1.21
0.21	$4.10\text{x}10^{-07}$	$4.18\text{x}10^{-07}$	$4.58\text{x}10^{-07}$	1.10

Table A.5
Ferrous iron oxidation rate at 68°C and pH=1.1

[Fe2+] M	$-r_{O-gas}$	$-r_{I}$	$-r_{b\,m}$	η
0.12	$2.83\text{x}10^{-07}$	$2.27\text{x}10^{-07}$	$2.99\text{x}10^{-07}$	1.32
0.15	$4.23\text{x}10^{-07}$	$3.65\text{x}10^{-07}$	$4.59\text{x}10^{-07}$	1.26
0.17	$5.24\text{x}10^{-07}$	$4.69\text{x}10^{-07}$	$5.78\text{x}10^{-07}$	1.23
0.19	$5.92\text{x}10^{-07}$	$5.60\text{x}10^{-07}$	$7.11\text{x}10^{-07}$	1.27
0.22	$7.63\text{x}10^{-07}$	$7.54\text{x}10^{-07}$	$9.29\text{x}10^{-07}$	1.23

Table A.6
Specific growth rate

$\frac{[Fe^{3+}]}{[Fe^{2+}]}$	Redox potential mV (Ag/AgCl)	$\mu\ h^{-1}$
0.17	419	0.1155
0.51	452	0.1067
1.65	482	0.0834

Appendix B

Analytical Procedures

The analytical procedure was as follows (Jeffrey et al., 1989):

1. For ferrous iron titrations

   - 5 ml of solution sample were collected in a 250ml conical flask using a pipette
   - 10ml of spekker acid solution were added to this sample
   - 3 to 4 drops of the indicator were also added to the sample solution and ferrous iron was titrated until the first permanent colour change from yellow/orange to intense purple was obtained. The volume V_T of $K_2Cr_2O_7$ solution used was then recorded and used in equation (B.1) for the calculation of ferrous iron concentration

$$[Fe^{2+}] = \frac{N_{K_2Cr_2O_7} * V_T * 55.84}{V_S} \qquad [g/l] \qquad \text{(B.1)}$$

where $N_{K_2Cr_2O_7}$ and V_T are the normality and the titration volume of $K_2Cr_2O_7$ solution, and V_S is the volume of the solution sample.

2. For total iron titrations

   - 5 ml of sample solution were collected in a 250ml conical flask using a pipette
   - 30ml of ferric acid solution were added to the sample solution and it was heated to the boiling point
   - Stannous chloride solution was added drop wise to the boiling sample solution until the yellow color completely disappeared. One extra drop of stannous chloride solution was added before the sample solution was left to cool at room temperature
   - 10ml of mercuric chloride were added to the cooled sample solution. A silky–white precipitate was expected to appear before proceeding to the next step otherwise the titration was aborted and repeated

- 4 to 8 drops of the indicator were added to the sample solution and the total iron was titrated until the first permanent colour change from yellow to intense purple was obtained. The volume V_T of $K_2Cr_2O_7$ solution used was then recorded and used in equation (B.2) for the calculation of total iron concentration.

$$[Fe]_T = \frac{N_{K_2Cr_2O_7} * V_T * 55.84}{V_S} \qquad [g/l] \qquad \text{(B.2)}$$

Then $[Fe^{3+}]=[Fe]_T-[Fe^{2+}]$ (B.3)

Appendix C

Concentration of Dissolved Oxygen

For the abiotic oxidation of ferrous iron the concentration of dissolved C_{O_2} can be assumed equal to the saturation concentration C* since the rate of the abiotic oxidation of ferrous iron is too small (Eq. 4.1). The following calculations were done to confirm this assumption.

van't Riet (1979) suggests that for salt solutions the coefficient of oxygen mass transfer k_La is given by:

$$k_L a = 2.0 \times 10^{-3} (P_g / V_L)^{0.7} U^{0.2} \qquad (C.1)$$

where

- P_g/V_L is the gassed power per unit volume of liquid (in W/m^3)
- U is the superficial gas velocity (gas flowrate divided by nominal cross-sectional area of the fermenter, in m/s)
- k_La is in units of 1/s.

The estimated value of k_La calculated using equation C.1 for this present study is 0.0585/s. The solubility of oxygen at different temperatures used for the abiotic oxidation of ferrous iron was calculated using equation C.2 (Tromans, 2000).

$$C^* = P_{O_2} . k . \phi \qquad (C.2)$$

where

- P_{O2} is the oxygen partial pressure
- $k = \exp\left(\frac{0.046T^2 + 203.35T.\ln(\frac{T}{298}) - (299.378 + 0.092T)(T - 298) - 2.0591.10^4}{8.3144T}\right)$
- $0<\Phi<1$, an estimated value of 0.9 was taken in this present study since the concentration of salt used is small (0.21M) (Tromans, 2000).

The values of C* and C_{O2} calculated at the temperatures of the abiotic experiments are reported in table C.1. C_{O2} was calculated by using equation 4.1 where the largest value of $-r_{Fe2+}$ was taken at each temperature.

Table C.1: Oxygen Solubility

Temperature (K)	314.4	324	333	341
C* (mol/l)	19.30×10^{-5}	17.54×10^{-5}	16.38×10^{-5}	15.66×10^{-5}
C_{O2} (mol/l)	19.24×10^{-5}	17.45×10^{-5}	16.19×10^{-5}	15.27×10^{-5}
$(C^*-C_{O2})/C_{O2}$ (%)	0.3	0.5	1	3

It can be seen from table C.1 that the assumption $C^* \approx C_{O2}$ is valid since the relative error is less than 5%.

It was assumed that there is no gas-liquid mass transfer limitation since the rates of ferrous iron oxidation and oxygen fixation were increasing without flattening out (Fig. 4.9-4.11, 4.13-4.15). A mass transfer limitation would have caused these figures to look like figure C.1.

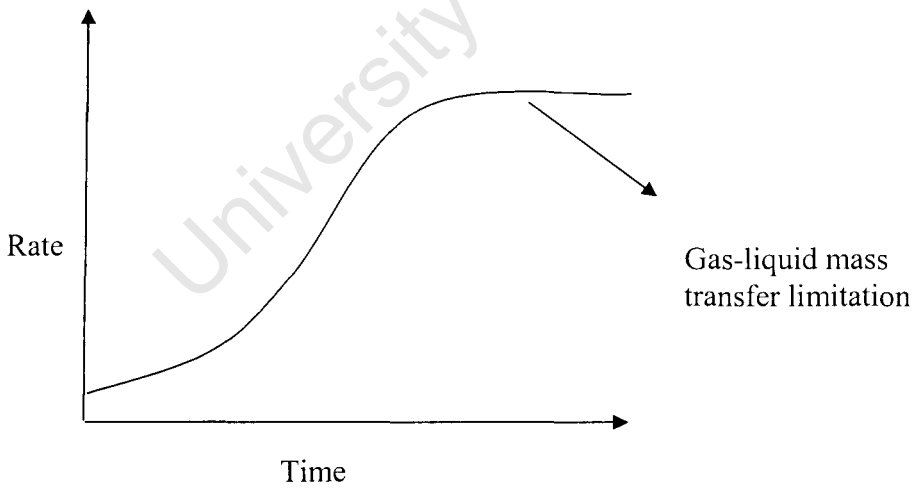

Figure C.1: Rate curve trend in case of gas-liquid mass transfer limitation

At 35°C oxygen solubility is about 20.86×10^{-5} mol/l (Eq. C.2) and the corresponding maximum rate of oxygen mass transfer is equal to 12.20×10^{-6} mol O_2/l.s or 43.92 mmol O_2/l.h

and this corresponds to a maximum rate of ferrous iron oxidation of 175.68 mmol Fe^{2+}/l.h (Eq. 4.1 with C_{O2}=0). These calculations confirm that there is no oxygen mass transfer limitation since these maximum rates are significantly larger than the maximum rates of oxygen fixation and ferrous iron oxidation obtained in this study (Fig. 4.9-4.11, 4.13-4.15).